Modelling of the Mechanical Properties of

Low-Density Foams

Proefschrift

ter verkrijging van de graad van doctor
aan de Technische Universiteit Delft,
op gezag van de Rector Magnificus Prof.ir. K.F.Wakker,
in het openbaar te verdedigen ten overstaan van een commissie,
door het College voor Promoties aangewezen,
op maandag 12 januari 1998 te 10.30 uur

door

Vladimir SHULMEISTER
werktuigkundig ingenieur

geboren te Nikolaev (de Oekraïne)

Dit proefschrift is goedgekeurd door de promotor:

Prof.dr.ir. R.Marissen

Samenstelling promotiecommissie:

Rector Magnificus, voorzitter

Prof.dr.ir. R.Marissen	Technische Universiteit Delft, promotor
Prof.dr.ir. E.v.d.Giessen	Technische Universiteit Delft
Prof.dr.ir. J.G.H.Joosten	Rijksuniversiteit Leiden, DSM-Research
Ir. A.H.J.Nijhof	Technische Universiteit Delft
Prof.dr.ing. K.Schulte	Technische Universität Hamburg-Harburg, Germany
Prof.dr.ir. F.Shutov	Tennessee Technological University, USA
Prof.dr.ir. I.Verpoest	Katholieke Universiteit Leuven, Belgium

ISBN 90-423-0025-6

Shaker Publishing B.V.
St. Maartenslaan 26
6221 AX Maastricht
tel.: 043-3260500
fax: 043-3255090

To my Father and Mother

Contents

List of Symbols

a	strut cross-sectional area	n	degree of initial anisotropy
A_{eff}	effective cross-sectional area	N	number of walls, fibres or struts
A_i	cell dimensions	p	coefficient
A_{ij}	ratio of geometrical anisotropy	p_0	gas pressure inside cells
A'_{ij}	initial anisotropy ratio	p_{at}	atmospheric pressure
A''_{ij}	secondary anisotropy ratio	q	radius of gyration of the cross-sectional area
b	edge length of virtual cube	r_i	radii
b_i	strut length	S	wall surface area
c	strut length	t	strut cross-section side
C	number of cells	V	number of vertices, volume
C_i	coefficients	x_i	coordinates
d	distance between nuclei	α	orientation angle
D	diameter	β, γ	coefficients
E	number of struts	δ	thickness of cell walls
E_{f}	foam Young's modulus	δ^i	distance
E_{s}	Young's modulus of solid	ε	strain, geometrical expansion ratio
E_{ij}	ratio of Young's moduli	ϑ	fraction of open cells in a closed-cell foam
F	force, number of faces	κ_i	curvatures
g	probability distribution	ν_{f}	Poisson's ratio of foam
G_{f}	shear modulus of foam	ν_{s}	Poisson's ratio of solid
I	second moment of inertia	ρ_{f}	foam density
K	geometrical factor	ρ_{s}	density of solid
l	strut length	σ	stress in a strut
L	edge length of a cube	Σ	global stress
M	scale factor	τ	stress in a strut
M_i	bending moment	ϕ	fraction of solid in struts

Abbreviations

2D	two dimensional
3D	three dimensional
bcc	body-centred cubic
fcc	faced-centred cubic
FE	finite element
FEM	finite element method
hex	hexagonal
PMI	polymethacrylimide
PS	polystyrene
PUR	polyurethane
PVC	polyvinylchloride
SEM	scanning electrone microscope
XPS	extruded polystyrene

1. Introduction

Almost any solid material can be foamed—from dough to ceramics. The result of the foaming of the first one is not very often used as a construction material but as a food and is called “bread”. Nevertheless, its specific mechanical properties are often very appreciated. Typical extremes are cake and rusk. Irrespective of the kind of the unfoamed solid material, the mechanical properties of the resulting foam are dependent on the mechanical properties of the original unfoamed material and of the geometry of the foam cells. In such a way, the mechanical properties of bread will be dependent on a kind of dough it is baked of. Moreover, the quantity of yeast in the dough will determine how friable the baked bread is. In terms of engineering foams, “yeast” would sound as “blowing agent”.

Foams are a medium composed of the two phases: solid and gas. Various solids are applied. Polymer foams are most widespread, but glass and metal foams are also produced. All three materials are subject of this thesis; most attention is given to polymer foams. Polymer foams are created by means of physical and chemical processes during their production, where gas bubbles nucleate and grow in liquid material like PUR (polyurethane), XPS (extruded polystyrene), PVC (polyvinylchloride), etc. After production, a cellular solid results containing a very wide range of cell sizes and shapes. The three dimensional (3D) cells fill the space and can consist of membranes, struts and concentrations of material in the vertices where struts meet. The membranes between the cells may be removed by reticulation or by chemical treatment. The result of membranes removal is an open-cell foam consisting of struts and vertices only. Depending on the amount of open cells, foams can be classified as either open-cell or closed-cell.

Foams find numerous applications because of their high mechanical properties relative to their low density. Open-cell foams are frequently used for sound absorption or are applied as filters, mattresses, etc. If a foam has a relatively high density, the mass of the material is mainly concentrated in the vertices. In a foam with a relatively low density, the mass is roughly distributed uniformly over relatively slender elongated struts.

Closed-cell foams show a higher stiffness and find applications as construction material, e.g., as core of sandwich panels. Closed-cell foams are also applied for thermal insulation purposes [see, for instance, the theses of Boetes (1986), du Cauze de Nazelle (1995) and Brodt (1995) at the Delft University of Technology]. The isolation and mechanical properties combined with the low density makes closed-cell polymer foams extremely useful for the panels in the refrigeration trucks. A recent example is the “Cold Feather”

developed at the Delft University of Technology in the group of Beukers *et al.* (1997).

Liquid base material with a gaseous blowing agent can be extruded with simultaneous foaming, as mentioned above. In these cases, differences in growth rates in the three principal directions occur, and the final foam can be characterized as geometrically anisotropic. The cells are elongated in the direction with the highest cell growth rate. Because of the geometrical anisotropy, the mechanical properties of the final foam are also anisotropic.

1.1 Production

A very wide range of materials, like metals, polymers, glass and ceramics, may be foamed. As a result, a "bi-material" system with gas as a continuous or disperse phase and a solid as a continuous phase occurs. Depending on the volumetric fraction of the solid phase, foams are classified at low- or high-density. According to Cunningham and Hilyard (1994), foams with a volumetric fraction of solid less than 0.1 are called low-density. The scope of this thesis is restricted to low-density foams.

It will be shown further in this thesis that foam geometry plays a vital role in the mechanical properties of foams. To understand the existing geometry of foams, the principles of the foaming process should be considered.

Foams may be produced in various ways. One of the most wide-spread of them is a method with a physical blowing agent. According to this method, a gas (the blowing agent) is initially dissolved in a homogeneous dispersing medium which may be a polymer, a metal melt or another material. As a result, a quasi-homogeneous medium appears and it must become a two-phase "gas-liquid" system. To achieve this, a number of conditions must be realised. First of all, the potential of evolving gas in the initial phase must exceed that of the new phase. And, secondly, surface forces should be overcome. This is the reason that nucleation of bubbles in a liquid with supersaturated gas can take place due to a fluctuation clustering of molecules of a new phase. If this condition is satisfied, bubbles start to grow. The growing process takes place until the supersaturation disappears. The degree of the gas saturation determines a final foam density ρ_f (if the foaming takes place freely).

The above mentioned fluctuations in the compound may be initialized artificially. The use of nucleating agents may lead to the nucleation process and so, to a more homogene-

ous foam structure and to control of the cell size. For example, the addition of finely dispersed metal or mineral particles to the composition of a polymer melt with a supersaturated gas and subsequent foaming of this composition leads to the creation of a uniform fine-cell foam structure.

1.2 Blowing agents

The most general classification of the blowing agent is based on the mechanism of the gas liberation. According to this classification, blowing agents may be chemical or physical. The first ones are individual compounds or mixtures of compounds which liberate gas as a result of chemical processes like thermal decomposition or as a result of their interactions with the other components of the composition.

Physical blowing agents are compounds that liberate gases as a result of evaporation or desorption when the pressure is reduced or at increasing temperatures. As opposed to the chemical blowing agents, physical blowing agents do not change the chemical constitution of the compound. This difference will be of a great importance for the determination of the mechanical properties of the solid phase of the foam.

The present thesis is devoted to the prediction of the mechanical properties of foams, based on solid properties and foam geometry only. Knowledge of solid properties is then essential of course. Chemical reaction may change the properties of the solid. Consequently, it is desired in this thesis for validation theory to use foams that are produced by use of a physical blowing agent. The properties of the solid in foam may be assumed to be very close to the properties of the solid before foaming. It should additionally be noted that even in the case of physical blowing agents, the properties of solid material in foam may differ to some extent from those of the original unfoamed solid. This can be caused by the influence of various additives, i.e., stabilisers, remaining of the blowing agent, etc. and even by geometry, like in PUR, where the solid temperature due to the exothermal reaction of the curing resin is influenced by the foam geometry (e.g., cooling). The temperature during curing may then influence the subsequent chemical reactions and consequently the solid properties.

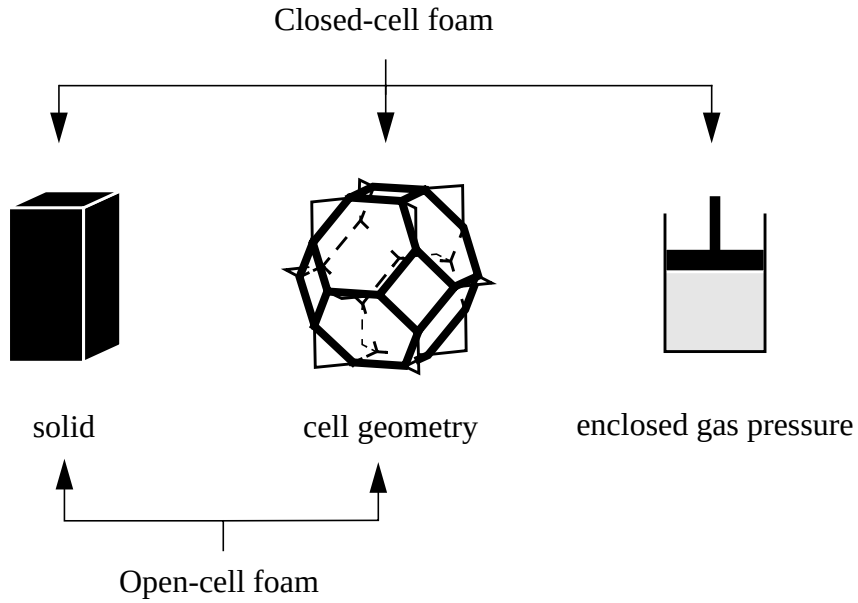

Fig. 1.1. Components affecting the mechanical properties of foams.

1.3 Mechanical properties of foams

In general, the mechanical properties of foams are dependent on three main components, schematically illustrated in Fig. 1.1. As far as open-cell foams do not contain gas enclosed in the foam cells, the gas pressure does not influence the mechanical properties of open-cell foams. In contrast, the two first features, the kind of solid from which the foam is made and the cell geometry, are of great importance for the properties of any foam.

1.3.1 Foam geometry

As mentioned above, foam geometry plays an important role in the behaviour of foams. From the geometrical point of view, a foam comprises a network of space-filling polyhedra. A cellular structure can be described as a number of cells, surrounded by walls (faces). Each face has struts as borders where the faces intersect. Furthermore, the struts intersect and form vertices (or knots). It has been shown by Euler (1746), that the number of struts E, vertices V and faces F of C cells in 3D are related as:

$$-C + F - E + V = 1. \tag{1.1}$$

This is Euler's law and it is valid for any foam structure. In this way, a foam structure consists of walls, struts and vertices.

To detect the relation between the morphology and properties of the cellular solids, it is important to consider the geometrical features of the foam structure which could be accepted as the most important. According to Berlin and Shutov (1980), these parameters are:

- relative number of open cells
- relative foam density
- cell size
- cell shape, or geometrical anisotropy
- cell walls thickness and distribution of solid between struts and faces
- geometry of a foam cell and its constituents

The consideration of all these parameters is presented below.

Relative number of open cells

According to their morphology, foams are subdivided in open- and closed-cell foams. The main difference between these two foam classes is absence of the membranes in the open-cell foam. But in most cases foam contains closed as well as open cells. This causes a necessity to introduce the degree to which cells are closed or open, because it influences the properties of cellular materials significantly. A study of closed-cell foams performed by Berlin and Shutov (1980) suggests, that the fraction of open cells, ϑ, is a function of the foams relative density. In the region of the low-density foams ($\rho_f / \rho_s < 0.06$, where ρ_s is the density of the solid material), the factor ϑ is approximately equal to 0.3 and decreases for foams of higher densities. They explain this effect by the fact, that in the low-density foams the membranes become very thin and can easily rupture during or after processing. However, the rheological behaviour of the foaming liquid will be important and possibly even dominate ϑ.

It is expected that the relative content of open cells in closed-cell foam will play a considerable role in the physical properties of cellular materials.

For example, Hagiwara and Green (1987) observed that the Young's modulus of closed-cell foam increased with the cell size. They explained this by the increasing fracture of the closed cells in the smaller cell size materials. The key is, that the smaller is the cell size of the foam with a constant density, the lower is the walls thickness and, hence,

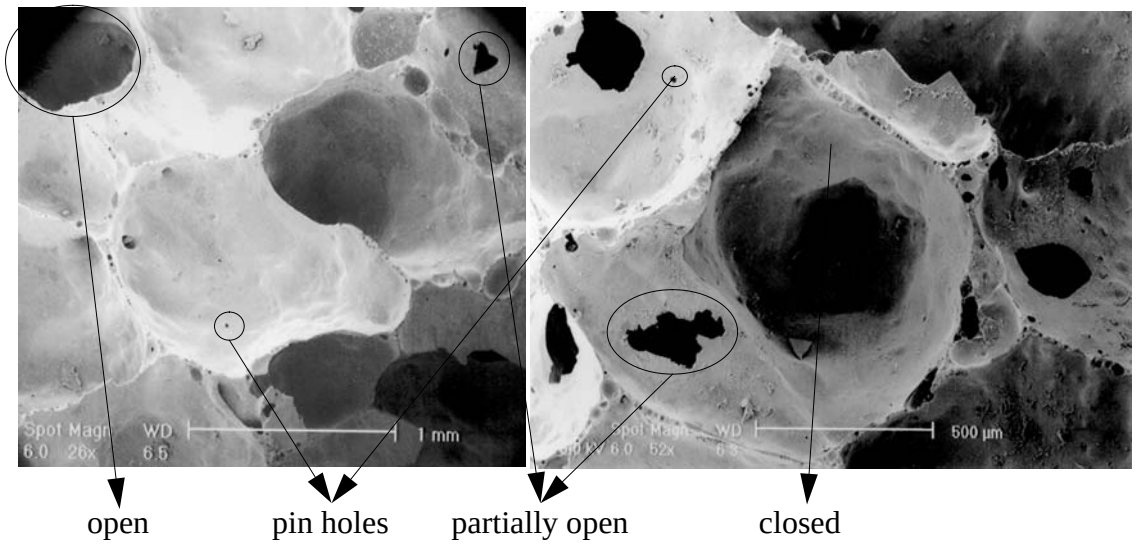

Fig. 1.2. Scanning electron microscope views of the closed-cell glass foam with various types of the cell opening.

the greater is the probability that the walls rupture during the production process or after.

A recent study of the morphological features of closed-cell PUR foam by Yasunaga *et al.* (1996) showed the importance of the amount of cell opening for the properties of closed-cell foam. The cell walls have been classified as:

- closed
- pin holes
- partially open (less than 50% area open)
- open

All these features are shown at the example of closed-cell glass foam in Fig. 1.2. The effective fraction of open cells is estimated then by the equation

$$\vartheta = \frac{N_{open} + (1/2)\, N_{part}}{N_{open} + N_{part} + N_{pin} + N_{closed}}, \qquad (1.2)$$

where N correspond to the number of walls of various classes.

In practice, it is difficult to make foam with only closed or only open cells. Open-cell foams contain mostly open cells (more than 90%), while the major number of cells in closed-cell foams is closed.

Relative foam density

The relative foam density ρ_f/ρ_s is a crucial parameter for the physical properties of foam. It shows the part of space which is occupied by the solid phase and, therefore, is very important for mechanical, thermal, electrical and many other characteristics of foams.

The foam density ρ_f can be calculated just by dividing the mass of the foam sample by its volume. But the obtained value is averaged over the volume of the sample, because the structure is not homogeneous and the foam density of the surface layers may be 3 to 10 times greater than the averaged value. This can be caused, for example, by temperature differences during the foam production process and the resulting different foaming rates. Moreover, gravity may cause the foam density to increase from top to bottom. This effect is dependent on the technological details of the foaming process, when the thickness of cell faces and struts decreases due to drainage of the liquid foam.

Nevertheless, the absolute majority of the models use a simplified averaged foam density ρ_f and do not take the density distribution into account.

Many empirical equations describing the mechanical properties of foams are connected to the relative foam density by the general formula

$$\frac{\Phi_f}{\Phi_s} = C\left(\frac{\rho_f}{\rho_s}\right)^p, \tag{1.3}$$

where Φ_f and Φ_s are mechanical properties of foam and solid phase correspondingly, C and p are the coefficients obtained from the experiments.

Cell size

The mean cell diameter $\bar{D}$ is one of the important geometrical characteristics of foam. As it has been shown above, the cell size can indirectly influence the mechanical properties of foams. Different investigators have very various and contradictory conclusions about this issue. For instance, Morgan *et al.* (1981) found out experimentally that the Young's modulus is independent of the cell size in a closed-cell glass foam, while Hagiwara and Green (1987) stated that increasing cell size makes closed-cell foams stiffer. Open-cell glassy carbon foam was studied by Brezny and Green (1990). The elastic modulus and fracture toughness have been found to be independent of the cell size, while a square root dependence on the toughness has been predicted. The compressive strength

decreased with increasing cell size.

The problem may be caused by the attempt to explain some phenomena by plotting mechanical characteristics of foams against the cell size, without sufficient considering the basics of the phenomena. It will be shown in this thesis that the distribution of cell sizes can have important influence on the mechanical properties of foams. Moreover, it will be shown that not only the cell size, but also the cell size distribution can be vital for the behaviour of foams.

Cell shape, or geometrical anisotropy

Due to the production, when foams are extruded and they rise during foaming, the final foam structure is often anisotropic. Based on this production process, mostly three main directions can be determined in foam with different cell dimensions in these directions. Consequently, many foam properties are dependent on the direction. Moreover, mechanical characteristics of foam are better in the directions where foam cells have greater dimensions.

Cell walls thickness and distribution of solid between struts and walls

The solid material in foams can be considered to be distributed between 3 geometrical groups: walls, struts and vertices. As far as only low-density foams are considered in this thesis, the material in vertices is neglected. The solid phase is assumed to concentrate in walls and struts for the closed-cell foams, and in struts for the open-cell foams.

Berlin and Shutov (1980) noted that a critical cell wall thickness, δ_{cr}, exists for their specific base material, which is the minimum thickness for that material to allow closed-cell foam formation. The critical cell wall thickness δ_{cr} is a lower boundary for the cell wall thickness in the closed-cell foam. The upper border is theoretically limited by the foam density ρ_f only. The solid material is distributed then between walls only.

The distribution of the material between walls and struts in the closed-cell foam will influence the mechanical properties of the foam considerably.

Form of a foam cell and its constituents

To achieve realistic results in the prediction of the mechanical properties of foam, the structural elements of a foam should be studied thoroughly. This, as well as the properties of the solid material in a foam, is the crucial point in the modelling.

An ideal geometry of a foam that has reached a thermodynamical equilibrium should comply with the following terms:

- A strut is an intersection of 3 walls [Plateau's law (1873)].
- A knot-point is an intersection of 4 struts and an intersection of 6 walls [Plateau's law (1873)].
- Struts are straight in the undeformed state.
- Several struts, belonging to the same cell wall and connected to each other, lay in one plane.
- As a result of the previous points, walls are flat in the undeformed state.
- During the production process of foam (growing), a dihedral angle (angle between faces) is equal to $120°$.
- Struts intersect in a vertex under the bond angle equal to $109° 28'16"$.

These laws are based at the principles of the minimizing surface energy during the foam growth.

Struts of the foamlike structures are known to have a cross-section in a shape of Plateau-Gibbs borders, well-known from the literature [see, for instance, Kann (1989) or Pertsov *et al.* (1992)]. An example of the strut cross-section in closed-cell polymethacrylimide (PMI) foam is given in Fig. 1.3.

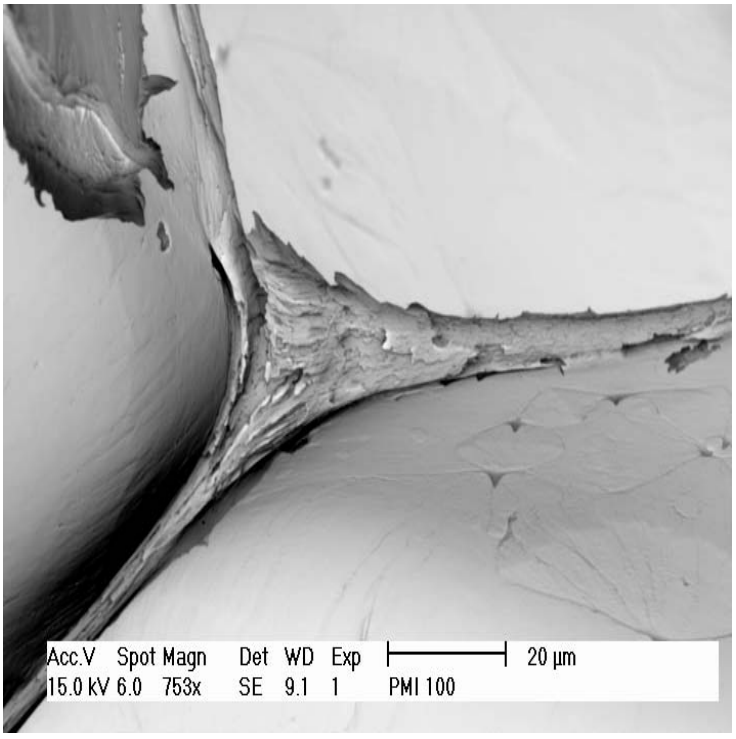

Fig. 1.3. Strut cross-section in the form of Plateau-Gibbs border in PMI foam.

There are some more geometrical details of foam that should be named here. First of all, the cell walls thickness is not constant within a wall but decreases from the wall border to the centre [see Yasunaga *et al.* (1996)]. The same effect is observed with the struts which are thicker near vertices and thinner in the middle part. Moreover, cell walls thicknesses and struts cross-sections are not constant for all struts and walls in a foam. They can vary and the distribution of the walls thicknesses and strut cross-sections may be large. The use of the mean values in the modelling can lead to the introduction of the errors. That is why, it is important to measure a considerable amount of struts and walls and to pay attention onto distributions. For many foam materials discussed in this thesis, these distributions are narrow. Nevertheless, application of variable strut cross-sections and walls thicknesses in the model can be useful.

1.3.2 Properties of the solid material

As mentioned above, only two features influence the behaviour of a foam: *kind of material* inside the foam and *geometry* of the foam (for the closed-cell foams gas pressure may be important too). All accents of the present thesis are concentrated on the last issue—foam geometry. Only this Chapter deals with solid materials.

One of the main aims of the modelling presented in this thesis is creation of a general-purpose model that would be valid for all low-density foams, any solid material and kind of geometry. This means that special attention should be given to the solid properties of the material inside the structural elements of foams.

Unfortunately, it is very often extremely difficult or even not possible to determine the mechanical properties of the base material inside the foam. The main problem is that the material before foaming almost always differs from that after the foaming process and solidification. A lot of factors influence the properties of the solid material and can even change its chemical composition. Polymers are especially sensitive to the foaming process. Macromolecules of a polymer might get orientation in a foamed medium and improve the mechanical properties of solid in the directions of the orientation. Furthermore, there are many other aspects that can influence the solid material, like stabilisers, nucleators, etc.

To conclude: the knowledge of the properties of the original unfoamed material does not mean the knowledge of the properties of the material inside the foam. This yields the necessity to determine the properties of the material inside the foam. This problem is very

often insuperable because of the scale of the foam structural elements. The strut length is often approximately 50 μm and a uniaxial test becomes challenging. Nevertheless, experiments are known [see, for instance, Warburton *et al*. (1990)], where a three-point bending test with a 1.3 mm span is accomplished on a wall of a foam cell. Unfortunately, such tests are exceptions.

What will be important to know about the solid material inside foam? It is dependent on the kind of mechanical properties of the foam that are of the interest. For instance, if it concerns the linear elastic properties of the foam only, the Young's modulus of the solid material will be sufficient. For a more advanced model, which includes nonlinearities, much more information about the solid material will be necessary. It should be noted here, that some materials exhibit time dependent behaviour (e.g., polymers) and that should also be incorporated in the model. Fracture of foams is controlled by the fracture of solid. That is why, if fracture of foam is being modelled, this aspect should be taken into account too.

The model to be presented in this thesis can in principle include all features mentioned above. However, some of them are not incorporated yet. For instance, the polymer behaviour is often very sensitive to the strain rate. Since this behaviour is not present in the model yet, all tests described below are accomplished at low speeds whereas the time scale of solid and foam behaviour is chosen to be similar. Consequently, time dependent behaviour is almost ruled out as a variable. A fracture model has not been created yet. Therefore, fracture of the solid will not be discussed here.

1.4 Existing Foam Models

Primary existing foam models found in the literature are shown in Fig. 1.4. The main drawback of the existing models is their unrealistic geometry, which is often regular in comparison with the irregular real foam structure. A vivid example of it is a tetrakaidecahedron used by Ko (1965), Dementjev and Tarakanov (1970a) and Zhu *et al.* (1997). This approach is doomed to yield inaccurate results due to the application of the regular geometry to model irregular structures. Another type of models are based on small volume elements which mechanical properties are averaged through all possible orientations in space. A wide-spread example of such a model, a tetrahedral element of Warren and Kraynik (1987), (1988) and (1994), is very limited in use because of its limited size and still the same regular geometry.

Some attempts to create a random model [see, for instance, the randomized tetrakaide-

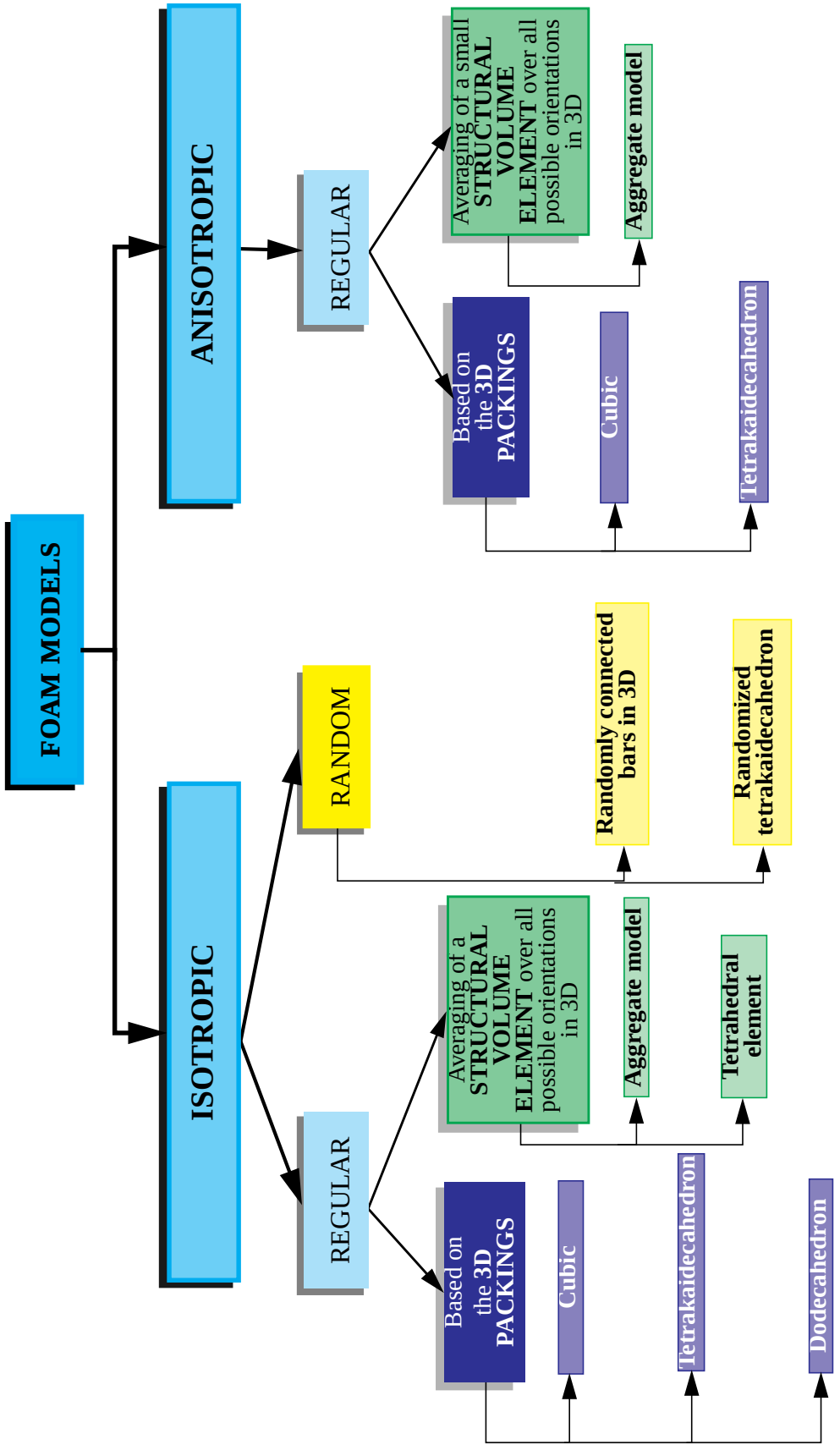

Fig. 1.4. Overview of the previously existing models.

cahedron of Valuyskikh (1990) or randomly connected rods of Lederman (1971)] are also not very successful. The randomized tetrakaidecahedron is obtained from the regular structure in an unnatural way and may be used for open-cell foams only (for details see Section 2.3.1). Several geometrical laws formulated in Section 1.3.1 are violated. The model of Lederman (1971) is created in a way never occurring in nature and, therefore, has an unnatural geometry. As a result, the model could not be applied to the closed-cell foam modelling. Moreover, bending of the rods has not being incorporated in the model, which occurred therefore to be extremely stiff.

The models will be discussed in more detail later in this thesis. The main conclusion made after analysis of the existing foam models was the necessity to create a foam model that could resemble the geometry of a real foam (including anisotropic foams) and that could be general-purpose, i.e., could potentially be used for any low-density foam type.

1.5 Scope of the thesis

The purpose of this work was to create a comprehensive model for all low-density foam types: open- and closed-cell, isotropic and anisotropic. Moreover, almost the entire deformation region in compression (but excluding the densification under contact phenomena) and in tension (excluding fracture) will be incorporated in the model. The complete structure of this thesis is schematically shown in Table 1.1.

Table 1.1. Contents of the thesis

<table>
<tr><th colspan="6">Open-cell model: Chapter 2</th></tr>
<tr><th colspan="3">Isotropic: Sections 2.3.1-2.3.3</th><th colspan="3">Anisotropic: Sections 2.3.4-2.3.5</th></tr>
<tr><td>Linear elastic</td><td>Large deformations</td><td>Nonlinear material</td><td>Linear elastic</td><td>Large deformations</td><td>Nonlinear material</td></tr>
<tr><td>Section 2.3.2</td><td colspan="2">Section 2.3.3</td><td>Sections 2.3.4-2.3.5</td><td></td><td></td></tr>
<tr><th colspan="6">Closed-cell model: Chapter 3</th></tr>
<tr><th colspan="3">Isotropic: Sections 3.3.2-3.4.1</th><th colspan="3">Anisotropic: Section 3.4.2</th></tr>
<tr><td>Linear elastic</td><td>Large deformations</td><td>Nonlinear material</td><td>Linear elastic</td><td>Large deformations</td><td>Nonlinear material</td></tr>
<tr><td>Section 3.4.1</td><td colspan="2">Section 3.3.2</td><td colspan="3">Section 3.4.2</td></tr>
</table>

Chapter 2 of the thesis will deal with open-cell foams. First, the random isotropic model will be constructed (*Section 2.3.1*). Consequently, linear elastic (*Section 2.3.2*) and nonlinear (*Section 2.3.3*) models will be created. Moreover, *Section 2.3.2* will also incorporate regular foam models and will show the influence of the irregularities on the linear elastic properties of the foam models. A new approach for the introduction of the anisotropy in foam will be presented in *Section 2.3.4*. With the help of this approach, a regular anisotropic tetrakaidecahedron will be created. The random anisotropic foam model will be developed in *Section 2.3.5* using the same principles as for the regular model in the foregoing Section. Nonlinear problems for the anisotropic foam model will not be taken in the scope of the thesis and comprise a possible future development of the model.

In **Chapter 3**, the closed-cell foam model will be created. *Section 3.4.1* will present the linear elastic modelling with some applications of the model to glass and polymer foams. Further development of the model in *Section 3.4.2* will result in a comprehensive anisotropic closed-cell foam model including material and geometrical nonlinearities. The model will be verified on glass and polymer foams.

The present thesis is partly based on the following papers:

Sections 2.3.1-2.3.2

Burg, M.W.D. van der, V. Shulmeister, E. van der Giessen and R. Marissen (1997). *On the Linear Elastic Properties of the Regular and Random Open-Cell Foam Models.* J. of Cell. Plast., 33, 31-54.

Section 2.3.3

Shulmeister, V., M.W.D. van der Burg, E. van der Giessen and R. Marissen. *Numerical Analysis of Large Deformations of Low-Density Elastomeric Open-Cell Foams.* Submitted for publication in J. of Mech. of Mater.

Section 2.3.5

Shulmeister, V., A.H.J. Nijhof and R. Marissen (1997). *Three Dimensional Modelling of Random Anisotropic Open-Cell Foams.* Proc. of the 4th Cell. Polym. Int. Conf., Shrewsbury, Great Britain, 14/1-6.

Section 3.4.1

Shulmeister, V., A.H.J. Nijhof, N.J.H.G.M. Lousberg and R. Marissen (1995). *On the Micromechanics of Polymer Foam Used as Thermal Insulator.* Book of Abstracts of the 19th

Int. Congr. of Refrig., The Hague, The Netherlands, 136.

Shulmeister, V., A.H.J. Nijhof and R. Marissen (1997). *Linear Elastic Closed-Cell Foam Modelling.* Proc. of the 5th Europ. Conf. on Adv. Mater. and Proc. and Appl., Maastricht, The Netherlands, 2/13-18.

2. Open-cell foams

2.1 Introduction

Open-cell foams contain hardly any walls. Cell walls are removed by physical or chemical treatments, which will not be described here. However, “open-cell” does not mean that all walls are removed from the structure. There is often a very small percentage of walls that still remains in the foam, as can be seen from the view of the open-cell PUR foam in Fig. 2.1. This phenomenon indicates that open-cell foams originate from closed-cell foams. Hence both open- and closed-cell foams have similar geometrical features. However, the presence of a very few number of walls in the open-cell foam does not influence mechanical properties of the foam and can be neglected.

An open-cell foam structure can be considered as an array of cells composed of struts. A great number of foam structures is geometrically anisotropic and the dimensions of cells that comprise the structure are dependent on the direction. This leads to differences in the mechanical properties of the macrostructure in various directions, so-called mechanical anisotropy. This effect occurs due to a rise process during the production of foam. This fact should be incorporated in the model when anisotropic foam is modelled.

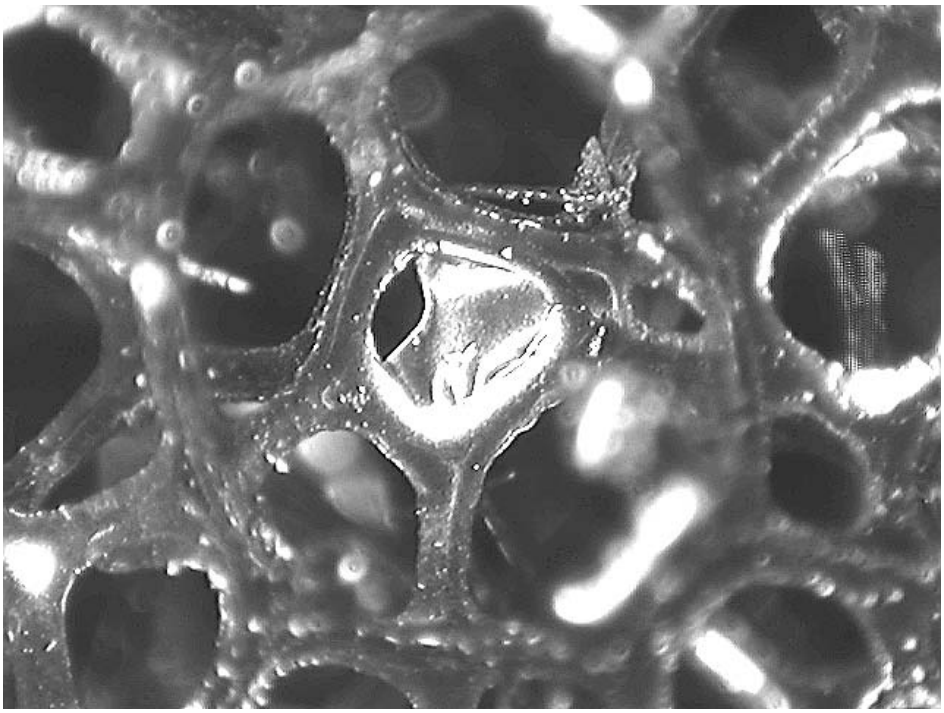

Fig. 2.1. View of open-cell PUR foam with a visible cell wall.

2.2 Survey of the existing models

2.2.1 Regular foam models

Several attempts have been made in the past to predict the bulk mechanical properties of open-cell polymer foams by relatively simple models using structural beams to represent the foam struts. These models have mostly been based on regular 2D or 3D packings.

2D models will not be considered here, because they are unsuitable for reproducing the deformation mechanisms of real 3D foams. The first group of the regular models in 3D comprises models which are based on regular, symmetrical packings of struts. The size of the unit cells of such models is approximately the same as the strut length.

Cubic model

Rectangular prism models shown in Fig. 2.2a represent one type. The most comprehensive description of this type of model was given by Gibson and Ashby (1988). The initial response of their unit cell on the uniaxial compression–tension deformation is governed by the bending of struts. The cross-section of the struts has been simplified to be square. An obvious advantage is the simplicity of these models, where the regular unit cells fill the space completely through repetition. On the other hand, these models are quite far removed from real foam geometry, which is never rectangular and is more or less irregular. Moreover, as can be seen in Fig. 2.2a, the model is only quasi–3D. The struts in the x_3-direction are not effective. Furthermore, the cubic structure does not satisfy Plateau's laws (1873).

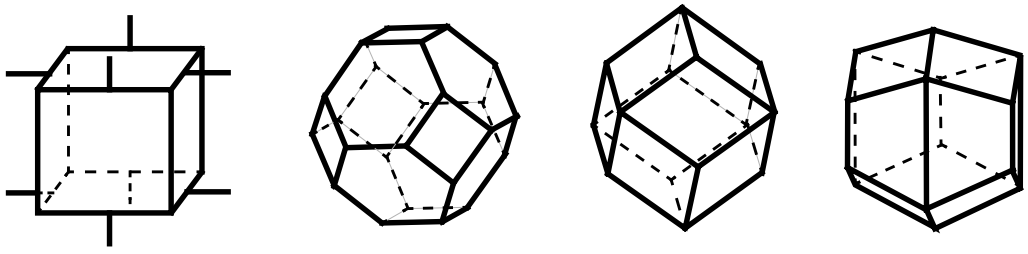

(a) (b) (c) (d)

Fig. 2.2. Regular models, based on the regular cells packings. (a) Cubic model. (b) Tetrakaidecahedron. (c) Rhombic dodecahedron. (d) Rhombic-trapezoidal dodecahedron.

Isotropic linear elastic model

Based on the model shown in Fig. 2.2a, Gibson and Ashby (1988) recognized the bending of struts to be the main deformation mechanism at small strains. To determine the Young's modulus E_f of an open-cell foam, they related the mass densities of foam ρ_f and solid material in struts ρ_s to the geometrical features of struts, the strut length l and the strut cross-section side t, as $\rho_f/\rho_s \propto (t/l)^2$. Further, the strut moment of inertia I is proportional to t^4. The global stress Σ is proportional to F/l^2, where F is the global uniaxial force; the strut deflection due to bending $\Delta \propto \varepsilon\, l$ is proportional to $Fl^3/(E_s I)$, where E_s is the Young's modulus of the solid material in struts. The foam Young's modulus E_f is then given by:

$$E_f = \frac{\Sigma}{\varepsilon} \propto \frac{F/l^2}{Fl^2/(E_s I)} \propto \frac{1}{l^2}\,\frac{E_s t^4}{l^2}\ , \text{or}$$

$$\frac{E_f}{E_s} \propto \frac{t^4}{l^4} \propto \left(\frac{\rho_f}{\rho_s}\right)^2. \tag{2.1}$$

Finally, the relative Young's modulus of the open-cell foam is represented by

$$\frac{E_f}{E_s} = C_1\left(\frac{\rho_f}{\rho_s}\right)^2, \tag{2.2}$$

where C_1 is a coefficient, incorporating the geometric constants of proportionality. Numerous experimental data for open-cell foams have been fitted by applying $C_1 = 1$. This led to the following elastic constants of the open-cell foam, given by Gibson and Ashby (1988) and based on the cubic model:

$$\frac{E_f}{E_s} \approx \left(\frac{\rho_f}{\rho_s}\right)^2, \qquad \frac{G_f}{E_s} \approx \frac{3}{8}\left(\frac{\rho_f}{\rho_s}\right)^2, \qquad \nu_f \approx 0.3\,, \tag{2.3}$$

where G_f is the shear modulus and ν_f is the Poisson's ratio of the foam.

Earlier, Rusch (1969) gave an empirical relation between the foam relative density and elastic modulus in compression as

$$\frac{E_f}{E_s} = \frac{1}{12}\,\frac{\rho_f}{\rho_s}\left\{2 + 7\frac{\rho_f}{\rho_s} + 3\left(\frac{\rho_f}{\rho_s}\right)^2\right\}. \tag{2.4}$$

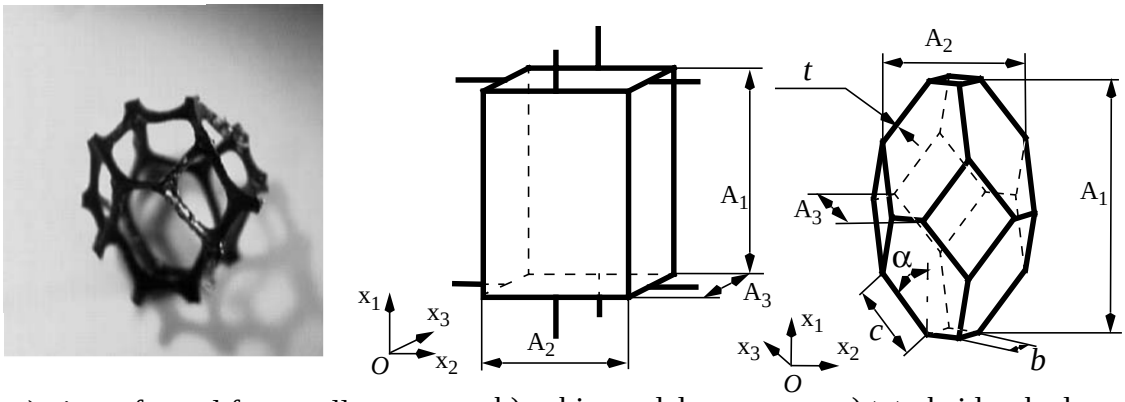

a) view of a real foam cell b) cubic model c) tetrakaidecahedron

Fig. 2.3. Anisotropic (a) real foam cell and (b)–(c) models.

Anisotropic linear elastic model

The cubic model of Gibson and Ashby (1988) has been modified to give the correlation between the geometrical anisotropy and the mechanical characteristics of anisotropic foams like Young's modulus. A typical example of an anisotropic foam cell is given in Fig. 2.3a. The corresponding anisotropic cubic model is shown in Fig. 2.3b. The geometrical anisotropy of foam is given in terms of a cell dimensions ratio, $A_{ij} = A_i / A_j$, where i and $j = 1, 2, 3$, $i \neq j$ and dimensions $A_1 \geq A_2 \geq A_3$.

The Young's moduli ratio of an anisotropic axisymmetric foam with $A_2 = A_3$ comprises

$$E_{13} = \frac{E_1}{E_3} = \frac{2A_{13}^2}{1 + (1/A_{13})^3}. \tag{2.5}$$

This anisotropic cubic model has been extended to orthotropic foams with $A_2 \geq A_3$ by Huber and Gibson (1988) and resulted in the Young's moduli ratios:

$$E_{ij} = A_{ij}^2 \left[\frac{1 + A_{kj}^3}{1 + A_{ki}^3} \right], \quad k \neq i, \quad k \neq j. \tag{2.6}$$

The described above fitting of the experimental data leads to doubts about use of such a "model" for the prediction of the mechanical properties of foams in general. The models depicted in Figs. 2.2a and 2.3b are used only to illustrate that the main deformation mechanism in foam is bending and will never give a detailed feedback between geometry and mechanical properties of foam. However, the model has extensively been fitted to experiments and may be used as "experimental result" for the verification of other models.

Isotropic nonlinear model

The cubic model has also been used to predict large-deformation behaviour of open-cell foams. When the tensile strains of the foam become sufficiently large (when the tensile strain ε_f exceeds a value of about 0.3), the struts become oriented in the loading direction. Consequently, the axial deformation of the struts increasingly dominates the foam response. The foam elastic response in this regime, in terms of the foam tangent modulus $E_{f,t}$, depends on the density according to

$$\frac{E_{f,t}}{E_s} = C_2 \left(\frac{\rho_f}{\rho_s} \right)_i , \tag{2.7}$$

where C_2 is a constant. Subscript i refers to the initial situation at zero strain. Gibson and Ashby (1988) accepted $C_2 \approx 1$ as a fair approximation. Equation (2.7) reflects a direct relation of the macroscopic foam deformation and the local tensile deformation of struts.

In case of compressive deformations of the foam, some struts will buckle, and henceforth initiate the collapse of the foam. Gibson and Ashby (1988) expected the elastic collapse stress Σ_{el} to be

$$\frac{\Sigma_{el}}{E_s} = C_3 \left(\frac{\rho_f}{\rho_s} \right)_i^p , \tag{2.8}$$

where C_3 and p are coefficients. It was found from experiments that $C_3 \approx 0.05$ and $p \approx 2$.

Tetrakaidecahedron

Another wide-spread model, based on the tetrakaidecahedron, has been considered by Dementjev and Tarakanov (1970a), Renz and Ehrenstein (1982), Lakes *et al.* (1993) and Zhu *et al.* (1997). The model is shown in Fig. 2.2c. It consists of six quadrilateral and eight hexagonal faces. According to the crystallography, it corresponds to the body-centred cubic (bcc) packing of spheres. The geometry of this regular foam model corresponds much better to the real foam geometry than the cubic model. The model has three orthogonal main directions and none of the struts is initially oriented in a main direction. This is more realistic than the cubic model which has a strong orthogonal character. The Young's modulus of the tetrakaidecahedron with struts having a square cross-section is found by Dementjev and Tarakanov (1970a) to be

$$\frac{E_f}{E_s} = \frac{2 + \frac{t}{l}}{18}\left(\frac{\rho_f}{\rho_s}\right), \tag{2.9}$$

where t is a side of the square cross-section and l is the length of a strut.

For an isotropic tetrakaidecahedron a correlation between the t/l ratio and the relative foam density ρ_f/ρ_s was given by Gibson and Ashby (1988) as

$$\frac{\rho_f}{\rho_s} = 1.06\left(\frac{t}{l}\right)^2, \tag{2.10}$$

which can be substituted in Eq. (2.9).

The most recent studies of the linear elastic properties of this model by Zhu *et al.* (1997) gave the following formula for the relative Young's modulus of the tetrakaidecahedron with struts having triangular cross-section

$$\frac{E_f}{E_s} = \frac{0.726\left(\frac{\rho_f}{\rho_s}\right)^2}{1 + 1.09\left(\frac{\rho_f}{\rho_s}\right)}, \tag{2.11}$$

which is much more convenient than the corresponding expression by Dementjev and Tarakanov [see Eq. (2.9)] because it does not contain geometrical features of the foam microstructure. The same model with the struts having Plateau-Gibbs border cross-section resulted in the stiffer model with the relative Young's modulus

$$\frac{E_f}{E_s} = \frac{1.009\left(\frac{\rho_f}{\rho_s}\right)^2}{1 + 1.514\left(\frac{\rho_f}{\rho_s}\right)}. \tag{2.12}$$

This model has been applied to anisotropic modelling by Dementjev and Tarakanov (1970b). For this, the isotropic tetrakaidecahedron was extended in the rise direction, as shown in Fig. 2.3c. An analytical relationship is given for the Young's moduli ratio of a transversely isotropic foam with $A_1 > A_2 = A_3$ as a function of the strut diameter t, struts lengths b and c and orientation angle α by

$$E_{13} = E_{12} = \frac{\left[\frac{1}{2K^3} + (\cos\alpha)^2\right]\cos\frac{\pi}{4}(\cos\alpha)^2(2+\beta)}{\left(\frac{2}{K}+\beta\right)(\sin\alpha)^3}, \tag{2.13}$$

where $K = c/b$ and $\beta = t/c$ are geometrical factors.

The rewriting of Eq. (2.13) yields to

$$E_{13} = E_{12} = \frac{(2c+t)\left(2c^2-b\right)\left(b^3-b^2c+2c^3\right)}{2(2b+t)b^3c^2}.$$

Dodecahedra

Other approaches for perfectly ordered 3D models are a rhombic dodecahedron and a rhombic-trapezoidal dodecahedron, depicted in Fig. 2.2c and Fig. 2.2d respectively. These two cells can be derived from two closest packing geometries of spheres: hexagonal (hex) and face-centred cubic (fcc) packing. The rhombic dodecahedron has a cubic symmetry (orthogonal), as a tetrakaidecahedron, so the mechanical properties of the unit cell structures are equal in the three principal directions. This is in contrast to the rhombic-trapezoidal dodecahedron which is relatively stiff in one direction due to the alignment of struts in that direction (x_1-direction in Fig. 2.2d). The elastic properties of these two unit cells have been studied by Ko (1965). The equivalent Young's modulus of the rhombic-trapezoidal dodecahedron is given by

$$\frac{E_f}{E_s} = \frac{\sqrt{3}}{4}\left(1 + \frac{9}{4\{13 + 8\nu_s + 2\sqrt{3}\frac{l^2}{a}\}}\right)\left[\frac{a}{l^2}\right], \tag{2.14}$$

where a is a strut cross-sectional area, l is a strut length and ν_s is Poisson's ratio of the solid material in struts.

The effective Poisson's ratio of the model is

$$\nu_f = \frac{1}{4}\,\frac{2(1+2\nu_s) + \sqrt{3}\frac{l^2}{a}}{\frac{13}{2} + 4\nu_s + \sqrt{3}\frac{l^2}{a}}. \tag{2.15}$$

The same constants for the rhombic dodecahedron give

$$\frac{E_f}{E_s} = \frac{63\sqrt{3}}{71 + 16\nu_s + \sqrt{3}\frac{l^2}{a}} \frac{a}{l^2} \tag{2.16}$$

and

$$\nu_f = \frac{7}{8} \frac{2 + 4\nu_s + \sqrt{3}\frac{l^2}{a}}{\frac{71}{4} + 4\nu_s + \sqrt{3}\frac{l^2}{a}} , \tag{2.17}$$

where

$$\frac{a}{l^2} = \frac{2}{9}\sqrt{3}\ \frac{\rho_f}{\rho_s} . \tag{2.18}$$

2.2.2 Irregular foam model

A completely different approach has been used by Lederman (1971) to compose an open-cell foam model. Irregularities are incorporated in the model using randomly distributed fibres. The slender fibres have an average length $\bar{l} = \left(\sum_{i=1}^{k} l_i \right) / k$, a cross-sectional area a and are connected in 3D to rigid spheres of diameter D_s (N fibres are connected to each sphere). A graphical representation of the model is illustrated in Fig. 2.4a. The main drawbacks of this model are that (i) it does not incorporate the bending of the struts, and (ii) the topological requirements of geometrical connectivity among the edges and vertices

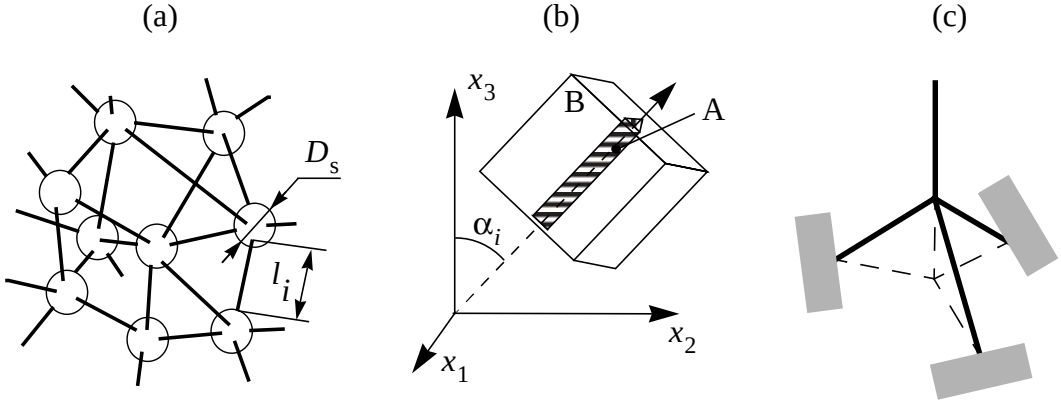

Fig. 2.4. (a) Irregular model of Lederman; (b) Aggregate model of Cunningham; (c) Tetrahedral element of Warren and Kraynik.

of cells are not satisfied, so that the random orientation of the fibres in the model has no physical foundation (violation of Plateau's laws). The concept of cells vanishes and such a structure violates Euler's formula [Eq. (1.1)]. The relative Young's modulus based on Lederman's model is

$$\frac{E_\mathrm{f}}{E_\mathrm{s}} = \frac{1}{5}\left(1-\frac{2}{3}\nu_\mathrm{f}\right)\frac{3\left(D_\mathrm{s}/\bar{l}\right)^2}{1+\left(D_\mathrm{s}/\bar{l}\right)}\frac{na}{\pi {D_\mathrm{s}}^2} \text{ with } \nu_\mathrm{f} = \frac{1}{4}, \tag{2.19}$$

where ν_f is Poisson's ratio of the foam.

2.2.3 Structural volume elements

Aggregate model

A model developed by Cunningham (1981 and 1984) comprises a structural unit consisting of strut "A" surrounded by a low modulus matrix "B", as illustrated in Fig. 2.4b. The effective constants are averaged over all possible orientations α_i of the structural volume element in 3D. For the isotropic structure, the Young's modulus is

$$\frac{E_\mathrm{f}}{E_\mathrm{s}} = \frac{1}{6}\left(\frac{\rho_\mathrm{f}}{\rho_\mathrm{s}}\right). \tag{2.20}$$

This result was explained by the fact that only approximately $1/6$ part of the volume elements are oriented close to the loading direction and are, therefore, effective loaded "structural elements". This clearly points out that this model is based on the axial deformation of struts as the dominant deformation mechanism. Consequently, it is not realistic, because bending is very important.

Tetrahedral element

Another model for predicting the mechanical properties of an open-cell foam is the tetrahedral element of Warren and Kraynik (1988), shown in Fig. 2.4c. It is a logical extension of the 2D structural element, described by Gioumousis (1963), Warren and Kraynik (1987) and later on used by Hall (1993), Papka and Kyriakides (1994). As opposed to the 2D case where the structural element may by assembled into a hexagonal honeycomb, the tetrahedral element cannot be assembled into an ordered network, as proved by Matzke (1946). Because of the limitations of size, only averaged properties can

be considered. The relative Young's modulus for low-density foams based on this model is given by Warren and Kraynik (1994) as

$$\frac{E_f}{E_s} = \frac{33\sqrt{3}}{5}\left(\frac{\rho_f}{\rho_s}\right)^2 \frac{q^2}{a}, \tag{2.21}$$

where q is the radius of gyration of the cross-sectional area a. The factor q^2/a represents the specific shape of the strut cross-section. In the case of a circular cross-section, $q^2/a = 1/(4\pi)$. Substituting this into Eq. (2.21) the relative Young's modulus becomes

$$\frac{E_f}{E_s} \approx 0.91\left(\frac{\rho_f}{\rho_s}\right)^2, \tag{2.22}$$

which is close to the Gibson and Ashby results given in Eq. (2.3).

A specific strut cross-section parameter q^2/a and the corresponding relative Young's moduli have also been determined for the triangular and Plateau-Gibbs cross-sections (for details see Fig. 2.11), as follows:

triangular: $q^2/a = 1/(6\sqrt{3})$ and

$$\frac{E_f}{E_s} = 1.10\left(\frac{\rho_f}{\rho_s}\right)^2; \tag{2.23}$$

Plateau-Gibbs: $q^2/a = (20\sqrt{3} - 11\pi)/6(2\sqrt{3} - \pi)^2$ and

$$\frac{E_f}{E_s} \approx 1.53\left(\frac{\rho_f}{\rho_s}\right)^2. \tag{2.24}$$

This model, as well as each of the regular unit cells from Fig. 2.2, contains a high degree of periodicity, because the size of these unit cells is of the order of the average strut length. However, it can be expected and will be demonstrated in other parts of this thesis that randomness in the microstructure of a foam exerts a significant influence on the mechanical properties.

2.3 Present modelling

2.3.1 Introduction of irregularities in the model

To approach a real foam, a model should satisfy Plateau's laws (see Section 1), yielding from the thermodynamical equilibrium of the growing foam structure.

A tetrakaidecahedron has been assumed to be the most suitable of the space-filling polyhedra for these conditions. Only the last criterion is somewhat violated: the mean angle between edges is equal to $110°$ with two peaks at $120°$ and $90°$. This geometrical violation may have an effect on the mechanical properties of the model.

The existing regular models can be improved by increasing the number of the enclosed cells, i.e., model dimensions, and by developing of a non-regular model. An effort has been done by Valuyskikh (1990) to randomize a regular model through the stochastic deviation of nodes of the tetrakaidecahedra. Because of the unnatural way of introducing randomness (a random structure is built on the initially regular structure), the resulting structure misses very important geometrical features of the real foam, e.g., the faces of cells become nonplanar and the closed-cell model is not valid anymore. It must be concluded that the model is hardly representative for real random foams.

Voronoi tessellation

To improve the prediction of the relative Young's modulus, a unit cell will be introduced with dimensions being about one order of magnitude larger then the average strut length, so that the geometrical disorder can be incorporated. As an improvement of the model of Gent and Thomas (1963) and of Valuyskikh (1990), the modelled foam structure corresponds better to the real foam microstructure. This is accomplished by taking the 3D foam microstructures in the unit cell from Voronoi tessellation of space described by Voronoi (1908). Weaire and Fortes (1994) pointed out that the structural randomness is important for the mechanical properties of the model. They also noted, that, as opposed to the 2D case, the 3D Voronoi model has not been explored yet. In the Voronoi tessellation, the final geometry is based on the distribution of nuclei (centres of the foam cells). This procedure resembles the physical process of nucleation and growth of gas bubbles in a liquid during cell formation. A created Voronoi geometry is topologically very similar to the geometrical structures resulting from the growth process according to the following assumptions, given by Boots (1982):

- all nuclei appear simultaneously,

Table 2.1. Geometrical features of various cells [from Kumar and Kurtz (1994)]

Structure	Mean number of struts in a face $\bar{N}$	Mean number of faces in a cell $\bar{F}$	Mean number of vertices in a cell $\bar{V}$
Tetrakaidecahedron	5.143	14	24
Rhombic dodecahedron	4	12	14
Cubic prism	4	6	8
Voronoi cell	5.228	15.536	27.086
Foamlike structures	~ 5.1	~ 14	~ 23

- all nuclei remain fixed in location throughout the growth process,
- at each nucleus, the growth of the foam cell proceeds at the same rate in all directions (i.e., isotropic growth),
- the growth rate is the same for each cell associated with a nucleus, and
- growth of a cell ceases whenever and wherever the cell comes into contact with a neighbouring cell.

The Voronoi tessellation, constructed in this way out of a distribution of nuclei randomly oriented in 3D, divides the space into an array of cells (or polygons) having planar faces. Furthermore, three cells meet at each edge and one vertex belongs to four cells (connects four edges). The geometry of a Voronoi cell agrees quite good to measured values, as shown in Table 2.1. Not only connectivity, but also angle requirements are approached. It was shown by Kumar and Kurtz (1994) that the mean dihedral angle and the mean bond angle of a Voronoi cell are $120°$ and $111.11°$ respectively.

The initial spatial distribution of nuclei completely determines the final geometrical structure of the Voronoi tessellation. This method is applied to construct the microstructure of the foam model, where the nuclei resemble the starting points of growing bubbles, and the subsequent Voronoi tessellation is considered to represent the foam geometry. Because only open-cell foams are analysed here, cell faces are neglected, and the cell edges are considered to be slender struts.

These struts fill a cubic unit cell with edges of length L_{uc}. The foam is constructed with this unit cell, in such a way that each face of the unit cell is a plane of local symmetry in the foam. Due to the symmetry, the unit cell faces may be considered to remain shear stress free and stay flat during deformation in the x_1, x_2, x_3-directions. Thus, the global principal stresses Σ_1, Σ_2, Σ_3 in the x_1, x_2, x_3-directions are imposed by prescribing uniform displacements on the faces of the unit cell (see Fig. 2.5).

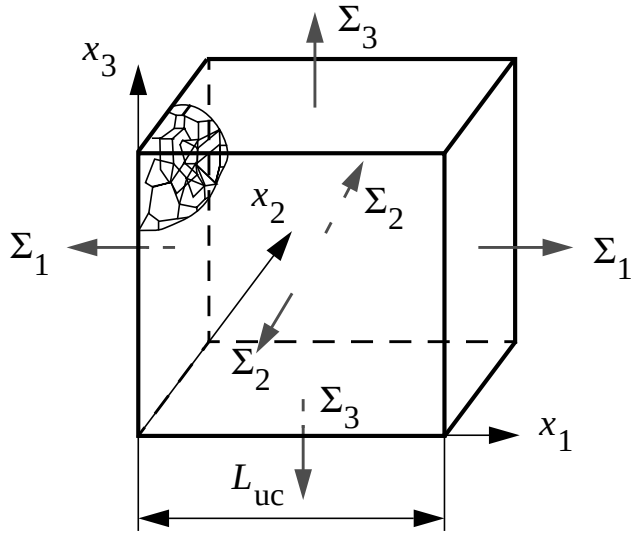

Fig. 2.5. The cubic unit cell, with the edge length L_{uc}, subjected to global principal stress Σ_i.

To construct some regular Voronoi geometries, regular packings of nuclei and corresponding small unit cells are often used [see, for example, Fedorov (1971) or Vainshtein *et al.* (1995)]. The three most appropriate regular nuclei distributions are (i) the bcc distribution, (ii) the fcc distribution, and (iii) the hex distribution. Figures 2.6a-c show the initial positioning of the nuclei before the application of the Voronoi tessellation, and Figs. 2.6d-f demonstrate the growth of the foam cells at a certain moment. Single cells of the resulting Voronoi tessellations are depicted in Figs. 2.2b-d respectively. Note that only the edges are depicted as the representation of the struts in open-cell foams. The bcc distribution of nuclei yields tetrakaidecahedron cells (truncated octahedra) as shown in Fig. 2.6g, the fcc distribution agrees with a 3D closest packing of spheres, the centres of which are the nuclei, and forms rhombic dodecahedron cells (see Fig. 2.6h), and the hexagonal variant of a closest spheres packing yields rhombic–trapezoidal dodecahedra as shown in Fig. 2.6i.

As it was noted above, the bcc and fcc nuclei distributions have a cubic symmetry. Consequently, the mechanical properties of the subsequent cell structures, the tetrakaidecahedron and rhombic dodecahedron, are equal in the three principal directions. This is in contrast to the structure obtained from the hex nuclei distribution, where the subsequent structure will be very stiff in one direction due to the alignment of struts in that direction. Real geometrically isotropic foams exhibit isotropic mechanical properties. The strong anisotropy of the foam model derived from the hexagonal closest packing is the reason that this model will not be considered further.

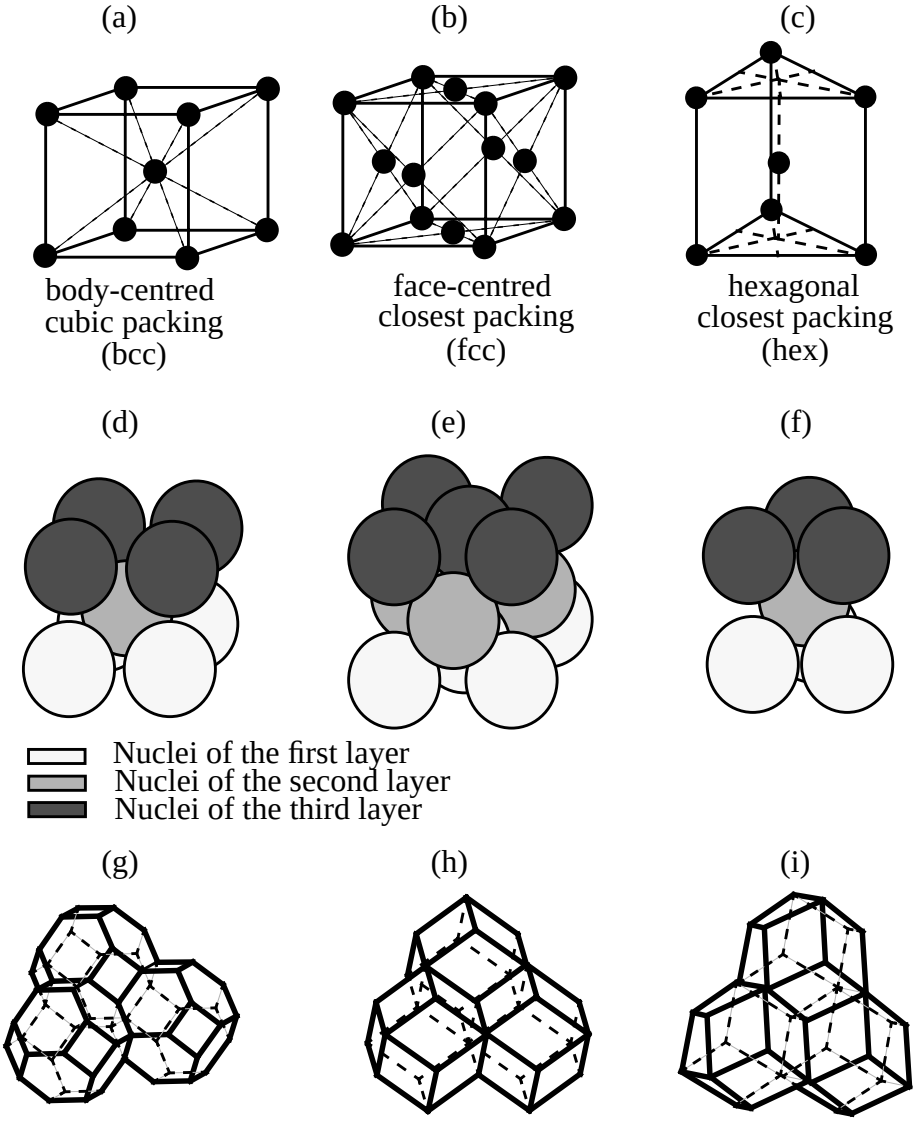

Fig. 2.6. Some nuclei distributions and their subsequent Voronoi cells; (a, d, g) body-centred cubic nuclei distribution leads to formation of a regular tetrakaidecahedron cell; (b, e, h) cubic closest (or faced-centred cubic) packing results in a rhombic dodecahedron cell; (c, f, i) hexagonal closest packing after application of the Voronoi tessellation yields a rhombic-trapezoidal dodecahedron cell. The first two cells, (g) and (h), have orthogonal symmetries.

Unit cell construction

To construct the irregular foam geometry of a large unit cell, the following steps are taken. First, a virtual cube having an edge length b_f or b_b, with nuclei according to the fcc or bcc distribution respectively, is placed periodically inside a large cubic box with edge

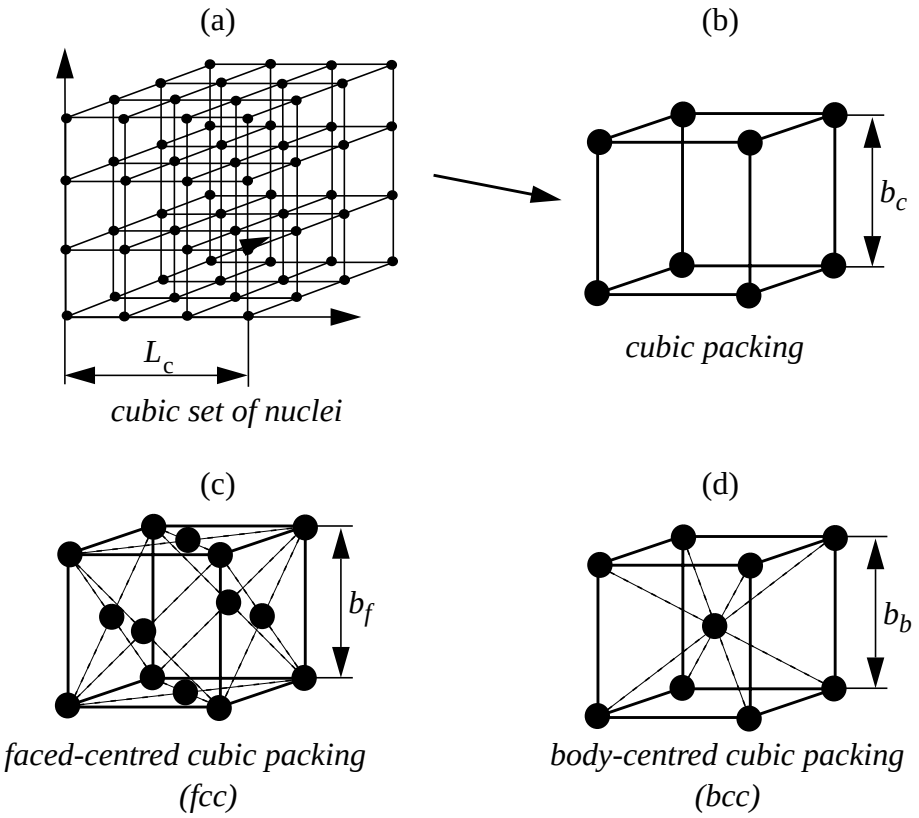

Fig. 2.7. Constructing of lattice of nuclei (a) by stacking cubic packings (b). The cubic packings consists of regular fcc (c) or bcc (d) packings.

length L_c, ($L_c > L_{uc}$), as displayed in Fig. 2.7. In this way, a large cubic box is obtained, containing a lattice of nuclei, arranged according to a bcc or an fcc distribution. The chosen virtual cube edge length (b_f or b_b) is different for the fcc and bcc packings, in order to keep the volumetric density of the nuclei equal for these two packings. Therefore, the cubic, bcc and fcc virtual cube edges lengths relate to each other as $b_c \div b_f \div b_b = 1 \div \sqrt[3]{4} \div \sqrt[3]{2}$. To introduce irregularity in the geometry of the final foam, the positions of nuclei are varied at random by giving a random orientation of the vector ii' (see Fig. 2.8a) of nucleus i and a certain deviation of the vector length. Thus, the nucleus is moved from its position in point i over a distance δ^i to a new position i', as shown in Fig. 2.8a. The deviation δ^i is taken from a uniform statistical distribution $[0,\delta_{max}]$. In this way nucleus i has its new position i' inside a sphere with a diameter of $2\delta_{max}$. An example of the deviations distribution is given in Fig. 2.8b. The deviation δ^i is related to the virtual cube edge length b between nuclei in a packing. The value of b is dependent on the kind of packing and is equal to b_c, b_f and b_b for the cubic, fcc and bcc lattices correspondingly. The normalized maximum deviation δ_{max}/b is a convenient measure of the geometric disorder.

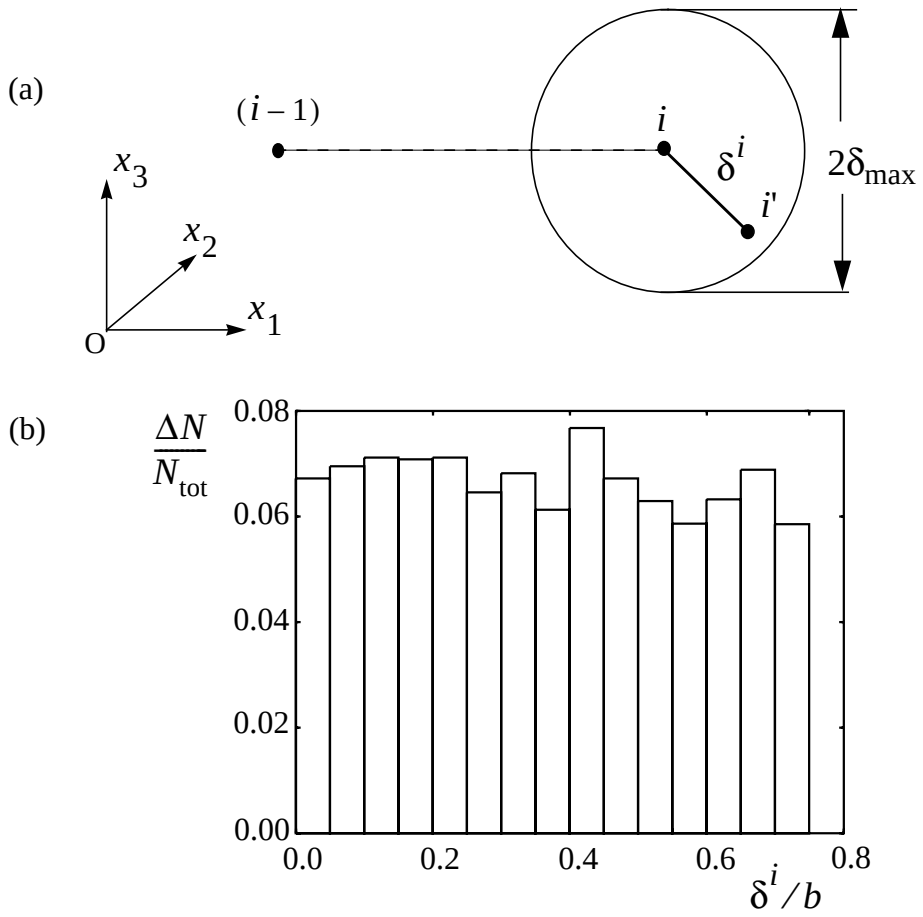

Fig. 2.8. (a) Disorder is created in the Voronoi geometry by imposing an arbitrary deviation of the nuclei positions. As an example, the regular nucleus position, point i, gets a deviation δ^i to its new random position, point i'. (b) Example of a histogram of the nuclei deviation δ^i/b of the bcc-based structure with the normalized maximum deviation $\delta_{max}/b = 0.75$. The step width of the δ^i/b ratio is 0.05.

Based on this random nuclei distribution, the foam microstructure is obtained using the Voronoi procedure. The Voronoi-software of Van de Weygaert (1991) has been adopted to generate the foam structure. In the final Voronoi tessellation, the foam cells at the boundaries may have shapes that are not suitable for the unit cell microstructure, as can be seen in the 2D analogue in Fig. 2.9. To avoid these boundary irregularities, the cubic unit cell with length L_{uc} is cut out of the cube with edge length L_c $(L_{uc} < L_c)$. In case of the bcc distributed nuclei, the cube edge length is $L_c = 8b$ and the unit cell edge length is $L_{uc} = 6b$, whereas for the fcc distributed nuclei, $L_c = 7b$ and $L_{uc} = 5b$. Due to the difference in b_f and b_b, the resulting unit cells contain approximately equal numbers of foam cells.

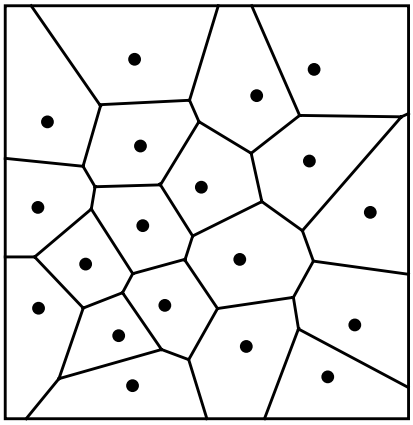

Fig. 2.9. 2D Voronoi representation. Voronoi boundaries are unwanted in the foam model, and will therefore be cut off.

In addition to the above nuclei distribution considerations, some microstructures are also based on completely random distributions of nuclei. These random nuclei distributions result in an irregular geometry of the foam model. The random nuclei are placed in a box with edge length L_c under the condition that the neighbouring nuclei are not closer than a distance d. The usage of d is necessary to obtain rather uniformly distributed cells. A random point process attempts to generate 10,000 times nuclei positions in the cube, with each coordinate taken from a uniform distribution $[0,L_c]$. If the generated nucleus is too close to its neighbours, the new nucleus is not placed. Choosing $d = L_c/16$, the final number of nuclei turns out to be always close to 800. With this random nuclei distribution, an additional Voronoi tessellation was created, and the cubic unit cell was cut out with edge length $L_{uc} = (3/4)\,L_c$.

The presumed symmetry of the unit cell requires that the struts crossing the unit cell face must be perpendicular to this face. Therefore all struts that cross the unit cell boundaries while cutting out of the unit cell cube, are rearranged to satisfy the symmetry conditions. This procedure is schematically depicted in Fig. 2.10a. The final structure comprises a framework of struts, as shown in Fig. 2.10b.

2.3.2 Linear elastic behaviour

All struts in the open-cell foam model are represented mechanically by beams that are rigidly connected in vertices. In real foams, struts have cross-sections in the form of Plateau-Gibbs borders, as shown in Fig. 2.11a, and have a variable cross-sectional area along their length. This occurs as a result of the growing process of bubbles, which is ruled by

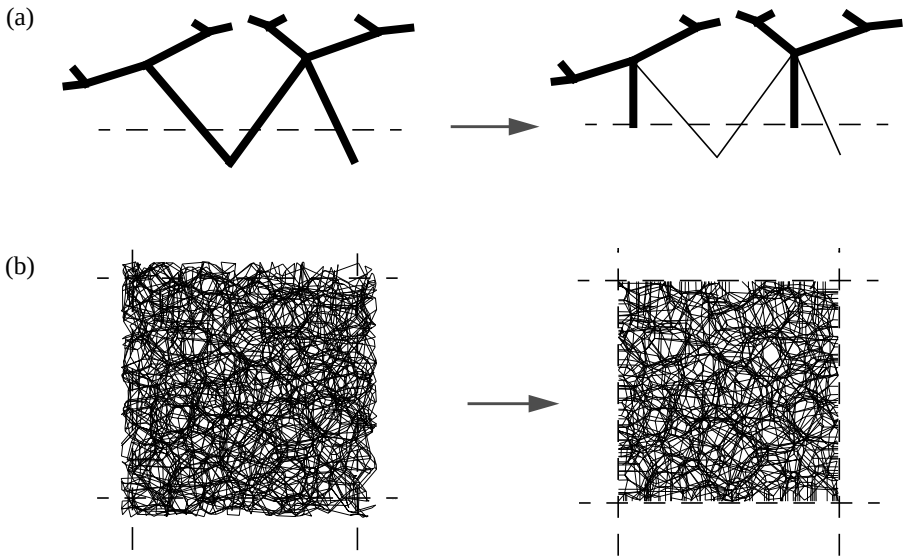

Fig. 2.10. (a) Rearrangement of struts passing the unit cell boundaries. (b) Example of a final microstructure inside the unit cell (projection of the 3D structure on a plane).

the effect of the surface area minimization. Hence edges appear with a cross-section in the shape of the Plateau-Gibbs borders, described, e.g., by Chan and Nakamura (1969) and Kann (1989). A typical strut cross-section, shown in Fig. 2.11a, changes its value along the strut from the thick vertices to the thin middle of the strut, while the shape remains quite similar. Figure 2.11b specifies the geometrical features of the strut. For the simplification of the model the following assumption is made: $r_1 = r_2 = \infty$. This leads to

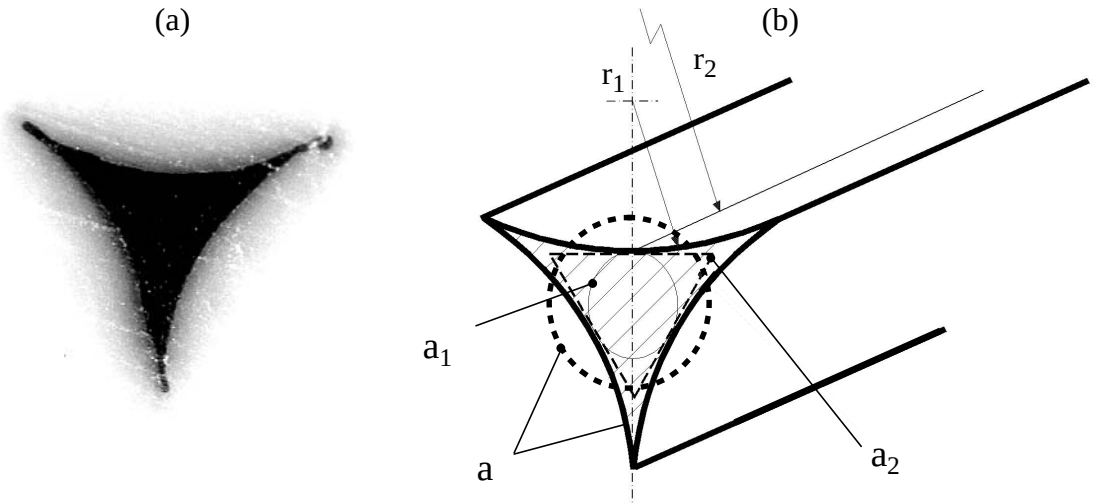

Fig. 2.11. Strut cross-section. (a) Open-cell PUR foam micrograph (only the completely black area is the strut cross-section). (b) Possible strut cross-section simplifications.

straight struts with the constant triangle cross-section, a_2, which is smaller than the original one. In a 2D simulation, Gioumousis (1963) demonstrated that struts in open-cell foams with densities below a critical relative foam density ρ_f/ρ_s get a middle part with a constant thickness. A further decrease of relative density causes an enlargement of such a region. The critical relative density was found to be equal to 0.0931. It was concluded that the critical density for the 3D case must be greater than that value. In this thesis only low-density open-cell foams with a relative density ρ_f/ρ_s less then 0.075 are considered. Consequently, the assumption that struts have a constant cross-sectional area along their length is allowable. The additional simplification of the cross-section to the circle, a_1, introduces greater error. Warren and Kraynik (1997) evaluated the ratio between the second moments of inertia of the circular, I_O, square, $I_\square$, equilateral triangular, I_Δ, and Plateau-Gibbs border, I_P, having equal cross-sectional areas as

$$I_O \div I_\square \div I_\Delta \div I_P = 1 \div 1.047 \div 1.209 \div 1.681 . \tag{2.25}$$

All struts in the thesis are assumed to have the same and constant circular cross-section with area a. Since the geometry of the foam model is determined in the above described procedure, the cross-section area a determines the relative density of the foam ρ_f/ρ_s:

$$\frac{\rho_f}{\rho_s} = \frac{\sum_{i=1}^{N} l^i a}{L_{uc}^3}, \tag{2.26}$$

where N is the number of struts in the unit cell.

By taking the circular cross-section, the moment of inertia of the strut is underestimated as compared to a real foam (for the same relative foam density ρ_f/ρ_s). This leads also to a certain systematic error in the mechanical properties of the model [see Eq. (2.22), Eq. (2.23) and Eq. (2.24)].

Each unit cell is uniquely determined by its initial nuclei distribution and relative foam density ρ_f/ρ_s. Then the initial linear elastic properties, like the relative Young's moduli, $E_{i,f}/E_s$, and the Poisson's ratios, $\nu_{ij,f}$, are defined. These properties of the unit cells are analysed by FE element techniques. Each strut is modelled as a beam element with a constant circular cross-section area a and of length l^i.

Geometries of the model microstructure can be divided into three types: (i) completely regular geometries based on the regular fcc and bcc nuclei distributions, (ii) completely random geometries based on random nuclei distributions and (iii) geometries,

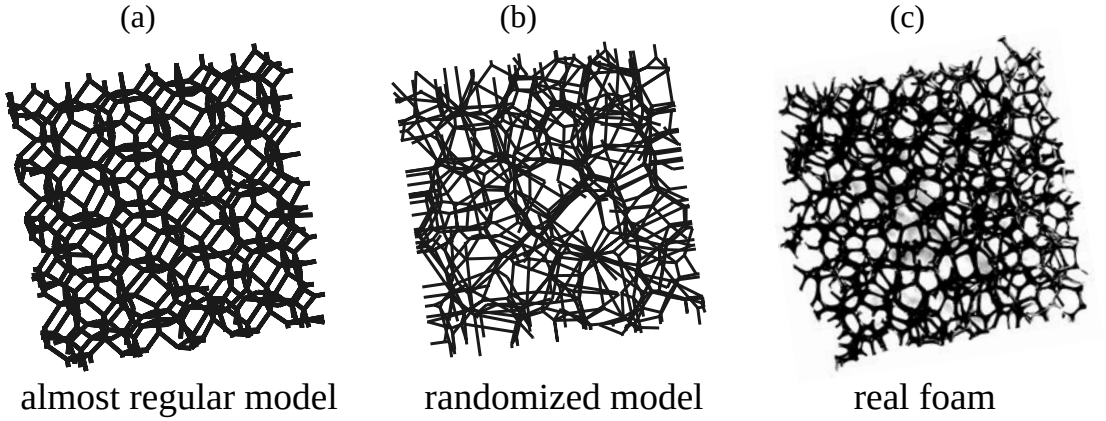

Fig. 2.12. Geometry of the foam models, based on the bcc nuclei distribution with (a) 15% and (b) 75% disorder. (c) A view of a real foam.

where nuclei of the regular distributions have a random offset δ^i. By increasing the range of the possible random offset δ^i/b, a transition can be made from the completely regular geometries to the completely random geometries. The directionality of the deviation was random while the deviation δ^i of the nuclei with respect to the regular fcc or bcc positions was taken from a uniform distribution $[0,\delta_{max}]$, where the following disorder factors have been taken: δ_{max}/b = 15%, 30%, 45%, 60% and 75%. Figure 2.12a shows an example of a microstructure based on the bcc distribution with a disorder factor δ_{max}/b = 15%. The typical features of the tetrakaidecahedra can still be recognized in the geometry. If the disorder factor δ_{max}/b exceeds 34.4% for bcc and 22.3% for fcc, the spheres with possible new positions of a nucleus (see Fig. 2.8a) start to overlap, with the result that the original bcc or fcc distribution cannot be distinguished any more. When δ_{max}/b = 75% the nuclei distribution is assumed to be completely random due to the overlapping of the relatively large spheres for the new nucleus position, resulting in a completely random unit cell geometry, which can be seen in Fig. 2.12b. A photograph of a real foam is displayed in Fig. 2.12c.

To compare the geometries of different unit cells, histograms of strut lengths and orientations of the strut with respect to a unit cell boundary normal are drawn. In the case of completely regular bcc and fcc nuclei distributions, both histograms of strut lengths of the final geometries have the same trivial shapes, namely one peak at the initial mean strut length $\bar{l}_I$. The histogram of the strut orientation for the fcc-based geometry has one peak at $\arcsin(\sqrt{2/3}) \approx 54.74°$, and for the bcc-based geometry two peaks at 45° and 90° (see Figs. 2.6h and g respectively).

If the disorder factor δ_{max}/b is relatively small, e.g., 15%, the strut lengths histogram shows one narrow peak for the bcc-based structure in Fig. 2.13a, and two peaks in the his-

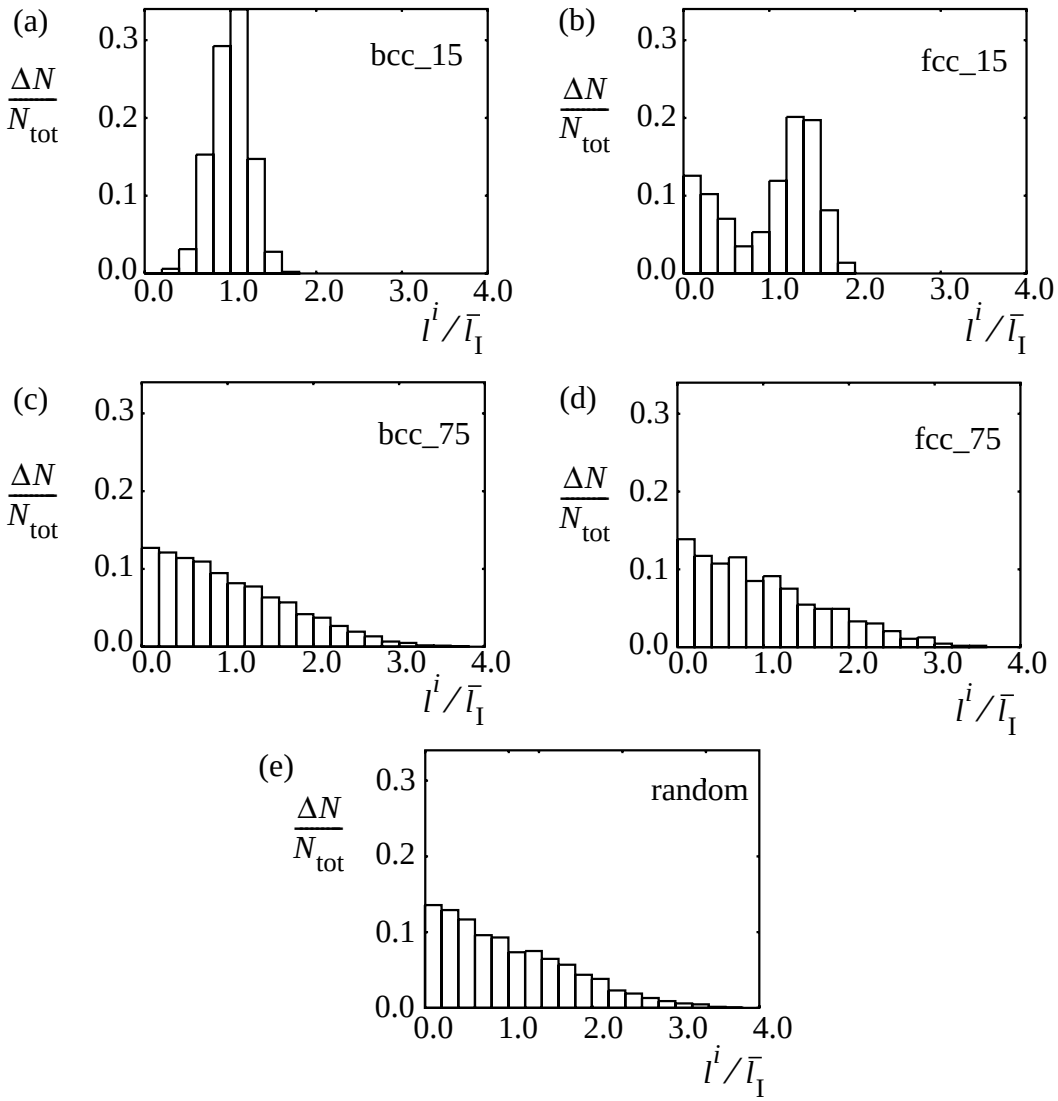

Fig. 2.13. Histogram of the strut lengths of bcc- and fcc-based models with low and high disorder and of the random model. The step width of the relative length is 0.2.

togram for the fcc-based foam model, as can be seen in Fig. 2.13b demonstrating an arbitrary implementation. The extra peak of very short struts in the fcc-based foam geometry stems from the drastic changes in the strut connectivity, e.g., the number of struts meeting at a vertex. It was equal to eight for the ideal regular structure (no disorder), but which becomes four when disorder is introduced. The same phenomenon can be observed in the struts orientation histogram, which identically to the regular model has two peaks in the bcc-based structure, as it is shown in Fig. 2.14a. Figure 2.14b demonstrates an occurrence of two additional peaks at 0° and 90° in the fcc-based unit cell. Note that this abrupt change in connectivity does not occur in the bcc-based structure, as strut connectivity is

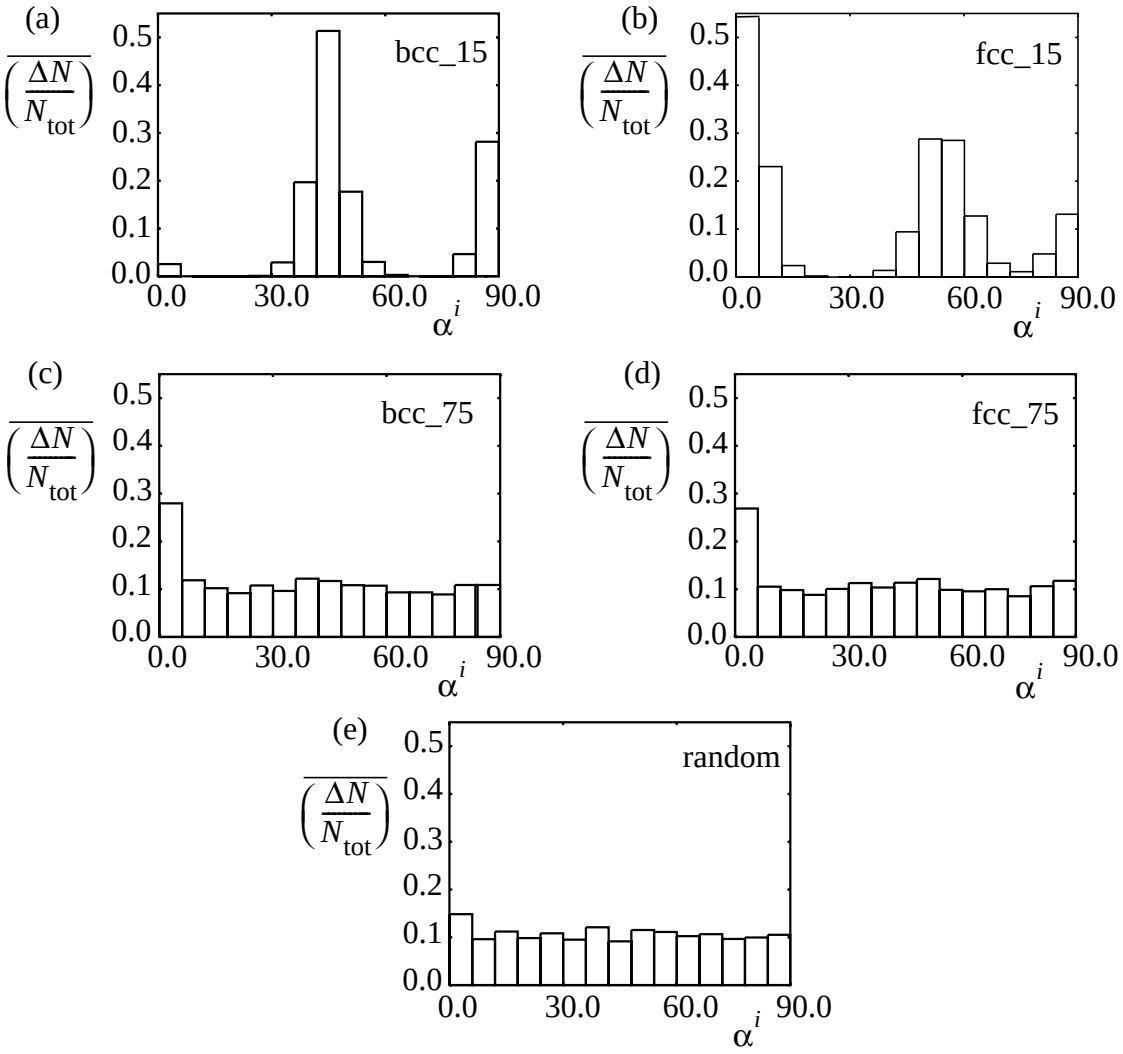

Fig. 2.14. Histogram of angles between struts and x_1-direction, in degrees. The step width of the angle orientation is $6°$. The number of struts $\Delta N/N_{\text{tot}}$ is normalized by a surface factor to obtain a uniform distribution of orientation vectors on the unit sphere. The normalized number of struts is defined as $\overline{(N/N_{\text{tot}})}$. This implies a normalizing factor $1/\sin\alpha$ as a function of the polar angle α under the assumption of rotational symmetry with respect to x_1-direction.

already four in that regular model.

As mentioned above, the nuclei distribution can be assumed to be completely random, when the disorder factor is increased above 75%. Indeed, histograms of strut lengths and orientations from Figs. 2.13c-d and Figs. 2.14c-d are close to the distribution of the completely random geometry from Fig. 2.13e and Fig. 2.14e. The relatively high number of struts with the angle orientation close to $0°$ is explained by the high sensitivity of the his-

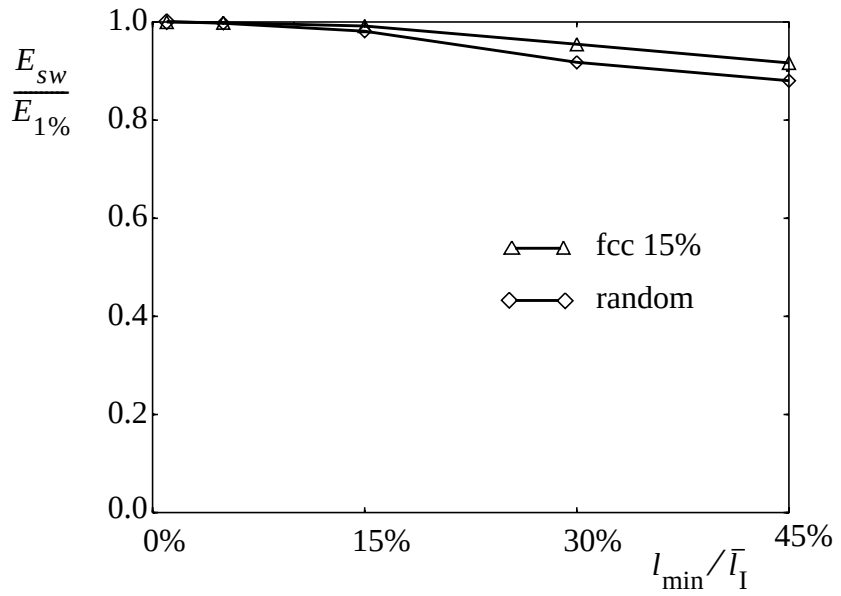

Fig. 2.15. Young's modulus of geometry with a sweep factor of 1% compared to Young's moduli using larger sweep ratios.

togram to that region in connection with the normalisation by $1/\sin\alpha$.

To determine the overall Young's modulus and Poisson's ratio, a uniaxial stress with magnitude Σ is applied. Since all disordered microstructures are geometrically isotropic, the three principal unit cell directions are assumed to be interchangeable concerning the elastic properties. Therefore, the elasticity parameters have been analysed in all three directions. The value $\rho_f/\rho_s = 0.025$ has been taken as the relative foam density.

To reduce the computation time, all short struts occurred in the model are to be eliminated. This procedure is called the "sweep mechanism". First, the influence of the sweep mechanism on the mechanical properties of the unit cell has to be studied. The parameter that governs the sweep process, i.e., the smallest allowable strut length relative to the initial average strut length, $l_{\min}/\bar{l}_{\mathrm{I}}$, has to be determined for further calculations. The influence of the sweep ratio on the mechanical properties has been analysed for the fcc structure with a disorder factor $\delta_{\max}/b_f = 15\%$ and for a completely random geometry. The sweep parameter $l_{\min}/\bar{l}_{\mathrm{I}}$ has been varied from 1% to 45% and the results are shown in Fig. 2.15. The accuracy is expressed in the ratio $E_{sw}/E_{1\%}$, where E_{sw} and $E_{1\%}$ are Young's moduli of the unit cells after sweeping with sweep ratio *sw*% and 1%, respectively. As expected, a slight sweep of the fcc-based structure with a small disorder factor leads to the elimination of the short struts without significantly affecting the mechanical properties of the whole structure. For a sweep ratio of 15%, the error in Young's modulus was about 1%, while the computing time was reduced by 50% for the fcc-based geometry.

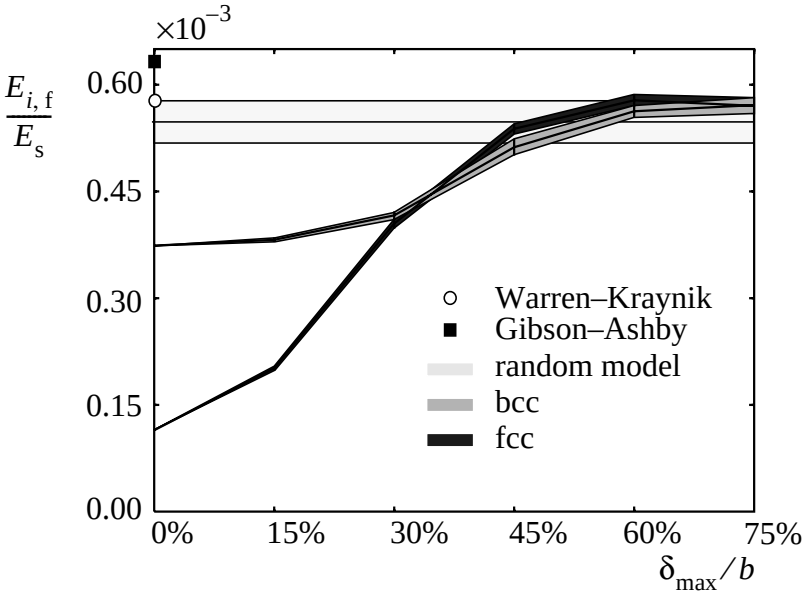

Fig. 2.16. The influence of disorder, expressed in $\delta_{\max}/b$, on Young's modulus of the unit cell. The band width of the unit cell results is four times the standard deviation.

For the random geometry, the sweep introduced a somewhat larger error while the computational profit was somewhat less. Based on Fig. 2.15, a sweep ratio of 15% was chosen.

Applying this sweep factor for all other unit cell geometries, the elastic properties could be determined numerically. The moduli have been determined for five geometries according to each disorder factor (for the bcc and fcc-based structures) as well as for the random model. This was done in all three directions per unit cell geometry. Consequently, 15 values were obtained for each situation. The average (of 15) results of the analyses, i.e., relative Young's modulus $E_{i,\mathrm{f}}/E_{\mathrm{s}}$ versus disorder factor, are plotted in Fig. 2.16.

The computation of linear elastic responses has been started from the regular structures based on tetrakaidecahedron and rhombic dodecahedron (bcc and fcc nuclei packings). Also the predictions of the small unit cells of Gibson and Ashby (1988) and of Warren and Kraynik (1994), calculated from Eq. (2.3) and Eq. (2.22), have been drawn in Fig. 2.16. The rhombic-trapezoidal dodecahedron yields $E_{\mathrm{f}}/E_{\mathrm{s}} \approx 4.2 \times 10^{-3}$ [from Eq. (2.14)] and the relative Young's modulus for the model of Lederman (1971) is $E_{\mathrm{f}}/E_{\mathrm{s}} \approx 14 \times 10^{-3}$ [from Eq. (2.19)], which are very high and far outside the range in Fig. 2.16. It is remarkable that the two predicted Young's moduli based on a regular small unit cell are relatively close to each other. This can be explained by the fact that in both models bending as well as axial deformations of the struts are considered. In the model of Lederman, bending of struts was excluded, thus making the foam model unrealistically stiff.

Struts, oriented in the direction of the global stress and penetrating the entire unit cell, increase the stiffness of the rhombic-trapezoidal dodecahedron. In the model based on the regular fcc distribution, all struts are oriented at an angle α of $45°$ to the principal global stress, so deformation takes place predominantly by bending, making the model too flexible.

The influence of disorder on the initial linear elastic mechanical behaviour can be seen in Fig. 2.16. An increase in the disorder of the geometry causes a rapid rise of the mechanical elastic constants. At a disorder factor of approximately 30%, the elastic coefficients of the fcc- and bcc-based geometries start to coincide. At 50% they are about equal to the moduli of the random model. Further randomization of the framework has almost no influence on the linear elastic properties of models; the geometry becomes sufficiently stochastic to erase the difference between the various models.

To trace the reasons for the increased stiffness of the random unit cells in comparison with the regular structures, the normal stresses σ_n^i and the maximum bending stress σ_b^i in each strut during the application of a uniaxial global stress Σ have been determined. Figures 2.17a and b demonstrate the histograms of maximum bending and normal stresses. Bending stresses in the bcc-based structure with a small disorder factor have two peaks, as illustrated in Fig. 2.17a. This can be explained by the fact that one group of struts is almost perpendicular to the global stress, while the other struts are at an approximately $45°$ angle to global stress direction (see Figs. 2.6g). In the case of the fcc-based structure with the same disorder factor, the bending stress distribution has only one peak, since nearly all struts are oriented at an angle of approximately $54°$ to each principal direction (see Figs. 2.6h). The average bending stress is seen to decrease for an increasingly random structure. At the same time, the normal stress distribution becomes wider (see Fig. 2.17b). Normal stresses then play a more considerable role in the stiffness of the foam model. Note that a global uniaxial tension results in compressive stresses in some struts, as can be seen in the left-hand part of the Fig. 2.17b. Figure 2.17c shows the maximum shear stress, τ^i, due to torsion of the struts, and it is seen that the stresses by torsion are negligible compared to normal or bending stresses in Figs. 2.17a and b. This indicates that torsion is of minor importance.

To understand the reasons for stiffness rising as disorder is increased, the distribution of the most highly loaded struts has been examined by visualizing the stress distribution over the geometry. It was found that in frameworks based on bcc and fcc nuclei distributions with small disorder, both the normal and the bending stresses are relatively uniformly distributed over the volume of the unit cell. Bending is the determining factor for the stiffness of the unit cell. The ratio of the maximum bending stress to the maximum

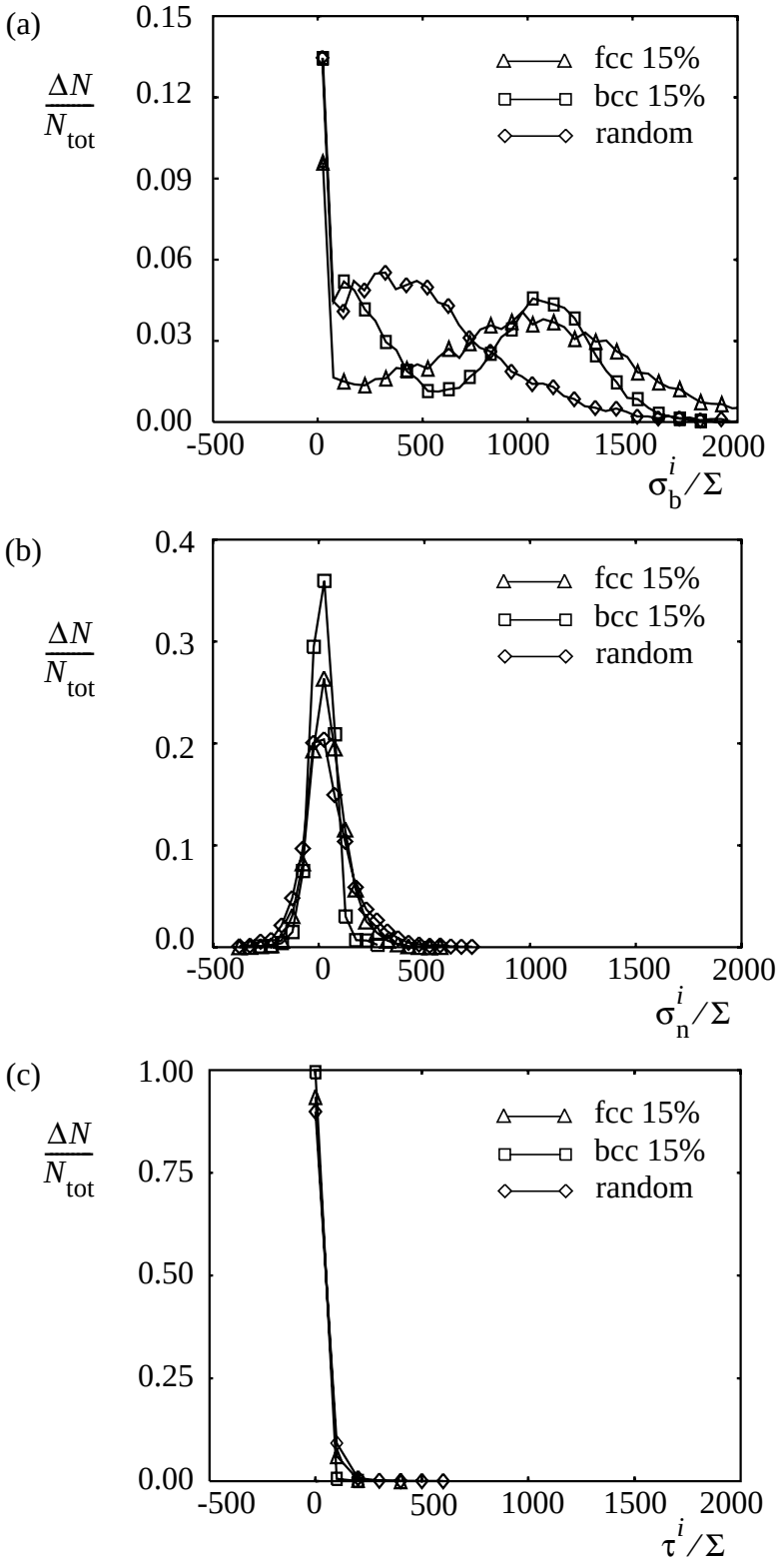

Fig. 2.17. Histogram of the (a) bending stresses, (b) normal stresses and (c) shear stresses due to torsion in struts of the unit cell. The interval of the relative bending stress is $\Delta\sigma_b^i/\Sigma = 50$, of the relative normal stress is $\Delta\sigma_n^i/\Sigma = 50$ and of the relative shear stress is $\Delta\tau^i/\Sigma = 100$.

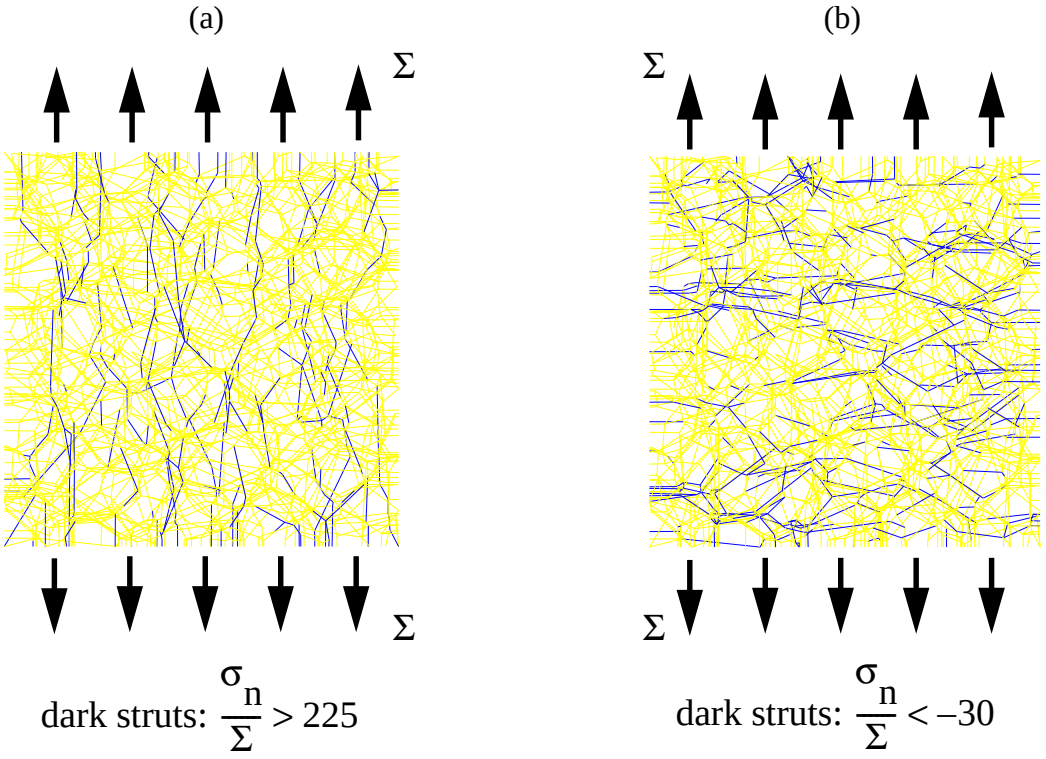

Fig. 2.18. (a) Distribution in the random unit cell of struts with a relatively high normal tensile stress. (b) Distribution of struts under compression.

normal stress, $\sigma_{b,max}/\sigma_{n,max}$, is around 6.5 for the bcc- and 5.7 for the fcc-based structures with 15% disorder factor. This ratio becomes 3.5 in the random model. This indicates that normal stresses are becoming more dominant for the linear elastic properties of the random model.

Figure 2.18a demonstrates the distribution of struts with normal stresses $\sigma_n/\Sigma > 225$ for the random foam geometry. The global uniaxial stress Σ appears to be transmitted from one cell face to the other by percolating chains of struts with high normal stresses. This implies that the presence of such chains oriented in the direction of the maximum global principal stress reinforces the foam. On the other hand, as a result of the global tensile stress, in combination with random geometry, some struts are under compression, as shown in Fig. 2.18b. The orientation of these struts is commonly in a plane about perpendicular to the direction of the global maximum principal stress. Again, chains of struts loaded in compression are observed. These chains percolate almost the whole unit cell. The presence of compressed struts points to the possibility of local buckling of struts, but this is not investigated further here.

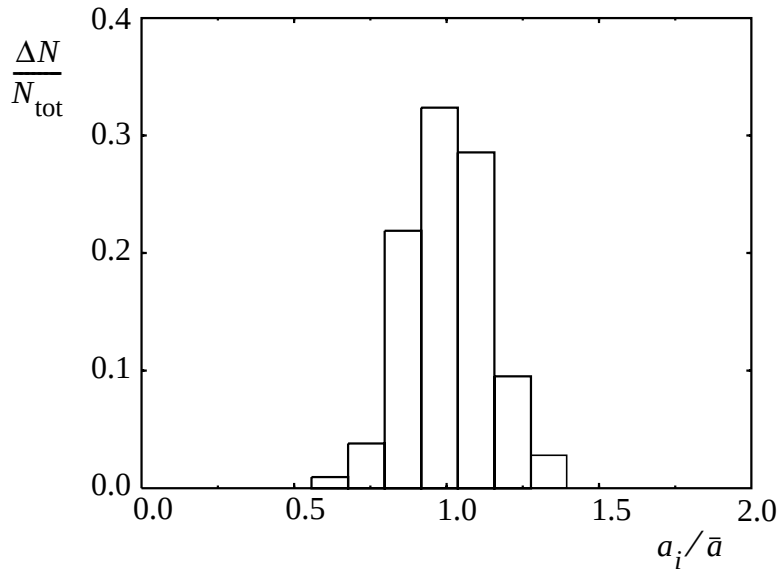

Fig. 2.19. Histogram of the measured strut cross-sectional areas a in the open-cell foam. The step width of the relative cross-sectional area is 0.12.

Influence of the variable strut cross-section on the random model stiffness

One of the most important simplifications, admitted in the random model described above, is the constant cross-section of struts throughout the model. The stochastic distribution of the strut cross-section might have a substantial influence on the mechanical properties of the open-cell foam model. To check this, the random model has been refined through the introduction of the struts having a varying diameter. For this purpose, a real open-cell foam has been analysed to establish the strut cross-section distribution. The result of this analysis is shown in Fig. 2.19. The measured coefficient of variation (standard deviation divided by mean value) is 0.2. The same form of the strut cross-section distribution has been applied to the random open-cell foam model six times in such a way, that the relative density ρ_f/ρ_s remained unchanged and equal to 0.025. The 95% confidence interval of the relative Young's modulus $(E_f/E_s)_{\text{var.}a}$ was found to be $(64 \pm 1) \times 10^{-3}$, which coincides with the result obtained from a geometrically identical model with the constant strut cross-section, $(E_f/E_s)_{\text{const.}a} = 64.2 \times 10^{-3}$. Obviously, a varying strut cross-section does not affect the open-cell foam stiffness. Therefore, a constant cross-section area a is adopted for further modelling.

The effect of the relative foam density on the mechanical properties

To investigate the dependence of mechanical properties on density, one unit cell with random geometry has been analysed with density ratios ρ_f/ρ_s varied from 0.0167 to 0.0542 (this corresponds to the range of the low-density foam classification, given, for example, by Cunningham and Hilyard (1994) as $\rho_f/\rho_s < 0.1$). The numerical results are displayed in Fig. 2.20. In other models, e.g., those of Warren and Kraynik and of Gibson and Ashby, the linear elastic response of open-cell foams is described by a linear function of the square relative density, as in Eq. (2.22) and Eq. (2.3).

The square dependence on the relative density points to bending as the dominant deformation of the struts. When density is low, the FE results of the large random unit cell model showed quite good agreement with the estimates of Warren and Kraynik (1994) and Gibson and Ashby (1988). However, with increasing density, the elastic modulus of the present model deviates from the linear function of the squared relative density, as can be seen in Fig. 2.20. In the more general formula

$$\frac{E_f}{E_s} = C_1\left(\frac{\rho_f}{\rho_s}\right)^p, \tag{2.27}$$

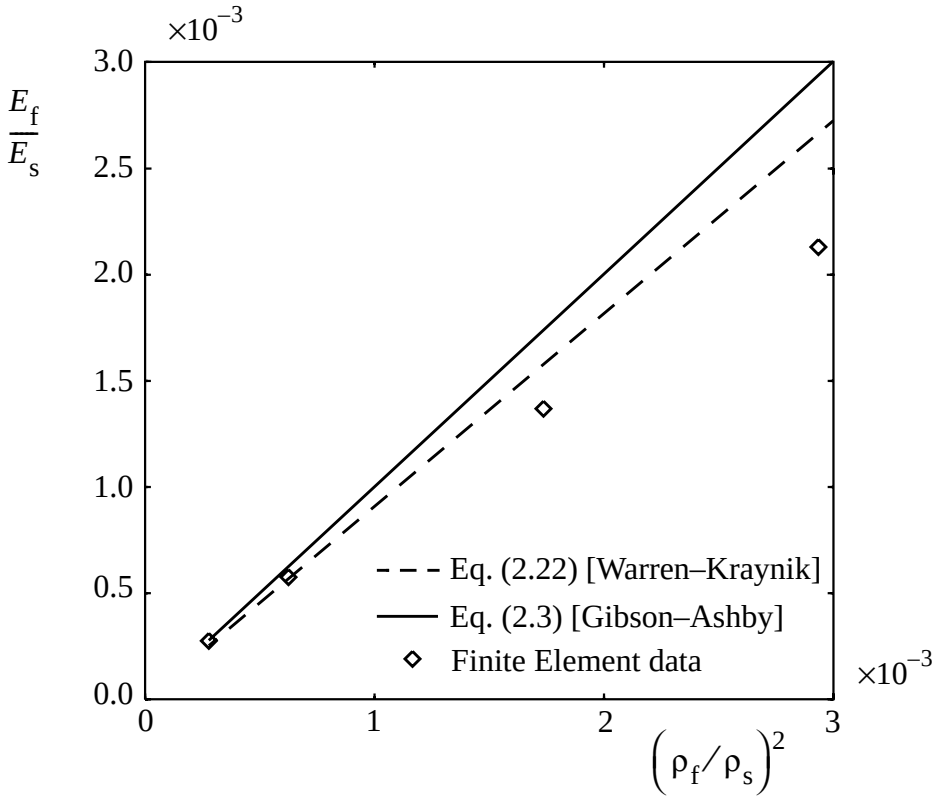

Fig. 2.20. Relative Young's modulus versus relative density.

the exponent p can range from $p = 2$ in case of bending behaviour only to $p = 1$ in case of axial deformation only. The progressive deviation with increasing density of the FE results in Fig. 2.20 from the straight lines of Warren and Kraynik [Eq. (2.22)] and Gibson and Ashby [Eq. (2.3)] where $p = 2$ indicates the progressive importance of axial deformations in the foam. This can be understood from the fact that the bending moment of inertia increases quadratically with respect to the strut area for increasing density. Thus, with increasing density, the normal stiffness of the struts becomes weaker relative to the bending stiffness, and therefore becomes more important in controlling the relative Young's modulus of the foam. For example, Hagiwara and Green (1987) studied open-cell alumina with relative densities varying from 0.08 to 0.25 and fitted the experimental data with Eq. (2.27), resulting in $p = 1.93$ and $C_1 = 0.303$.

Figure 2.21 demonstrates the influence of the relative foam density on the bending stress, normal stress and the shear stress due to torsion. It shows that the average maximum bending stress and the average shear stress due to torsion decrease much faster than the average normal stress. Also this difference in dependency can be partially explained by the fact that the moment of inertia increases faster with respect to the strut area during density increase.

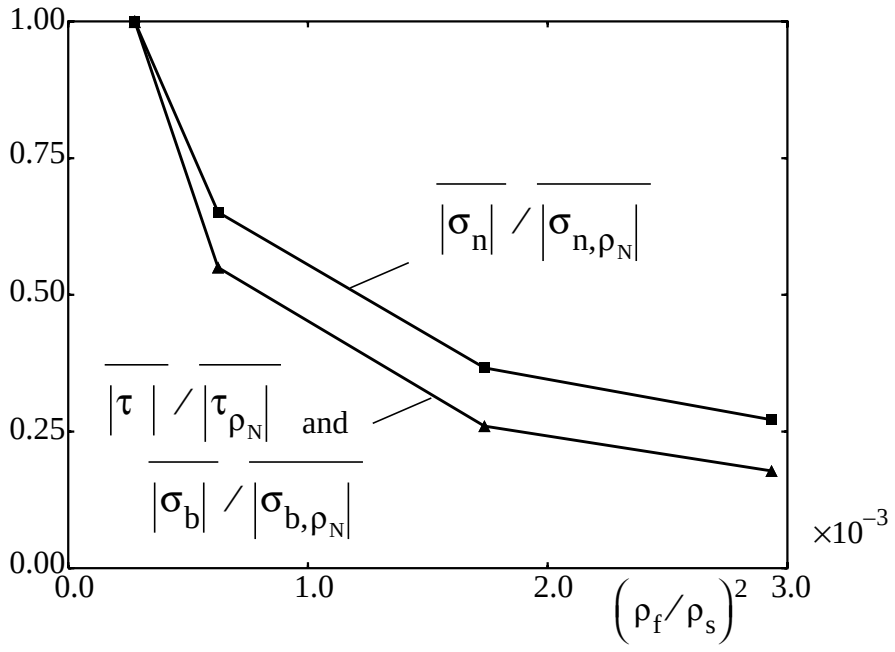

Fig. 2.21. The absolute bending stress, normal stress and maximum shear stress due to torsion, normalized at ρ_N, where $\rho_N = \rho_f/\rho_s = 0.0167$, as function of the relative density. At $\rho_f/\rho_s = 0.0167$ the average absolute bending stress is $\overline{|\sigma_b|}/\Sigma = 1130$, the average absolute normal stress is $\overline{|\sigma_n|}/\Sigma = 149$, and the average absolute maximum shear stress is $\overline{|\tau|}/\Sigma = 77$.

Table 2.2. Example of relative Young's moduli of various open-cell foam models at $\rho_f/\rho_s = 0.0231$, $E_f/E_s \times 10^{-3}$

Gibson–Ashby cubic model Eq. (2.3)	Rusch Eq. (2.4)	Tetrakaideca-hedron (square) Eq. (2.9)	Tetrakaideca-hedron (triangular) Eq. (2.11)	Tetrakaidecahed-ron (Plateau-Gibbs border) Eq. (2.12)	Rhombic dodeca-hedron Eq. (2.16)
0.535	4.17	2.76	0.44	0.61	3.59
Stochastic model of Lederman Eq. (2.19)	Aggregate model of Cunningham Eq. (2.20)	Warren–Kraynik (round) Eq. (2.22)	Warren–Kraynik (triangular) Eq. (2.23)	Warren–Kraynik (Plateau-Gibbs border) Eq. (2.24)	Present random model
13.3	3.86	0.487	0.588	0.818	0.53 ± 0.03

Numerical experiment

To verify the linear random model, Young's moduli of various open-cell foam models have been determined. The density of the foam is $\rho_f = 28.1\ kg/m^3$ and of the solid material $\rho_s = 1215\ kg/m^3$. The relative foam density is then $\rho_f/\rho_s = 0.0231$. Table 2.2 demonstrates the elastic moduli of the empirical (two first), regular (3 through 6), stochastic (7 through 11) and random models.

It was discussed before and illustrated in Fig. 2.16 that the empirical model of Ashby and Gibson which is implicitly based on a regular foam structure turns out to give a good approximation of the relationship between E_f/E_s and ρ_f/ρ_s for an irregular foam. This seems to validate this model. However, the model was fitted to real foams, that means to irregular foams. In this way, the random model is found to be in a good agreement with the data represented by the model of Gibson and Ashby, which should be considered as experimental, because of the extensive fitting to real foams.

2.3.3 Nonlinear model

The low-density open-cell foam is constructed from a unit cell, assuming that each unit cell boundary is a plane of reflective symmetry. Loading is applied through uniform normal displacements in the three directions (see Fig. 2.5); the average corresponding tractions on the cell faces define the macroscopic principal stresses Σ_1, Σ_2, Σ_3 acting on the foam.

The unit cell containing a strut framework used to model the foam is generated on the basis of the same Voronoi tessellation of space technique as used for the linear elastic

model in Section 2.3.2.

The FE analyses are performed using the standard program MARC. Geometrical nonlinearity occurs at large foam deformations. To obtain a good description of, for example, the buckling of the struts, all struts are meshed in relation to their length. This allows to achieve a rather uniform distribution of the element length throughout the unit cell. In this way, shorter struts, which need quite high compressive load before they buckle, contain less elements than the longer struts which will buckle first and, hence, are subdivided into more beam elements. A view of a cubic unit cell in 3D with the finite elements distribution is given in Fig. 2.22.

In addition to the foam geometry, the behaviour of the solid material in the struts is of the great importance for the macroscopic behaviour of the foam. In the analyses, the solid material can have various types of constitutive behaviour. Three types of idealized behaviour are used in the present analyses. Linear elastic (A) and two nonlinear elastic types of behaviour (B, C) are displayed in Fig. 2.23. Material A from Fig. 2.23 is used in the geometrically nonlinear analysis. In the nonlinear analysis, the behaviour of the solid material of the struts is described either by the bilinear curve (material B) or the nonlinear constitutive relations (material C). Both descriptions involve a limit stress σ_{ys}, which is here taken to have the value $0.28E_s$. The material C is characterized by the uniaxial stress–strain law

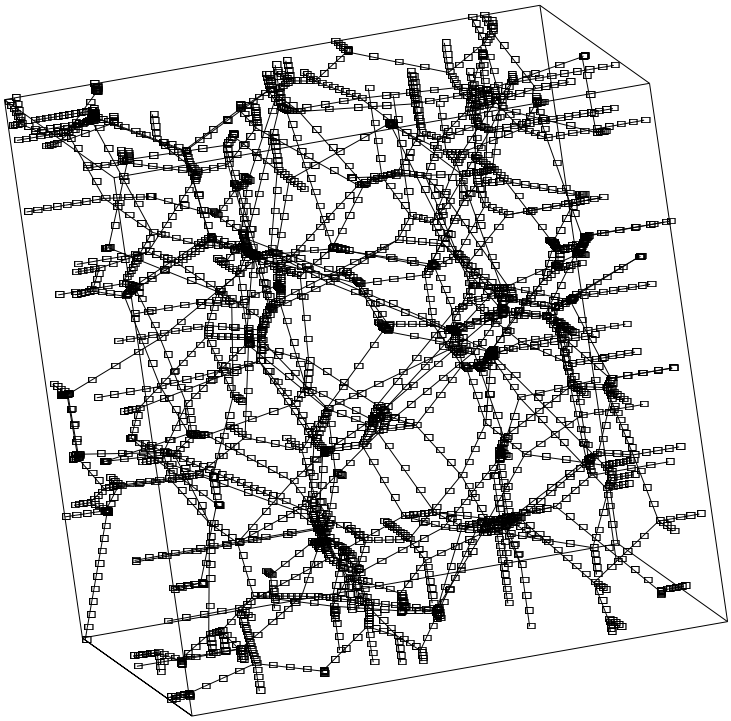

Fig. 2.22. Finite element mesh of a unit cell.

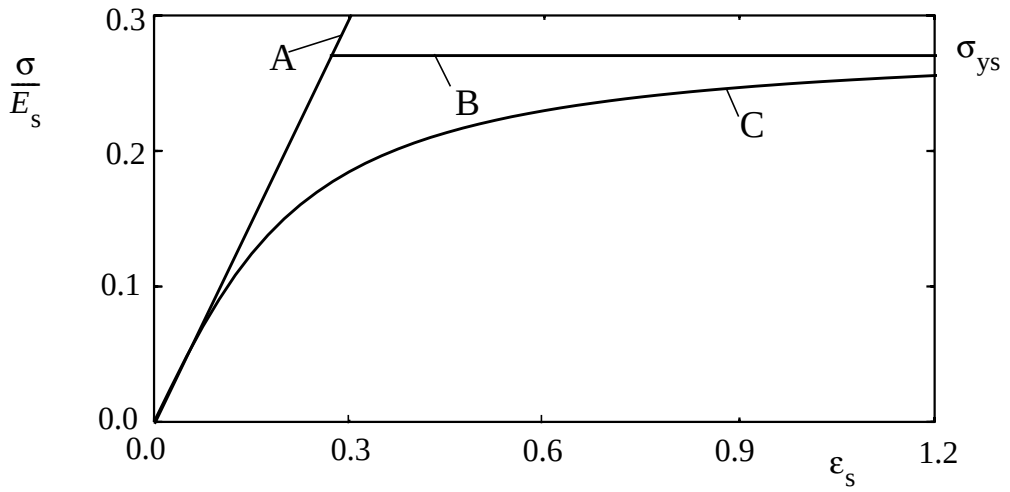

Fig. 2.23. Three different solid material behaviours of the struts: A –linear elastic; B –bilinear; C –nonlinear.

$$\frac{\sigma}{\sigma_{ys}} = \frac{2}{\pi}\arctan\left(\frac{\varepsilon_s}{\varepsilon_{s0}}\right) \tag{2.28}$$

with $\varepsilon_{s0} = 0.18$. These two strut material behaviours are idealized representations of a real rubber-like strut material of open-cell foams. Additionally, the material behaviour is assumed to be the same in tension and compression.

During large deformations, especially in compression, contact between struts may arise. This contact problem has not been incorporated in the numerical analysis and, therefore, the densification region of the foam observed during compression cannot be investigated.

Sensitivity to unit cell size

First, a number of unit cell analyses are performed in order to determine the minimum size of the unit cell that supplies an accurate solution. The unit cells are created by the Voronoi tessellation technique for randomly distributed nuclei sets. The dimensions of the unit cell for the detailed analyses are chosen on the basis of preliminary computations of unit cells with various sizes. The number of foam cells per unit cell is controlled by the size parameter L_{uc}/d (d is a minimum distance between nuclei in a unit cell), which is here chosen to be 2, 4 or 6. To demonstrate the reproducibility of the random model, the Voronoi tessellation is applied for at least five different random nuclei distributions per L_{uc}/d and the corresponding unit cells are generated for each size parameter. The corresponding unit cells contain on the average 63, 383 and 616 struts for L_{uc}/d=2, 4 and 6,

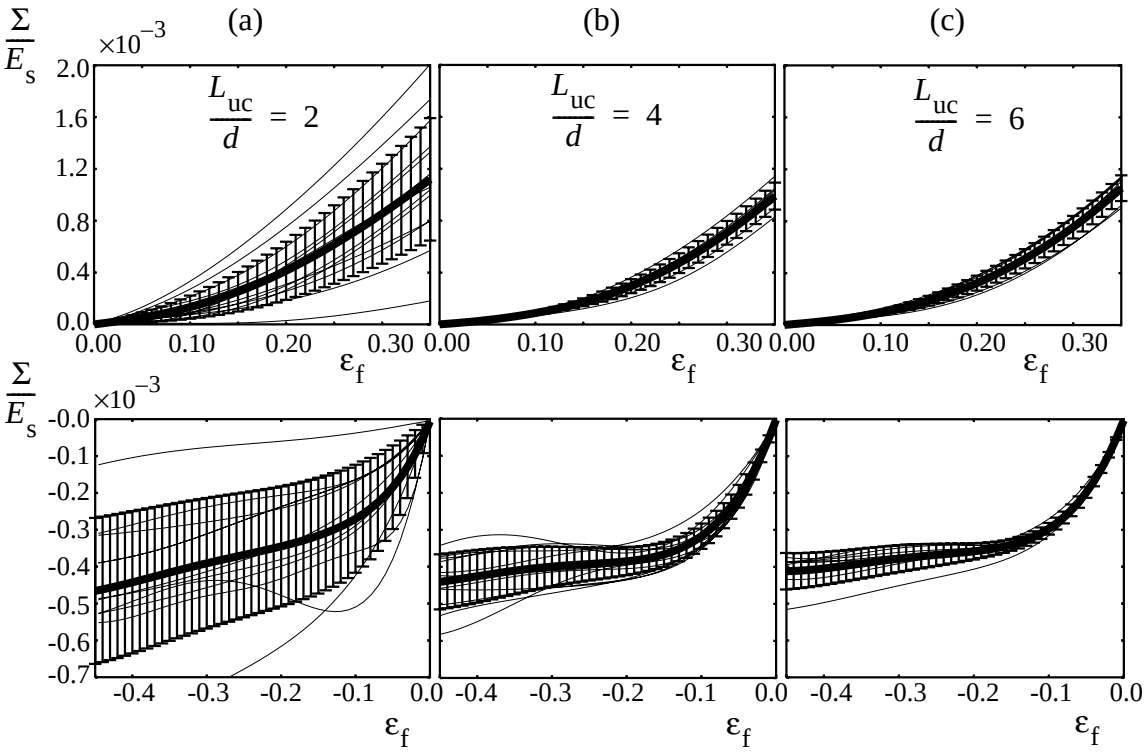

Fig. 2.24. Stress–strain diagrams and mean value (thick line) with 95% confidence interval for tension and compression for different random realizations per size parameter. (a) $L_{uc}/d = 2$; (b) $L_{uc}/d = 4$; (c) $L_{uc}/d = 6$.

respectively. The solid material is assumed to behave linear elastically (material A) for the moment, and the relative foam density ρ_f/ρ_s is taken equal to 0.025. This corresponds to the range of low-density foams. To achieve a good convergence during buckling of the struts, a minimum number of 4 and a maximum number of 8 elements per strut are chosen. Uniaxial tensile or compressive loading is applied in an incremental manner through displacement control.

Figures 2.24a–c show stress–strain curves under tension or compression of unit cells with the size parameters L_{uc}/d being 2, 4, or 6. The smallest unit cell with nearly 10 nucleation centres ($L_{uc}/d = 2$) shows a rather wide variation in the predicted stress–strain curves (see Fig. 2.24a). This scatter can be explained by the small sizes of the unit cell. Some unit cells exhibit stiff behaviour due to the influence of the rearranged boundaries which may reinforce the model. An increase of the unit cell size to $L_{uc}/d = 4$ with nearly 50 nucleation points per unit cell leads to a considerable reduction of the scatter and a clear plateau in the stress–strain compression diagram. A further increase of the parameter L_{uc}/d to 6 (128 cells) shows a raise of the computation times with a factor 10 in comparison with the unit cell with $L_{uc}/d = 4$, while the results for tension and compression

remain almost the same (compare Figs. 2.24b and c). Obviously, the unit cell should be sufficiently large compared to d. Based on the shown results, the unit cell with $L_{uc}/d = 4$ can be recommended to be used in the random foam modelling as the smallest unit cell that combines small scatter with low computing times.

Geometrically nonlinear model

Tension

The above study on the effect of the unit cell size presents a reference for the foam response based on linear elastic strut material. In the FE analysis, the tensile stress–strain response of the foam is determined for the linear elastic strut material (line A in Fig. 2.23). Three random models with L_{uc}/d equal to 2, 4 and 6 having behaviour closest to the averaged behaviour from Fig. 2.24 are chosen as representative models.

Additionally, two regular foam models, fcc- and bcc-based, with the same relative foam density are analyzed. As shown in Fig. 2.25a, both regular structures (bcc and fcc) show an initial stiffness that is lower than the stiffness of the random structures. Moreover, the stiffness of the fcc-based microstructure at large strains is much larger then the bcc-based. This can also be seen in Fig. 2.25b where the tangent modulus $E_{f,t}$ of the foam is plotted as a function of the logarithmic strain of foam, $\varepsilon_f = \ln(1 + U_i/L_{uc})$ (U_i is a displacement of one of the unit cell boundaries). For both regular microstructures, three distinct deformation regions can be seen in Fig. 2.25b. In the first region, the stiffness changes hardly and bending of struts is mainly responsible for the deformation. This is the

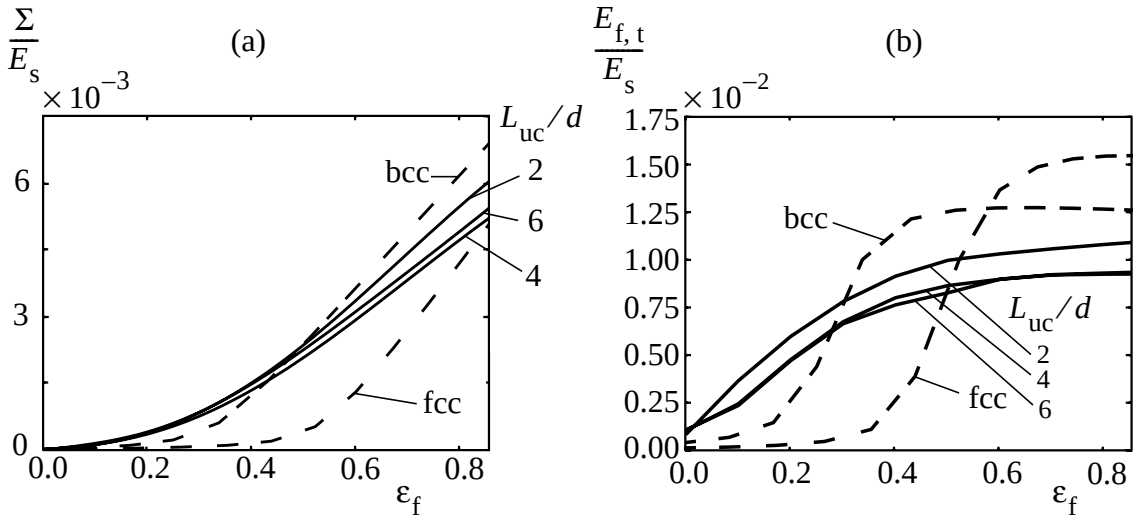

Fig. 2.25. (a) Stress–strain diagrams of different geometrically nonlinear foam models. (b) Corresponding tangent moduli.

so-called ‘strut bending region’. Subsequently, the axial deformation of struts start to play an increasing role in the global deformation of the foam. The increasing stiffness can be explained by the gradual re-orientation of struts towards the direction of the global stress Σ_i. This stage corresponds to the second, transitional region with a highly variable tangent modulus due to the mixture of bending and axial deformation in the struts. At a strain of $\varepsilon_f \approx 0.4$ for the bcc-based model and $\varepsilon_f \approx 0.7$ for the fcc-based structure, the third region starts. In this region, the foams deformation is almost completely determined by axial deformation of the struts that are aligned with the macroscopic stress.

Comparing with the regular models, the first deformation region is not present for all the random unit cells. This indicates that even in the initial deformation of the random model, axial deformation influences the overall foam behaviour. The large initial stiffness of the random model is explained by percolation of oriented chains of struts loaded mainly in tension. This effect has been discussed in Section 2.3.2. These percolations are absent in regular structures. However, due to the strain-induced strut re-orientation, the same effect occurs in regular models at large deformations. The bcc-based structure shows this effect earlier than the fcc-based model. Regular foams exhibit the alignment of many struts at the same time, thus explaining the reversed trend at large deformations. Regular foams are stiffer than random foams at large strains because of simultaneous strut alignment. Further considerations of the large strain stiffness will be presented in a forthcoming section.

To investigate the influence of the initial relative foam density ρ_f/ρ_s on the mechanical properties of the random model, the random unit cell with $L_{uc}/d = 4$ is loaded uniaxially in tension. The various relative foam densities are taken to be 0.0125, 0.0250, 0.0375 and 0.0500, and obtained by changing the diameter t of the struts. Figure 2.26a shows the stress–strain response for the various densities. In Fig. 2.26b, the tangent moduli $E_{f,t}/E_s$ are displayed as function of the foam strain. Again, the second and the third regions can be distinguished clearly. A first conclusion from this figure is that the stress–strain curves become linear at a certain strain. Moreover, this strain becomes larger with increasing density. This is due to the fact that with increasing strut diameter, the bending stiffness of struts increases as t^4 while its axial stiffness increases as t^2.

The results for $E_{f,t}/E_s$ of the random model in the small deformation region (to be precise, at $\varepsilon_f = 0.05$) from Fig. 2.26b are given as a function of $(\rho_f/\rho_s)^2$ in Fig. 2.27a. The results of the cubic model of Gibson and Ashby [see Eq. (2.7)] for the initial strain are plotted also, as well as $E_{f,t}/E_s$ of the random model in the undeformed state ($\varepsilon_f = 0$), which are taken from Section 2.3.2. If bending is the main deformation mechanism, the FE results would be on the Gibson–Ashby model line. Indeed, at 0% strain, the FE analy-

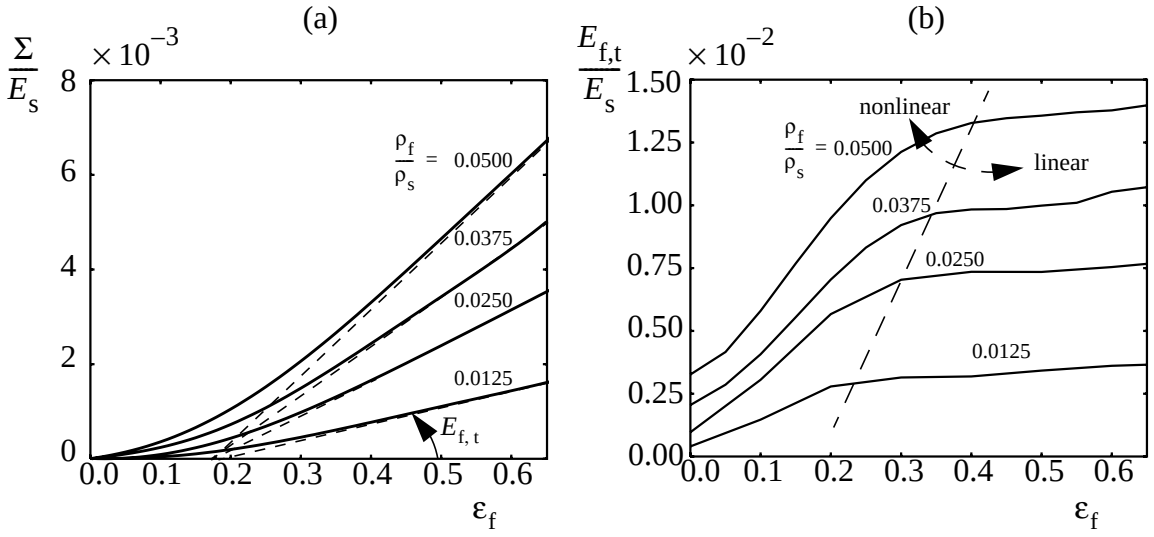

Fig. 2.26. (a) Stress–strain diagrams of the geometrically nonlinear random foam model with various densities. (b) Corresponding tangent moduli.

ses show that bending is the main deformation mechanism. However, at higher densities, axial deformation becomes more important. At a relatively small strain of 5%, the importance of the axial deformation in struts in the random model has increased substantially in comparison with that at $\varepsilon_f = 0$. Due to the rapidly increasing importance of the axial deformation, the cubic model of Gibson and Ashby loses accuracy with increasing strain.

At large strains of the foam ($\varepsilon_f > 0.4$), the random model exhibits an asymptotic stiffness due to the alignment of several strut chains in the direction of maximum principal stress. The values of $E_{f,t}/E_s$ for the random unit cell and for the fcc-based regular model at large strains are plotted against the initial relative foam density ρ_f/ρ_s in Fig. 2.27b. The random model is less stiff in this region than the fcc-based unit cell and both models do not reach the stiffness given by the cubic model of Gibson and Ashby by Eq. (2.7). If deformation is purely by uniaxial tension of the struts, $E_{f,t}/E_s$ should be linear with ρ_f/ρ_s. Any deviation is due to bending. The lower lines indicate that bending is still of importance or that not all struts deform axially. In the fcc-based microstructure, severe bending of the struts takes place at the ends of the struts, close to the vertices. Finally, the relative tangent modulus of a foam model under a large tensile strain is linear with respect to ρ_f/ρ_s. It is clear from Fig. 2.27b that neither the fcc-based nor the random model reaches such a high modulus; therefore, $C_2 < 1$ in Eq. (2.7).

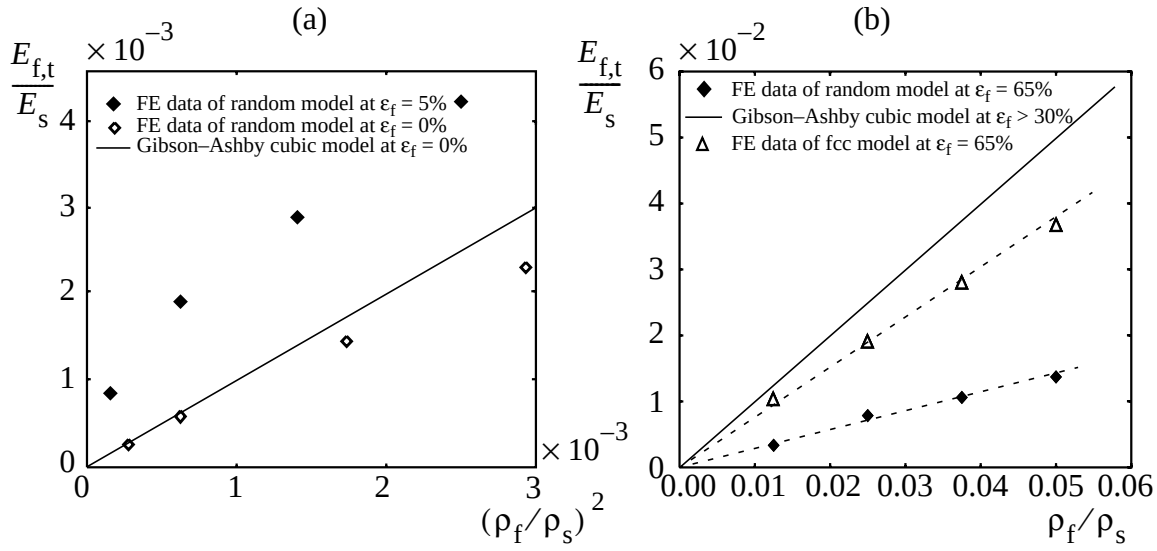

Fig. 2.27. Tangent modulus of the fcc-based and random models with linear elastic material (a) at small strain and (b) at large strain as a function of the relative foam density.

Compression

Similarly, the fcc-based model and the random unit cell built up of linear elastic struts are loaded in compression. The initial density of the foam is again $\rho_f/\rho_s = 0.025$. The two foam models predict a very different behaviour, as can be seen in Fig. 2.28. The random model is initially much stiffer than the regular one and exhibits a “maximum”, which

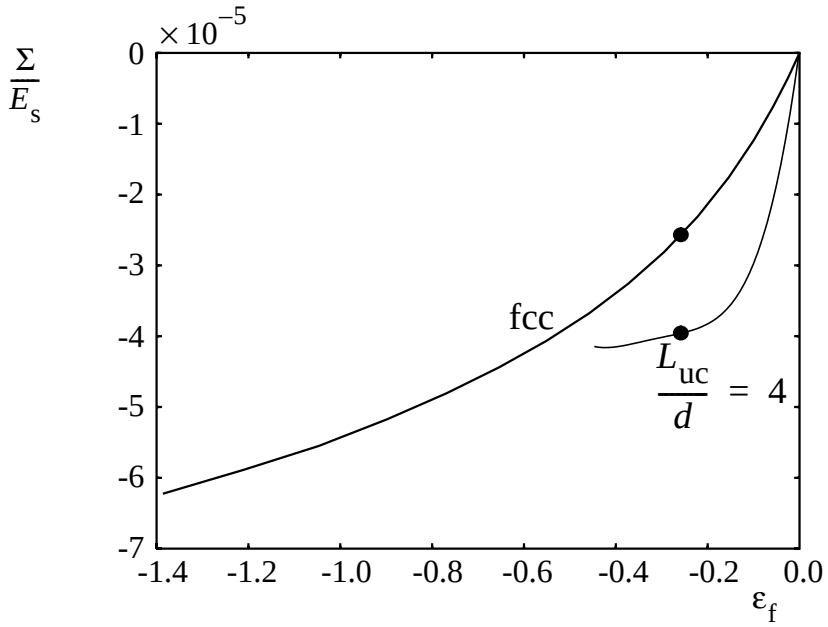

Fig. 2.28. Stress–strain diagram of the foam models under uniaxial compression. The deformed networks at the strains indicated by the dots are shown in Fig. 2.29.

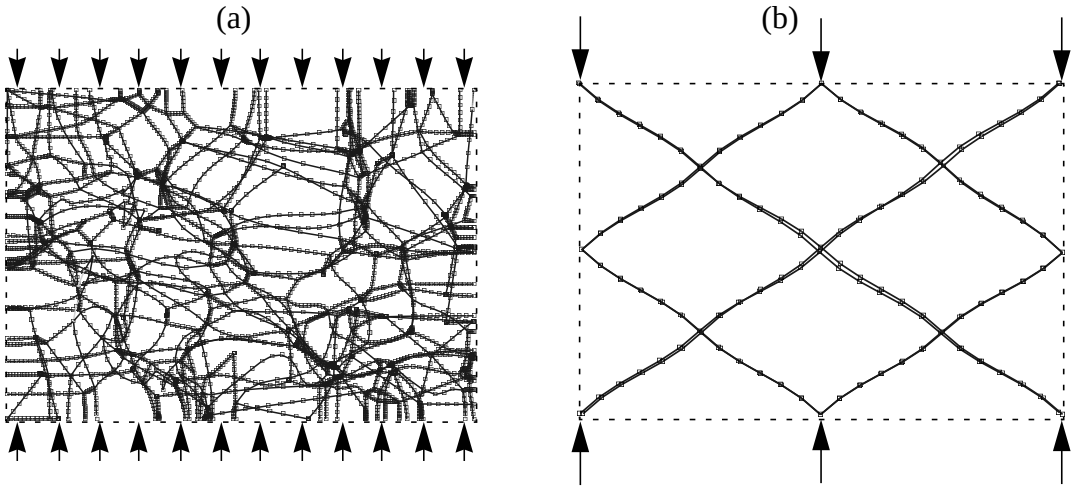

Fig. 2.29. (a) The random and (b) the fcc-based foam models at a compressive strain of $\varepsilon_f = -0.25$ (see Fig. 2.28).

is termed the elastic collapse stress Σ_{el}. Figure 2.29a depicts the random unit cell in the post-collapse regime when a considerable number of struts is buckled. In contrast, the local buckling of struts does not occur in the fcc-based model what is also seen in Fig. 2.29b, showing bending of the struts only. This explains the absence of a collapse stress.

To determine the coefficients C_3 and p appearing in Eq. (2.8), numerical experiments with unit cells of various relative densities are performed here. The coefficient p appears to depend on the ratio between the two deformation mechanisms in the struts, namely axial deformation ($p = 1$) and bending ($p = 2$). In a foam under global compressive stress, the buckling of struts is responsible for the maximum stress. For this reason, p is expected to be close to but lower than 2. Figure 2.30 shows how the elastic collapse stress of the foam model under compression depends on the relative foam density. Based on these FE results, the coefficient C_3 in Eq. (2.8) is found to be equal to 0.057 if $p = 2$. Similar experimental results have been obtained by Gibson and Ashby (1988) in Eq. (2.8). The minor discrepancy with the numerical results can be explained from the fact that the material in the struts of the random model behave linear elastically. The model of Gibson and Ashby is implicitly linear elastic and nonlinear behaviour of solid has been obscured. Real material behaviour in the random model would cause a lower elastic collapse stress of the model in Fig. 2.30. If the strut diameter increases with the relative foam density, it becomes more likely that the material in struts will behave in a nonlinear elastic fashion during buckling (it corresponds to the region of the solid material behaviour when $\varepsilon_s > 0.1$ in Fig. 2.23). In the region of relatively high foam densities, for example, the numerical simulation point in Fig. 2.30 with $(\rho_f/\rho_s)^2 = 0.0025$, the relative error becomes too high and the nonlinear behaviour of the solid material in the struts may not be neglected anymore.

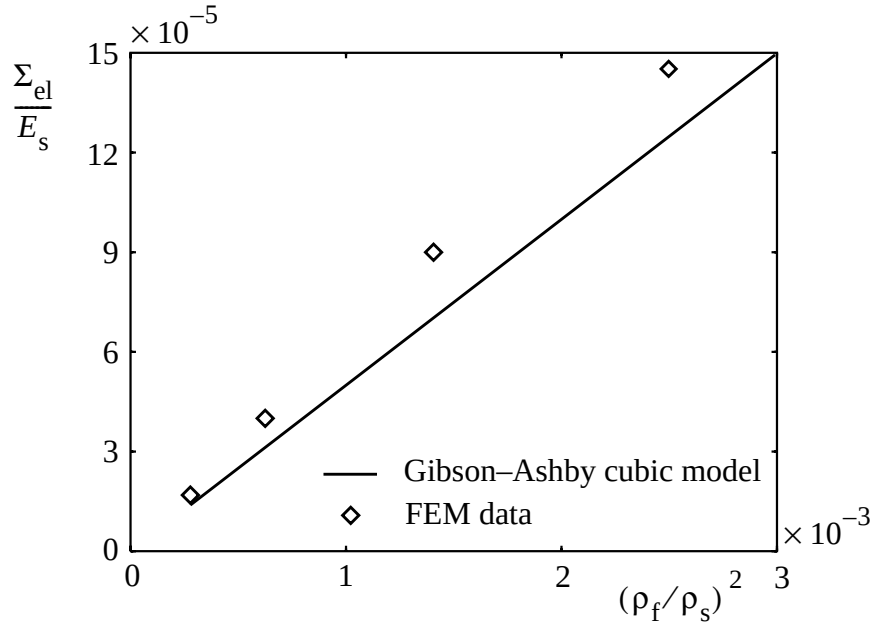

Fig. 2.30. Elastic collapse stress as a function of the relative foam density.

Nonlinear elastic material in struts

In order to study foams with nonlinear strut material (lines B and C in Fig. 2.23), three-dimensional finite strain beam analyses should be possible with such constitutive behaviour. Unfortunately, most FE codes do not have this capability. To make numerical analysis with nonlinear material behaviour possible, the cross-section of the strut with radius r is discretized in radial and tangential directions, as described in the Appendix. Application of the nonlinear constitutive behaviour to the solid material in the standard FE program used caused a number of numerical problems, especially when strut buckling would occur. Therefore, to investigate the influence of the constitutive behaviour of the solid material in the struts, only tensile deformation of the representative random foam model with $L_{uc}/d = 2$ has been analyzed.

The results of the simulations for the bilinear elastic material (curve B in Fig. 2.23) and nonlinear function (curve C in Fig. 2.23) are displayed in Fig. 2.31. Both these curves will ultimately approach the same maximum value of the stress. The effect of nonlinear solid behaviour is reflected in the foam properties in a similar way as may be expected. Contrarily to the linear elastic solid behaviour (curve A), where the foam stiffness increases monotonically with strain (Fig. 2.25), the presence of a limit stress σ_{ys} in the solid response induces a maximum of the stiffness after some strain level. The global tensile stress asymptotically approaches some maximum value $\Sigma_y \approx 2.3\times10^{-3}E_s \approx 0.82\times10^{-2}\sigma_{ys}$.

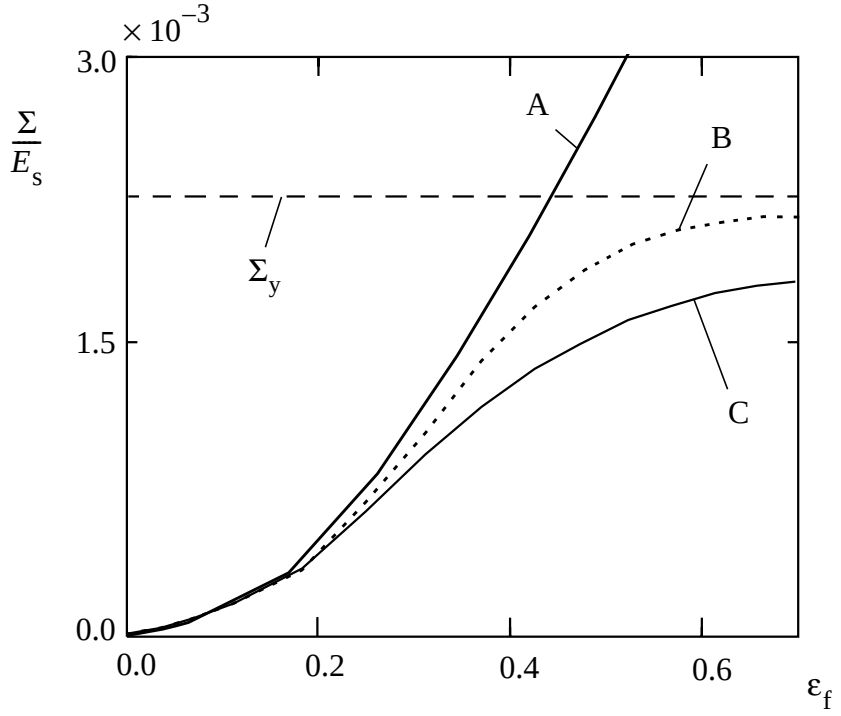

Fig. 2.31. Stress–strain diagram of the random model with various constitutive behaviours.

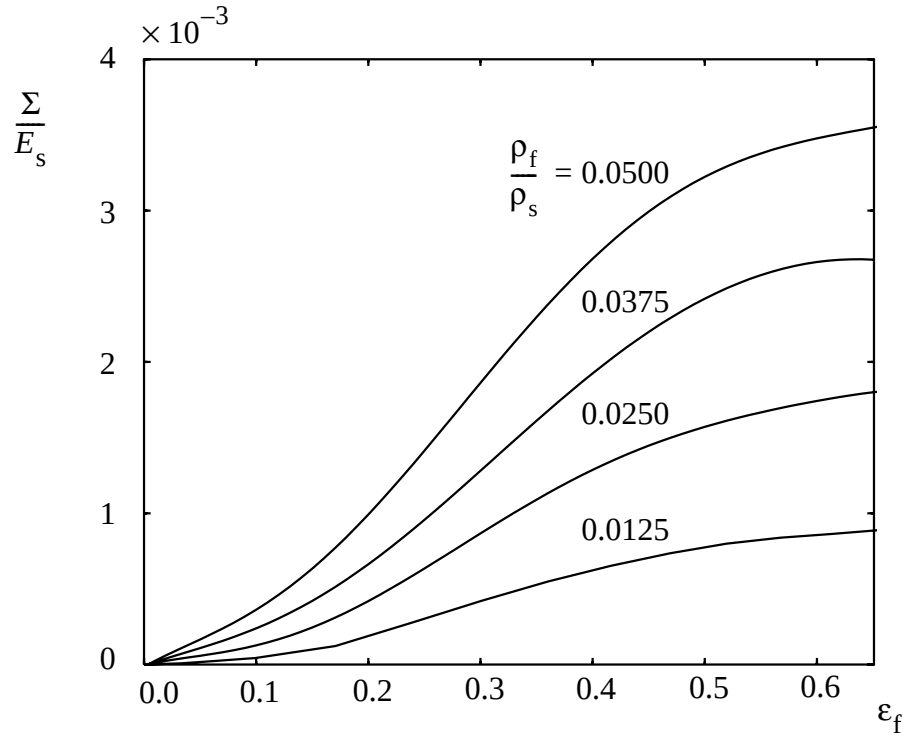

Fig. 2.32. Stress–strain diagrams for the nonlinear analysis.

The stress–strain curves for several densities of the random model with nonlinear strut material behaviour (curve C in Fig. 2.23) are shown in Fig. 2.32. Not unexpectedly, the one with the higher density has also the highest ultimate strength. Moreover, there is a linear correspondence between relative foam density ρ_f/ρ_s and maximum global tensile stress.

Effective unit cell cross-section

Nonlinear elasticity of foam

It was shown in the previous section that alignment of struts with the tensile direction occurs with increasing strain. Figure 2.33 actually demonstrates this in terms of the deformed strut network. It suggests that the percentage of struts, aligned in the direction of the maximum principal stress due to the large strain, determines the final tensile stiffness. These struts deform at large strains primarily by axial stretching.

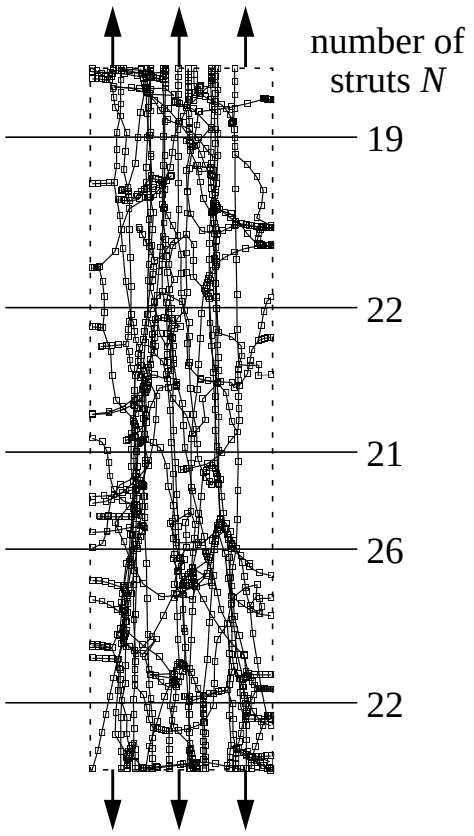

Fig. 2.33. Random model under a tensile strain of $\varepsilon_f = 0.6$, including the number of struts at various cross-sections of the model. The small squares are the nodal points in the FE mesh.

First, the difference in stiffness of the two regular foam models—the rhombic dodecahedron (fcc) and the tetrakaidecahedron (bcc)—at large tensile strains will be explained. The first shows a much higher stiffness at large strains than the bcc-based microstructure. Then, an arbitrary cross-section through the unit cell is made, normal to the global maximum principal stress direction. For this cross-section, the area of the solid phase in the unit cell cross-section is the total projected area of the N struts which pass through this unit cell cross-section and which are oriented at angles $\alpha_i \approx 0°$ to the global stress direction. This area of the cross-section is termed the effective cross-sectional area $A_{\text{eff}} = Na$.

In the undeformed rhombic dodecahedra unit cell, all struts are oriented under the same angle to the global direction, which is $54.74°$. As far as the regular structure deforms uniformly, the fcc-based strut structure at large strains has a constant effective unit cell cross-section with area

$$A_{\text{eff}}^{\text{fcc}} = A_{\text{uc}} \left(\frac{\rho_{\text{f}}}{\rho_{\text{s}}} \right). \tag{2.29}$$

Alternatively, the undeformed tetrakaidecahedron contains two groups of struts oriented under $45°$ and $90°$, correspondingly (see Fig. 2.6g), so that the bcc-based unit cell includes two groups of cross-sections of the unit cell. The smallest of them is expected to determine the large deformation of foam in tension, caused by the axial deformation of the struts completely oriented in the direction of the global stress Σ_i. This means, that the regular tetrakaidecahedron model in tension is less stiff under the large global strains than the regular rhombic dodecahedron. The corresponding tail ends of the curves in Fig. 2.25b for the bcc- and fcc-based models support this argument.

From the above discussion it is clear that a foam model with a constant effective unit cell cross-section will be the stiffest under large strains. As opposed to a regular model, the random model never possesses a constant A_{eff} along the unit cell length. It is strongly dependent on the position of the cross-section in the unit cell. It means that in any isotropic open-cell foam model, the stiffness at large strains will not exceed that of the fcc-based regular model. The effect will be more pronounced for small unit cells. An example in Fig. 2.33 demonstrates various number of struts in various unit cell cross-sections taken perpendicular to the global tensile stress direction. In this case, the model stiffness is determined by the cross-section with the lowest effective area, i.e., with the minimum number of struts in the cross-section. This is why the random model is less stiff in the large strain region than the fcc-based regular model.

The stiffness of a random model at large strains will always be lower than of the regular fcc-based model, because the random model will always contain struts that are oriented

in the direction perpendicular to the principal stress. These struts do not contribute to the effective cross-section and decrease the stiffness at large strains. For the ideal elastic model with all struts completely oriented in the principal stress under the large tensile strain, one would find

$$\frac{E_{\mathrm{f,t}}}{E_{\mathrm{s}}} = \frac{\rho_{\mathrm{f}}}{\rho_{\mathrm{s}}}. \tag{2.30}$$

This is similar to Eq. (2.7) with $C_2 = 1$ for a foam having a uniform cell-size distribution and no struts perpendicular to the principal stress direction. A great variation in the cell diameter can lead to a decrease of the minimum effective cross-sectional area A_{eff} and therefore, to smaller values of the coefficient C_2. The influence of the relative foam density on the tangent modulus at large strains of the fcc-based and random unit cells is shown in Fig. 2.27b. Struts of the fcc-based structure are connected with each other in vertices as shown in Fig. 2.29b and even under large tensile strains they are bent and are not completely rotated towards the global stress direction. This leads to a lower tangent modulus of the fcc-based structure in comparison with the ideal Gibson–Ashby model with the coefficient $C_2 = 1$ shown as the solid line in Fig. 2.27b. The dashed lines in Fig. 2.27b characterize an imperfection of the model in comparison with the ideal model. In other words, the coefficient C_2 in Eq. (2.7) can be estimated through the ratio of the minimum effective unit cell cross-section to that of the ideal model,

$$C_2 = \frac{A_{\mathrm{eff}}}{A_{\mathrm{eff,ideal}}}, \text{ or } C_2 = \frac{A_{\mathrm{eff}}}{A_{\mathrm{uc}}}\frac{\rho_{\mathrm{s}}}{\rho_{\mathrm{f}}}. \tag{2.31}$$

Yielding collapse of foam

For bilinear or nonlinear elastic solid material in the struts, the insight that the struts align during deformation can be exploited to estimate the global yield stress (see Fig. 2.27). If the yield stress of the solid σ_{ys} is reached in all struts of the certain unit cell cross-section, the macroscopic yield stress of the foam unit cell, Σ_{y}, follows directly from equilibrium

$$L_{\mathrm{uc}}^2\Sigma_{\mathrm{y}} = Na\sigma_{\mathrm{ys}}, \text{ or } L_{\mathrm{uc}}^2\Sigma_{\mathrm{y}} = A_{\mathrm{eff}}\sigma_{\mathrm{ys}}, \tag{2.32}$$

where N is the number of struts in the unit cell cross-section. It means that global yield of foam in tension occurs in the unit cell cross-section with the minimum effective area, i.e., in the cross-section with $N = N_{\mathrm{min}}$. Eq. (2.32) can then be rewritten as

$$\Sigma_y = \frac{N_{\min} a}{L_{uc}^2} \sigma_{ys}. \tag{2.33}$$

The normalized yield collapse stress Σ_y / σ_{ys} for the unit cell with $L_{uc}/d = 2$ is shown in Fig. 2.31 and equals nearly 0.008. Determined by Eq. (2.33), the foam global yield stress Σ_y in Fig. 2.31 is an asymptote for the bilinear and nonlinear elastic behaviour, according to the curves B and C in Fig. 2.23 respectively.

A random unit cell with a wide variation of A_{eff} may have poor mechanical properties at large strains, when it has a wide cell-size distribution. This effect has been observed by Gent and Thomas (1959), who characterized the non-uniformity of foam by the ratio of the largest observed cell diameter to the average diameter, D_m'/D_m. Samples with the highest D_m'/D_m ratio exhibited the lowest tensile strength and strain at failure. This effect can be explained by a local drop of the minimum effective cross-sectional area A_{eff}.

For foams with identical unit cell geometries but with different relative densities ρ_f/ρ_s, only the strut cross-sectional area a changes. Since a is a linear function of the relative foam density, the dependence of the yield collapse stress in foam caused by strut yielding and the foam density ρ_f/ρ_s is given as

$$\frac{\Sigma_y}{\sigma_{ys}} \propto \frac{\rho_f}{\rho_s}. \tag{2.34}$$

It must be noted that these considerations apply only to an isotropic foam model. In the case of an anisotropic foam, the effective foam cross-section A_{eff} is dependent on the direction.

2.3.4 Anisotropic regular model

Natural origins of the geometrical anisotropy

Polymers are foamed by nucleation of gas bubbles in a liquid hot polymer with subsequent growth of the bubbles and stabilizing of the foam. In most cases the growth of foam occurs in one direction, that is called rise direction, x_1. When the liquid substance saturated with the blowing agent is extruded, the resulting foam is also extended in the direction of extrusion, x_2. This leads to differences in the mechanical properties of the macrostructure in different directions, so-called mechanical anisotropy. A capability of foam to exhibit anisotropic properties is important for various applications, for instance, in vacuum panels filled with open-cell foams described, for example, by Vos *et al.* (1994). In these constructions, the foam is desired to have high mechanical properties in the load

direction, while other directions are of less importance.

Processes of nucleation, bubble growth and extrusion take place simultaneously and have an essential influence on the microstructure of the foam. Assumptions that were made for the Voronoi tessellation about the growth of foam do not take all these phenomena into account. To incorporate the effects of non-simultaneous nucleation and bubble growth and displacement of nuclei in the process of growing, two kinds of geometrical anisotropy will be considered. The first is associated with the primary anisotropy of the nuclei before their growth. For the 3D Voronoi tessellation it means that the nuclei are distributed in an anisotropic way. The other one is related to the extension of the foaming structure due to the effects of extrusion and growth in rise direction. In the case of the 3D Voronoi tessellation it implies the extension of the isotropic structure in the directions of anisotropy.

Model

Seven sorts of open-cell PUR foam (one of them, S08, is shown in Fig. 2.34a) of Recticel N. V. (Belgium) with various cell sizes are studied. If the largest principal dimension of a cell, also called the rise direction, is A_1, the second largest dimension (the extrusion direction) is A_2, and the smallest dimension (the transverse direction) is A_3, then geometrical anisotropy factors are

$$A_{13} = \frac{A_1}{A_3} \text{ and } A_{23} = \frac{A_2}{A_3}. \tag{2.35}$$

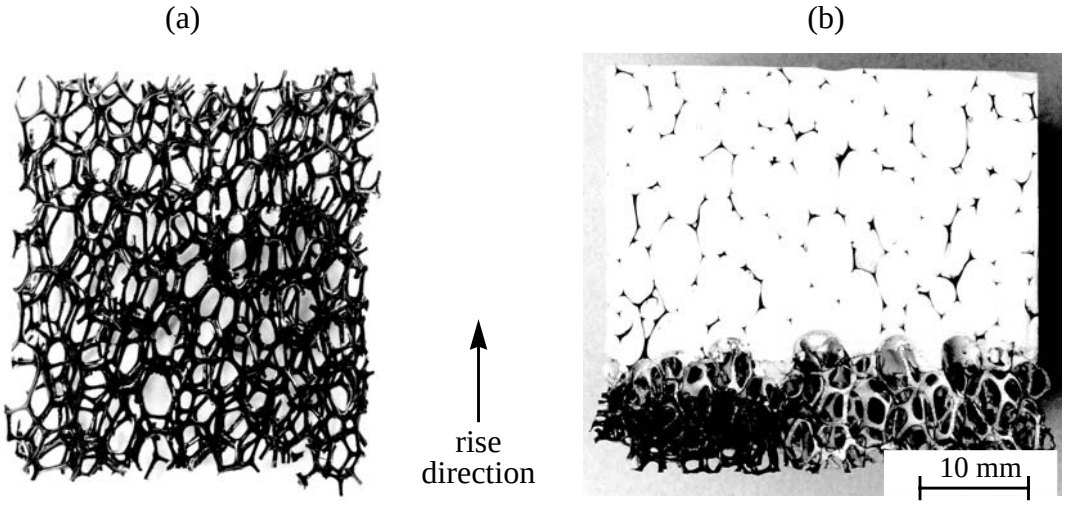

Fig. 2.34. (a) PUR S08 foam and (b) the same foam embedded in a polyester resin with low profile additives.

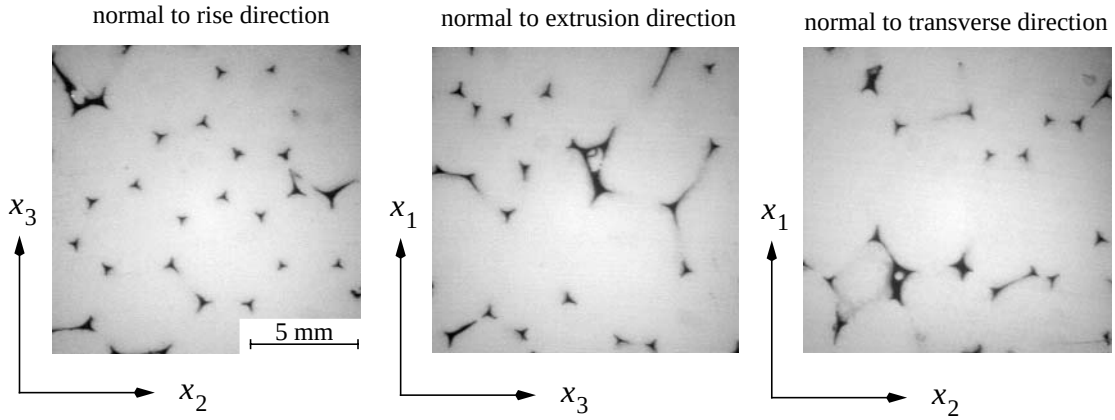

Fig. 2.35. Cross-sections of S08 foam embedded in a resin (dark areas are struts and light areas is resin).

Figures 2.3b-c illustrate the geometrical anisotropy factors. The dimensions of cells for each foam type have been measured. For this purpose, foam was embedded in a polyester resin with low profile additives (low profile additives reduce resin curing shrinkage), as it is shown in Fig. 2.34b, and cut in planes normal to three foam main directions. Examples of the resulting 2D views are shown in Fig. 2.35. They are studied with an image processing technique, as described by Waterman and Phillips (1974). Their average values varied between $6.57 \times 4.21 \times 3.7$ mm^3 for S08 foam and $0.57 \times 0.44 \times 0.4$ mm^3 for S90 foam (A_1, A_2 and A_3 correspondingly).

To define the influence of the anisotropic effects, both the primary anisotropy of the nuclei before their growth and the extension of the foaming structure due to effects of extrusion and growth, onto the geometry of the final structure (cells), two anisotropy factors, A'_{ij} and A''_{ij}, are introduced. Here i and j correspond to the principal directions of foam. The first (primary) anisotropy factor A'_{ij} refers to an anisotropic nuclei distribution. The second anisotropy factor A''_{ij} refers to the anisotropy of cells due to the stretching of already existing cells in the rise and extrusion directions.

The total anisotropy factor A_{ij} can be expressed in terms of the primary A'_{ij} and the secondary A''_{ij} anisotropy factors by

$$A_{ij} = A'_{ij}A''_{ij} . \tag{2.36}$$

Figure 2.36 explains the influence of primary and secondary anisotropy on cell geometry.

To characterise the proportion between primary and secondary anisotropy factors, the degree of the initial anisotropy, n, has been adopted. It is assumed that n is the same for all principal directions. The anisotropy factors consequently are:

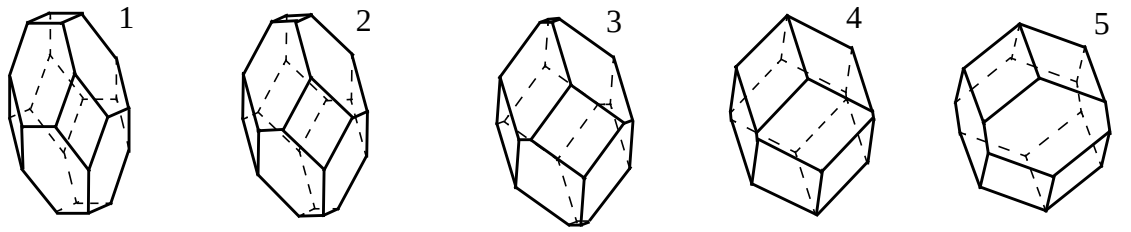

$n = 0$ (due to deformation [rise] only) $n = 0.25$ $n = 0.5$ $n = 0.75$ $n = 1$ (due to anisotropic nucleation only)

Fig. 2.36. Influence of the correlation between primary and secondary anisotropy on the final cell geometry when A_{ij}=*const.*

$$A'_{ij} = A_{ij}^{n} \quad \forall i, j \tag{2.37}$$

and

$$A''_{ij} = A_{ij}^{(1-n)} \quad \forall i, j\,. \tag{2.38}$$

The degree of initial anisotropy, n, varies from 0 to 1.

The shape of a cell changed in accordance with n, from an elongated tetrakaidecahedron (n=0 according to the model of Dementjev and Tarakanov) to an elongated rhombic dodecahedron (n=1) (see cells 1 and 5 in Fig. 2.36 respectively).

It is evident from Fig. 2.36 that by decreasing factor n, while keeping the total anisotropy A_{ij} the same, struts can be oriented in the rise direction of the foam. This may strongly increase the foam stiffness in this direction, because bending of struts being the determining factor in the elastic properties of foam is reduced.

Because foam density is a function of foam geometry and of the density of solid plastic, ρ_s, it can be calculated by Eq. (2.26). The densities of seven sorts of open-cell foams S08...S90 (PUR of Recticel N.V.) with various cell sizes and shapes have been measured and compared to those, calculated with Eq. (2.26) as shown in Table 2.3. The cross-sectional area of struts, a, has been measured using an image processing technique and assumed to be the same per foam type for all struts. To complete the measurements, a strut cross-section was rotated to get cross-section normal to the strut axis. The same technique was used to measure the strut length l.

Calculated with Eq. (2.26), the density of foam S08 varied from 29.9 kg/m^3 for the elongated tetrakaidecahedron (cell 1 in Fig. 2.36) to 28.1 kg/m^3 for the elongated rhombic

Table 2.3. Measured and calculated densities of foams

Foam type	S08	S20	S30	S45	S60	S75	S90
Measured density ρ_f [kg/m^3]	28.1	29.4	28.6	31.5	28.9	29.3	32.7
Calculated density $\overline{\rho}_f$ [kg/m^3]	29.0	36.6	36.0	28.3	17.2	20.1	24.9
Errors [%]	+3	+24.5	+25.9	-10.2	-40.5	-31.4	-23.9

dodecahedron (cell 5 in Fig. 2.36). This difference in densities can be neglected and the calculated values in Table 2.3 are averaged over 5 models (Fig. 2.36).

Correlation between geometrical and mechanical anisotropy factors

To determine the extent to which the mechanical properties of foam are affected by the kind of microstructural anisotropy, the FEM has been used. Seven sorts of open-cell PUR foam have been modelled in the standard MARC FEM program. Edges were represented as elastic beam elements, that had constant and same round cross-section a (Fig. 2.37a). For every kind of foam, 5 cells shown in Fig. 2.36 with different degrees of initial geometrical anisotropy n were loaded with a compression force in three main directions and linear elastic analysis was performed. An example of undeformed and deformed structures is shown in Fig. 2.37. For each case, the elastic moduli of the foam model in three

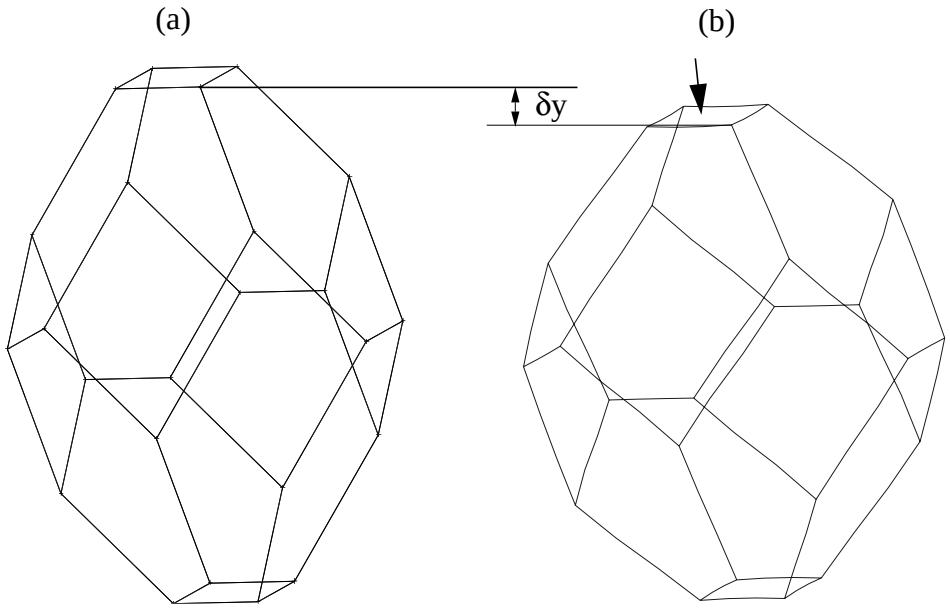

Fig. 2.37. (a) Undeformed and (b) deformed open-cell foam model.

main directions E_i (i=1...3) and the mechanical anisotropy factors

$$E_{13} = \frac{E_1}{E_3} \text{ and } E_{23} = \frac{E_2}{E_3} \tag{2.39}$$

were determined. The correlation between the kind of geometrical (through factor n) and mechanical anisotropy factors of foam E_{13} and E_{23} is presented in Fig. 2.38.

For all foam types (S08...S90) the mechanical anisotropy has been measured by performing the compression test in three directions with the cubic foam samples of a side length 40 *mm*. The deformation rate was kept low (0.25 min^{-1}). The corresponding factors n per foam type and direction has been found (solid straight lines in Fig. 2.38). The averaging of n over all tested foam types in each direction gave a mean value of $\bar{n} = 0.15$.

Assuming the value of $\bar{n}$=0.15 to be applicable for the cell shapes of all seven foams, the corresponding value of mechanical anisotropy was found (broken lines in Fig. 2.38). Table 2.4 demonstrates the values of the geometrical and mechanical anisotropy factors. The relative error of mechanical anisotropy suggested by this model is at most 23% and 9% on the average, while that calculated with the model of Dementjev and Tarakanov (1970) comprised 79% and 33.6% correspondingly.

This obvious advantage of the described regular anisotropic model as compared to the elongated tetrakaidecahedron of Dementjev and Tarakanov is related to the more realistic

Table 2.4. Geometrical and mechanical anisotropy factors of open-cell foams

Foam type	Geometrical anisotropy factors		Mechanical anisotropy factors E_{13}		Mechanical anisotropy factors E_{23}		Errors [%]	
	A_{13}	A_{23}	measured	calculated with $\bar{n}$=0.15	measured	calculated with $\bar{n}$=0.15	ΔE_{13}	ΔE_{23}
S08	1.78	1.14	3.80	4.19	1.31	1.18	10.2	9.9
S20	1.54	1.01	2.70	2.77	1.07	1.01	2.6	5.6
S30	1.44	1.15	2.11	2.17	1.19	1.26	2.8	5.9
S45	1.39	1.24	2.20	1.98	1.33	1.45	9.8	9.1
S60	1.21	1.13	1.80	1.50	1.14	1.24	16.4	8.4
S75	1.31	1.14	2.17	1.77	1.25	1.27	18.6	1.4
S90	1.43	1.10	1.82	2.24	1.21	1.18	22.9	2.7

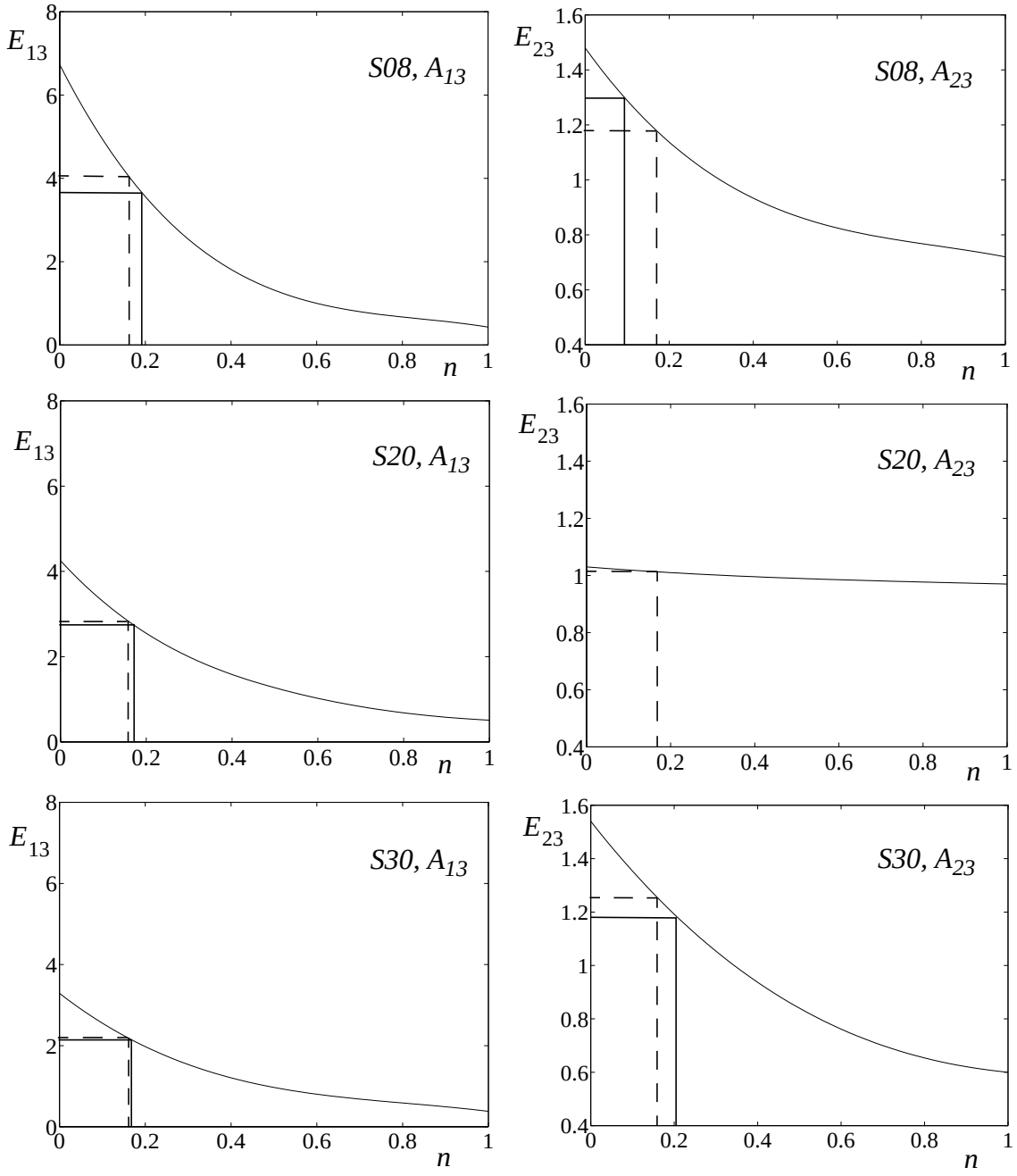

Fig. 2.38. Correlation between geometrical and mechanical anisotropy factors. Solid straight line corresponds to the measured n and broken line is associated with the accepted $\bar{n} = 0.15$.

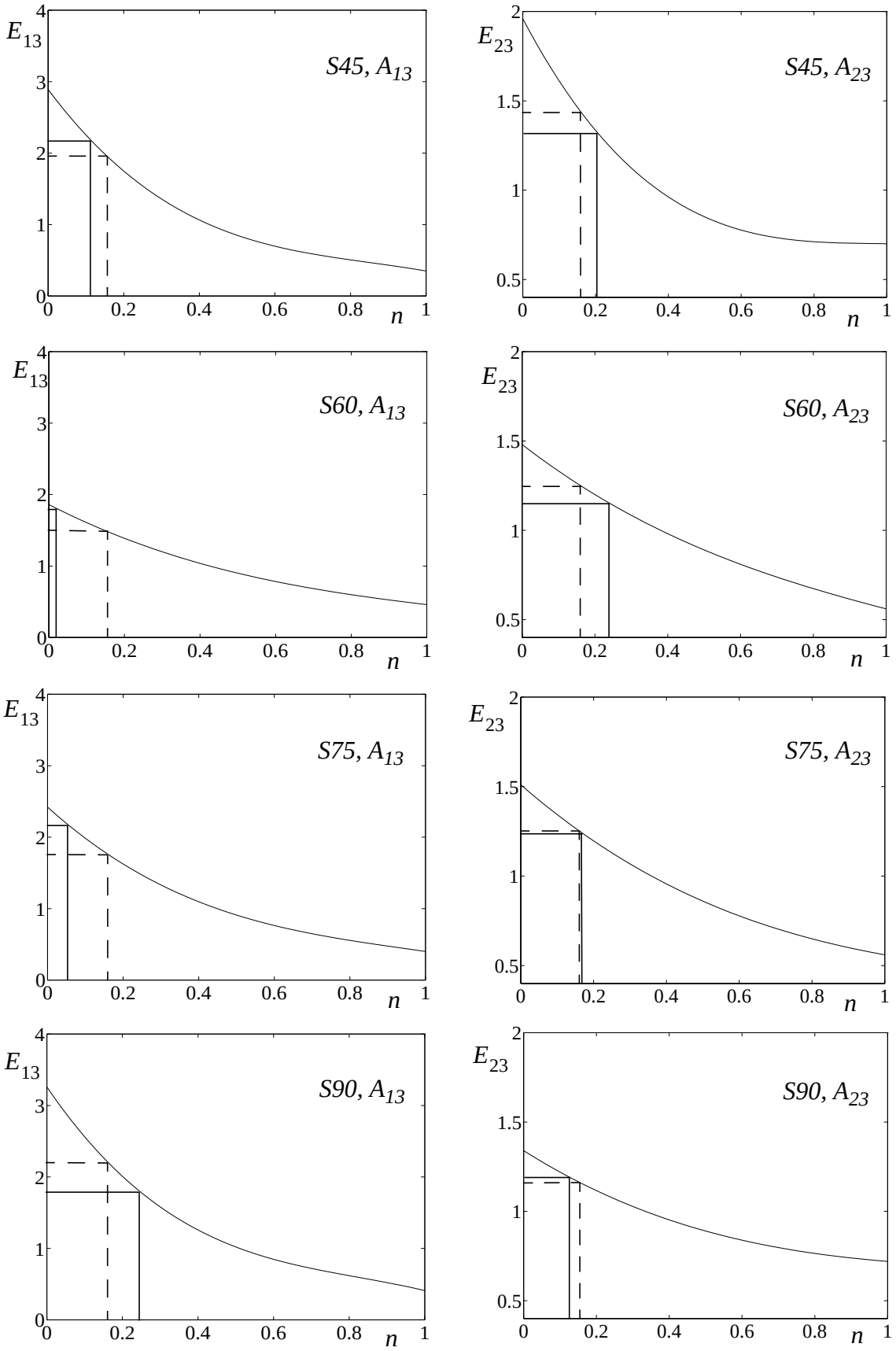

Fig. 2.38. (continuation) Correlation between geometrical and mechanical anisotropy factors. Solid straight line corresponds to the measured n and broken line is associated with the accepted $\bar{n} = 0.15$.

(but still regular) foam geometrical features, namely, struts orientations. Nevertheless, the regular nature of this modelling makes it impossible to approach a real foam geometry closely. This causes the necessity to incorporate anisotropy in the random model.

2.3.5 Anisotropic random model

An idea to apply the previously described method of the anisotropic arrangement in a regular foam model to the random model from Section 2.3.1 is evident.

First, the randomly distributed nuclei are generated in a box, as shown in a 2D analogue in Fig. 2.39a (a presentation of the actual 3D structure would be hardly interpretable from a figure). Then, the nuclei set is extended in the rise and extrusion directions with the primary anisotropy ratios A'_{13} and A'_{23}. The resulting set of random anisotropic nuclei is displayed in Fig. 2.39b as dots. Subsequently, Voronoi tessellation is applied to this ("stretched") nuclei set. The resulting Voronoi structure is shown in Fig. 2.39b as lines. The final structure is obtained by the extension of this structure in the rise and extrusion directions by secondary anisotropy ratios A''_{13} and A''_{23} and is demonstrated in Fig. 2.39c. Finally, a random unit cell is created, as described in Section 2.3.1. The main problem in this modelling is to determine the degree of the initial anisotropy n of the real foam to be modelled.

It must be noted that the anisotropic foam structure resulting from this modelling does

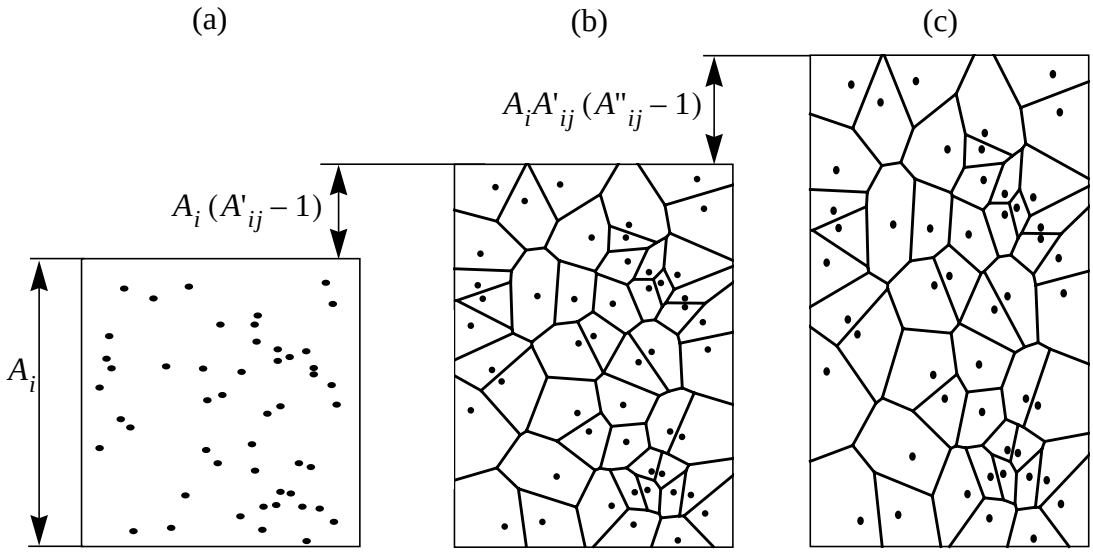

Fig. 2.39. Creation of an anisotropic unit cell (2D analogue). (a) Random nuclei set. (b) Extended random nuclei set with anisotropy factor A'_{ij} and Voronoi tessellation based on it. (c) Extended Voronoi structure with anisotropy factor $A_{ij} = A'_{ij}A''_{ij}$.

not possess a typical property common to the isotropic model, namely, lines connecting neighbouring nuclei are not perpendicular to the cell walls (see Fig. 2.39c). This results from the sequential application of the primary and secondary anisotropy, while in practice, nucleation and growth take place simultaneously.

Determination of the initial anisotropy degree

As it has been shown above, it is possible to create cells with the same geometrical anisotropy A_{ij}, but with various shapes. The struts orientation related to the main directions is of great importance. It is the dominant parameter that changes in the modelled cells in Fig. 2.36. This causes the necessity to study the real foam microstructure in detail. The orientation of struts in the S08 foam has been studied. No operational experimental method was found so far to determine the 3D distribution of strut angles of real foams sufficiently accurate. Therefore, another method is used. Namely, the 2D projections of the real foam, as shown in Fig. 2.34a, are analysed by the image processing technique. The orientation angles of more than 2000 struts per plane are measured in the planes x_1x_2, x_2x_3 and x_1x_3. The corresponding histograms are shown in Fig. 2.40. Since the difference between the geometry in the transverse and extrusion direction is not pronounced, as can be seen from the first view in Fig. 2.35, the corresponding histogram for the strut angles distribution in the plane x_2x_3 in Fig. 2.40 has fluctuations that are caused by too large scatter and, therefore, this plane is neglected and two other planes, x_1x_3 and x_1x_2, are considered. The histograms in these two directions are fitted by straight lines. This lin-

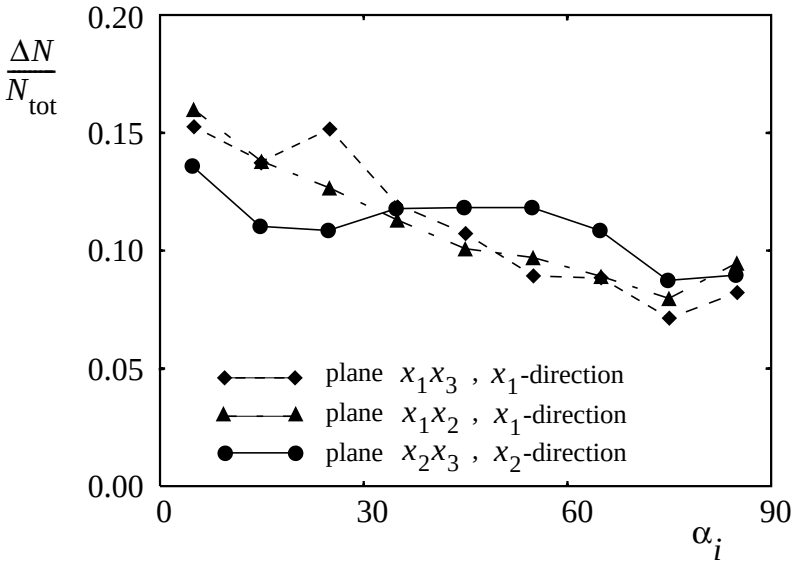

Fig. 2.40. Histograms of measured angles between strut projections and the three directions, in degrees. Step width of the strut angles orientation is 10^o.

earization leads to 2 slopes of -0.0609 and -0.0503 correspondingly. These slopes of the fitting lines characterize the strut angles distributions in the real foam.

Further, a series of models with various initial anisotropy degrees is created. n varies from 0 to 1, with the step of 0.1. In this way, eleven models of the S08 foam are simulated, all with the same total geometric anisotropy ratio obtained from real foam measurements, but with different strut angles distributions due to the variable n. The number of struts varies between 6500 and 3700 per model. The aim of the analysis is the determination of a model with strut angles distributions, similar to the real foam. For this purpose, histograms of strut angles distributions in planes x_1x_2 and x_1x_3 of all models are generated in a way similar to the real foam. The fitting of the corresponding histograms by straight lines allows the determination of the slopes of strut angles distributions per model. A plot of these slopes against the initial anisotropy degree n is given in Fig. 2.41. By applying the measured strut angles distributions in two planes of the real S08 foam to this plot, i.e., by adopting the empirical slopes of the real foam as values on the vertical axis, the corresponding degrees of initial anisotropy are found. The values of n are characteristic for the specific structure and may be applied in the modelling. Two different values of n are obtained, namely, 0.35 and 0.41. The average n equal to 0.38 can be applied in the present random anisotropic foam model.

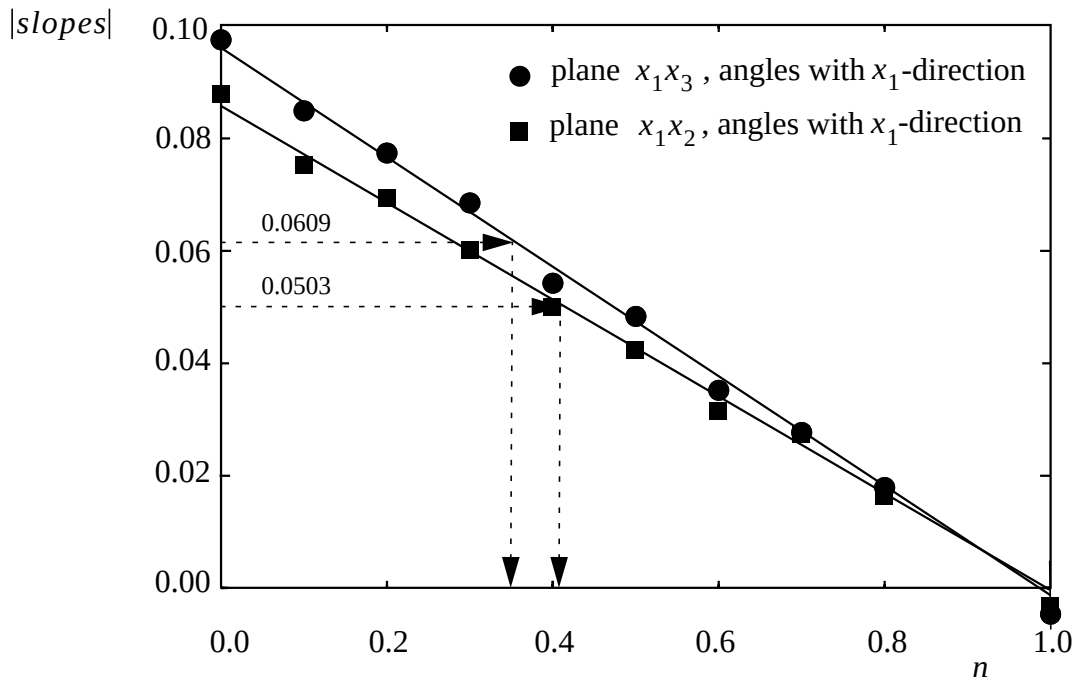

Fig. 2.41. Determination of the initial anisotropy degree n. Slopes here correspond to the linear fitting of angles distributions as shown in Fig. 2.40.

Determination of the degree of initial anisotropy from the measured distribution of strut angles

The method used above is based on the comparison of strut angles distributions of the real foam and of models to choose the correct model. In this analysis, histograms of the strut angles projections on planes are fitted by straight lines to determine the slope of these lines, which is used as a decisive factor in the choice of a model. But the correctness of such a fitting may be subjected to question because struts distributed in an anisotropic way may have a non-linear probability density function. To find this function, which is also a fit-function, first, a uniform isotropic distribution of struts in 3D is assumed. The projection of the arbitrary strut r_i on the plane x_1x_3 has an angle α_i with the x_1-axis, as shown in Fig. 2.42 by thick lines. The probability of angle α_i lying between angles α_I and α_{II} is equal to the ratio of the length of the arc AB to the length of the half-circle with the radius r_i. It turns out that the density of probability distribution is uniform and equal to

$$g = \frac{1}{\pi}. \tag{2.40}$$

After the expansion of the structure in the x_1 direction with the geometrical expansion ratio ε, what corresponds to the secondary geometrical anisotropy factor A''_{13} by

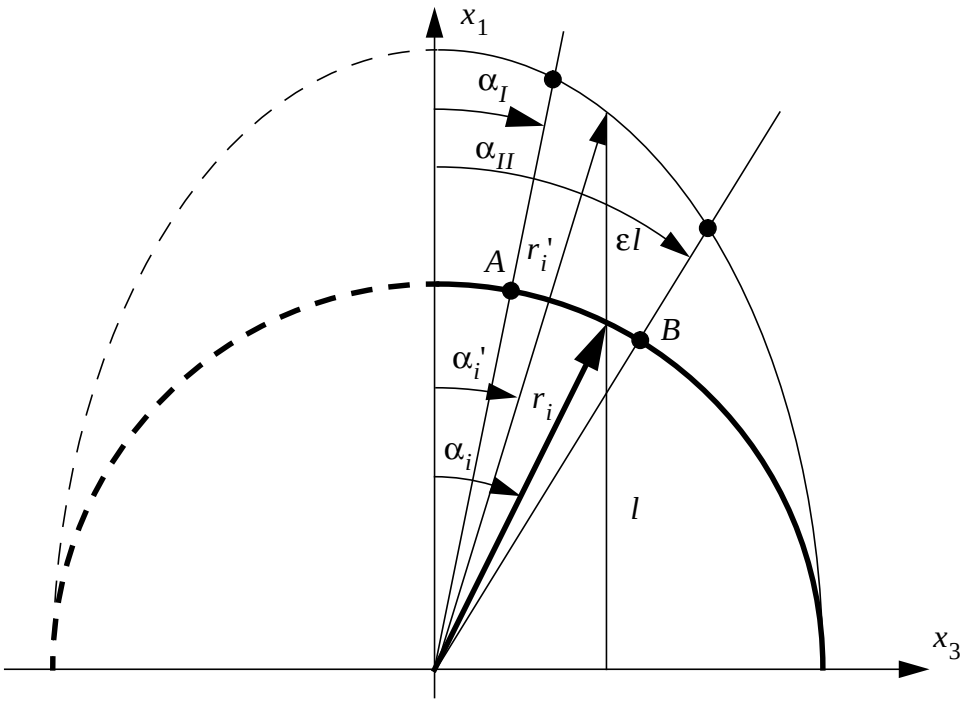

Fig. 2.42. Projection of a strut before (r_i) and after (r'_i) the anisotropic extension A''_{13}.

$$A''_{13} = 1 + \varepsilon, \tag{2.41}$$

the projection of the arbitrary strut r_i gets a new position r'_i with a new orientation angle α'_i to the x_1-axis. The correlation between the original orientation α_i and the new orientation α'_i is

$$\alpha'_i = \arctan\left(\frac{\tan\alpha_i}{1+\varepsilon}\right) \text{ or } \alpha_i = \arctan\{(1+\varepsilon)\tan\alpha'_i\}\,. \tag{2.42}$$

The probability distribution function is then:

$$g'd\alpha' = gd\alpha \text{ and } g' = g\frac{d\alpha}{d\alpha'}. \tag{2.43}$$

From Eq. (2.42) it follows that

$$\frac{d\alpha}{d\alpha'} = \frac{d}{d\alpha'}[\arctan\{(1+\varepsilon)\tan\alpha'\}]\,. \tag{2.44}$$

Substituting the solution of Eq. (2.44) in Eq. (2.43) leads to the following probability distribution function for the case of the anisotropic structure

$$g' = \frac{1+\varepsilon}{1+\varepsilon(2+\varepsilon)(\sin\alpha')^2}\,g\,. \tag{2.45}$$

At small ε, the probability distribution g' as a function of ε may be approximated by a straight line. In general, this function is not a linear one and should be used to fit measured strut angles distributions from Fig. 2.40. The fitting with the smallest squares method shown in Fig. 2.43 yields the values of the expansion ratio ε from Eq. (2.45). This expansion ratio is determined per projection plane and is given in Table 2.5. The corresponding values of the initial anisotropy degree n can be derived from Eq. (2.38) and Eq. (2.41),

Table 2.5. Values of the expansion ratio ε with standard deviation and corresponding initial anisotropy degree n

Projection plane	A_{ij}	ε	n
x_1x_3	1.78	0.41 ± 0.05	0.40 ± 0.06
x_1x_2	1.56	0.36 ± 0.04	0.31 ± 0.07
x_2x_3	1.14	0.13 ± 0.05	0.06 ± 0.35

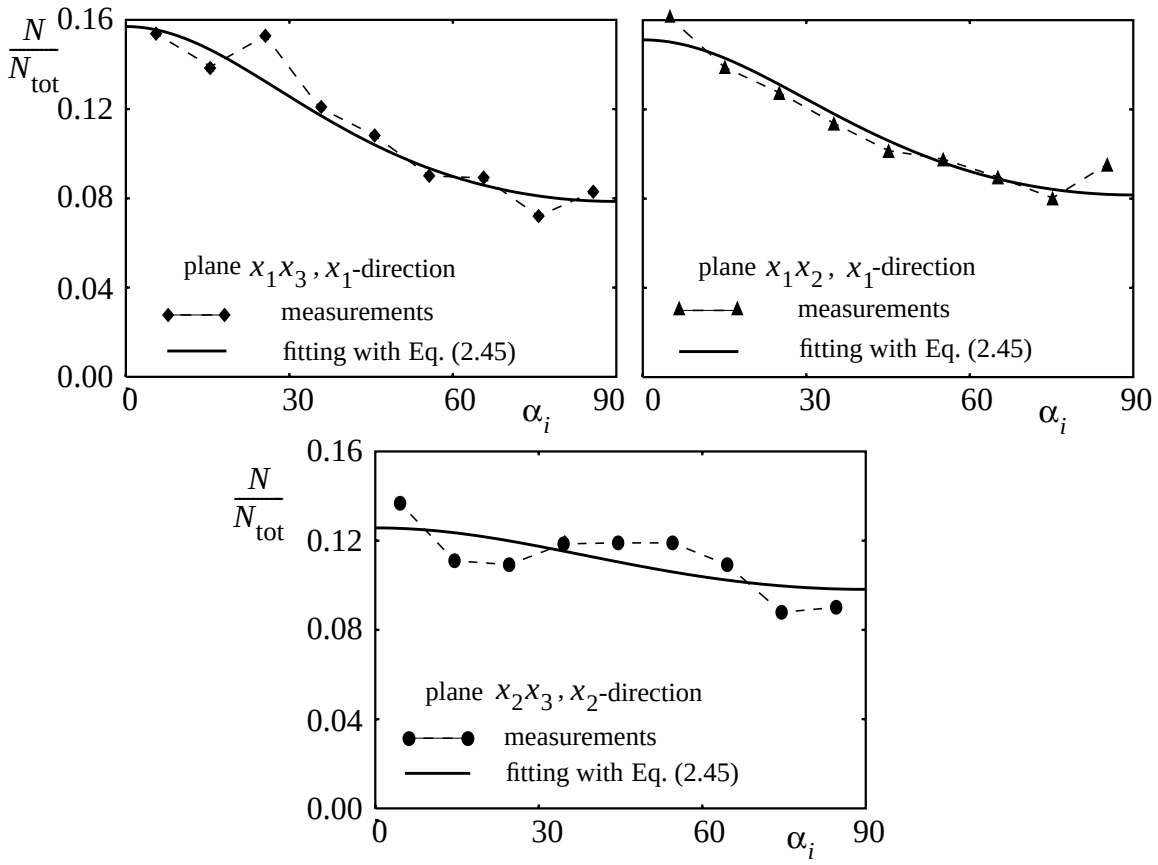

Fig. 2.43. Histograms of the measured strut angles distributions from Fig. 2.40 and their fitting by Eq. (2.45).

leading to:

$$n = 1 - \frac{\log(1+\varepsilon)}{\log(A_{ij})}. \tag{2.46}$$

The initial anisotropy degree n is also given in Table 2.5. The obtained results demonstrate that the measurements of the strut orientations in 2D are quite accurate for planes x_1x_3 and x_1x_2 (see the values of n for these two planes in Table 2.5), but exhibit considerable deviation in case of the plane x_2x_3. The latter results are, therefore, inaccurate and are not used in this analysis.

From the two values of n for the planes x_1x_3 and x_1x_2 the averaged n would be nearly equal to 0.36. This result is not far from that obtained earlier by another method, when the measured strut angles distributions were compared to those of the models (see Fig. 2.41). The initial anisotropy degree accepted then was equal to 0.38.

The primary geometrical anisotropy A'_{ij} has almost no influence onto the changes of the strut orientation distributions. It is clearly seen from Fig. 2.41, where random models

with the initial anisotropy degree $n = 1$, i.e., $A''_{ij} = 0$, have practically uniform strut angles distributions. The primary anisotropy affects lengths of struts making struts oriented in the rise and extrusion directions more elongated.

Young's moduli of the anisotropic model

To study mechanical properties of the anisotropic foam S08, a set of five random anisotropic unit cells with approximately 250 foam cells per unit cell has been created. This procedure follows that described in Section 2.3.1, but with several exceptions. Firstly, the 3D Voronoi tessellation is based on the anisotropic nuclei set which is obtained from the isotropic one by the extension of the nuclei in the rise and extrusion directions with the primary anisotropy ratios $A'_{ij} = A_{ij}^{0.38}$. Secondly, the unit cell created in this way is subjected to geometrical extension in the same directions with the secondary anisotropy ratios $A''_{ij} = A_{ij}^{0.62}$.

The resulting unit cell is assumed to have the same strut angles distribution as a real foam. The macroscopic foam properties are subsequently analysed by application of the standard MARC FE program to the generated unit cells. Struts are represented as elastic beam elements that have a constant and same circular cross-section. All 5 unit cells are loaded uniaxially in three main directions and an elastic analysis is performed.

For each case, elastic moduli of the foam model in three main directions are determined with Eq. (2.39). The computational results are summarized in Table 2.6 which also reveals the experimental results.

The other two anisotropic models (cubic and tetrakaidecahedron illustrated in Figs. 2.3b and c respectively) are also used to predict the mechanical anisotropy factors E_{13} and E_{12}. The results of the cubic model obtained from Eq. (2.6) are given in Table 2.6. The mechanical anisotropy factors of the tetrakaidecahedron are computed using a unit cell based on the bcc-distributed nuclei set.

It is clear from the comparison of these three models that the random model gives results which are in a good agreement with the measured values. The cubic model and the tetrakaidecahedron lead to models that are far too stiff and, therefore, are obviously not suitable.

The present analysis, based on the application of two types of anisotropy described by n obtained from the real foam measurements, leads to a correct model. For the S08, the initial anisotropy degree n is nearly equal to 0.38. It is assumed that this degree of initial anisotropy as related to for the physical processes during foam production and will be

Table 2.6. Mechanical anisotropy of open-cell PUR foams

Foam type	Measured mechanical anisotropy [Eq. (2.39)]		Mechanical anisotropy of random model		Mechanical anisotropy of cubic model [Eq. (2.6)]		Mechanical anisotropy of tetrakaidecahedron model	
	E_{13}	E_{23}	E_{13}	E_{23}	E_{13}	E_{23}	E_{13}	E_{23}
S08	3.80	1.31	3.30 ± 0.20	1.36 ± 0.08	6.22	1.80	6.65	1.48
S20	2.70	1.07	*2.43± 0.13*	*1.05± 0.03*	3.76	1.04	4.15	1.02
S30	2.11	1.19	*2.18± 0.03*	*1.35± 0.06*	3.46	1.78	3.25	1.54
S45	2.20	1.33	*1.97± 0.16*	*1.63± 0.16*	3.28	2.35	2.86	1.94
S60	1.80	1.14	*1.41± 0.07*	*1.18± 0.10*	1.97	1.59	1.90	1.48
S75	2.17	1.25	*1.69± 0.06*	*1.27± 0.06*	2.57	1.68	2.42	1.50
S90	1.82	1.21	*1.98± 0.11*	*1.19± 0.05*	3.28	1.49	3.28	1.36

Note: results presented with italic characters are based on n obtained from the measurements of the S08 foam

approximately the same for the other 6 available foam kinds S20...S90, also present in Table 2.6. To check this assumption, these foams have also been modelled by an anisotropic random model with $n = 0.38$. Each foam kind is modelled five-fold and mechanical anisotropy factors E_{13} and E_{12} are determined and shown in Table 2.6. These values are presented with italic characters, because they are all based on $n = 0.38$ as obtained from the S08 foam.

Modelling of aluminium foam

To evaluate the model, open-cell aluminium foam is studied. This foam has been chosen because of the known mechanical properties of the solid aluminium inside the foam. First, the density of the foam ρ_f was measured (see Table 2.7). Then, the microstructure of the foam has been studied with a SEM. Figure 2.44 demonstrates a view of the foam, which clearly shows that the structure is geometrically anisotropic. The geometrical anisotropy ratios A_{ij} have been determined through the measurements of the cell dimensions in three orthogonal directions. Further, it should be noted that the vertices contain a considerable part of the solid material. This detail is important for the modelling, because the solid concentrations in vertices are hardly deformed during the global deformation and will be neglected in the modelling. This yields a foam model with lower density.

Table 2.7. Geometrical features and Young's modulus of the aluminium foam

Foam feature	Values
Density of solid, ρ_s [kg/m^3]	2700
Measured foam density, ρ_f [kg/m^3]	217
Measured struts cross-section, a [mm^2]	0.0258
Measured average cell diameter in the transverse direction, D [mm]	2.0
Model average cell diameter in the transverse direction, D' [m]	0.15
Scale factor, $M = D/D'$	0.0133
Model cell struts cross-section, a' [mm^2]	145
Total struts length in the random model, $\sum l_i$ [m]	200.1
Calculated foam density of the random model, ρ_f' [kg/m^3]	56
Young's modulus of solid, E_s [MPa]	70000
Measured foam Young's modulus in the rise direction, $E_{1,f}$ [MPa]	85
Measured foam Young's modulus in the extrusion and transverse directions, $E_{2,f} = E_{3,f}$ [MPa]	30
Foam Young's modulus of the random model with the circular struts in the rise direction, $E_{1,f}$ [MPa]	65
Foam Young's modulus of the random model with the circular struts in the extrusion and transverse directions, $E_{2,f} = E_{3,f}$ [MPa]	20
Foam Young's modulus of the random model with the struts having Plateau-Gibbs cross-section in the rise direction, $E_{1,f}$ [MPa]	92
Foam Young's modulus of the random model with the struts having Plateau-Gibbs cross-section in the extrusion and transverse directions, $E_{2,f} = E_{3,f}$ [MPa]	29
Measured Young's moduli ratio, E_{13}	2.83
Young's moduli ratio of the model, E_{13}	3.25

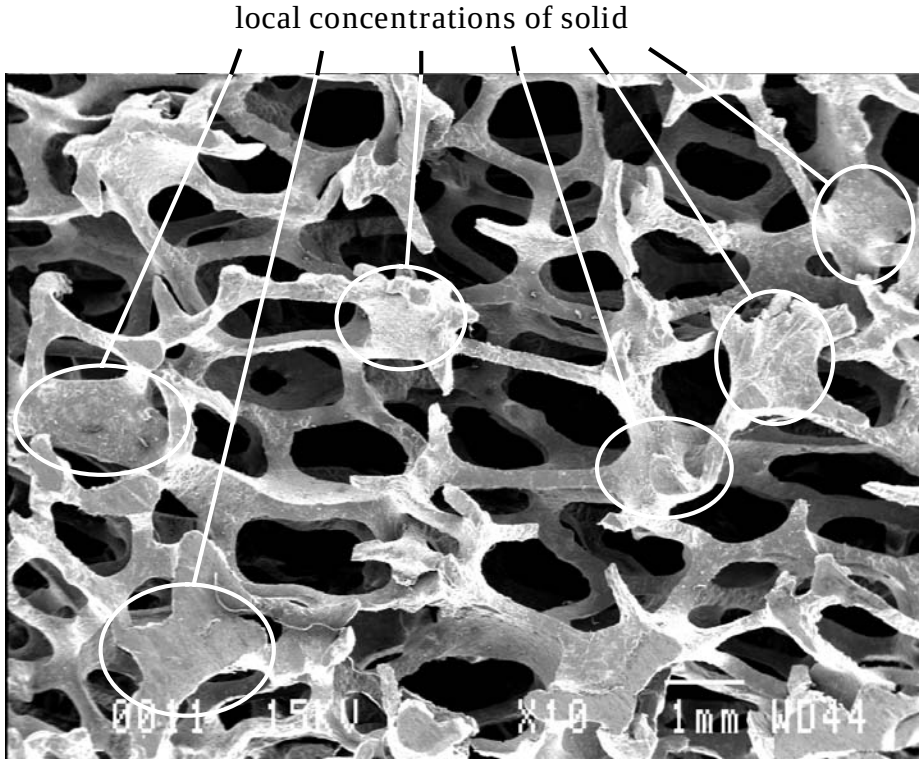

Fig. 2.44. View of open-cell aluminium foam.

The anisotropic foam model is created based on the measured cell geometry and on the assumption that the initial anisotropy degree n is equal to 0.38, as determined for the PUR foam. The cell diameters D in the three directions are measured with the image processing technique. The foam cells in the extrusion direction have almost the same dimensions as in the transverse direction, i.e., $A_{23} \approx 1$, and this foam is assumed to be transversely isotropic. The results of the measurements are given in Table 2.7 together with the mean cell diameter of the model in the transverse direction D'. The scale factor between the model and real foam comprises then $M = D/D'$. This scale factor is used to translate the strut cross-sectional area a of the real foam measured with the image processing technique to the circular cross-section of the struts in the model a'. Further, the total strut length $\sum l_i$ in the model is computed and, therefore, the density of the foam model ρ_f' is determined by Eq. (2.26). The discrepancy in the measured ρ_f and modelled foam densities ρ_f' in Table 2.7 can be explained by the concentration of the very large part of the solid material in the vertices which is not considered in the model.

The Young's moduli of foam are measured in the compression experiments completed at cubic samples in the three directions at a deformation rate of 0.015 min^{-1}. The resulting moduli in the rise and extrusion–transverse directions are, on the average, 85 *MPa* and 30 *MPa* respectively.

The anisotropic random FE model is created as described above. The Young's modulus of the unit cell is determined in the linear elastic analysis in FEM through the application of a uniaxial global compressive stress to the unit cell boundaries in the three orthogonal directions. The resulting Young's moduli $E_{i,\,\mathrm{f}}$ of the random foam model with density $\rho_{\mathrm{f}}' = 56\ kg/m^3$ was found to coincide quite good with the measured values (see Table 2.7). The further improvement of the model may be achieved by the introduction of the struts having Plateau-Gibbs cross-section with the second moment of inertia taken from Eq. (2.25) as given by Warren and Kraynik (1997). The resulting Young's moduli of the foam were predicted with a good accuracy.

2.4 Discussion and Conclusions

Low-density open-cell foam is modelled using the geometry of Voronoi tessellation. Nuclei in the Voronoi technique resemble the location of the gas bubbles. In this sense, the final foam geometry in the model is reasonably physically based. Starting from regular bcc and fcc lattice nuclei distributions, and subsequently giving the nuclei positions an increasing random offset, a smooth continuous transition has been made from regular foam geometries to completely random geometries.

To analyse the mechanical properties of the foam, a unit cell was cut out of the strut network. The open-cell foam unit cell constitutes a framework of struts in 3D. To incorporate the randomness adequately in the unit cell, the cell length scale is much larger than the average strut length. Assuming the struts to deform like beams and using FE techniques, the elastic foam model properties were determined for an overall uniaxial tensile stress.

The linear elastic properties of these unit cells have been compared with other models from literature, often based on a much smaller unit cell size. Thus, it is shown that disorder significantly determines the mechanical properties of the foam. Starting from regular geometries, Young's modulus and Poisson's ratio increased strongly with increasing disorder. This effect is explained by the appearance of chains of struts under high normal stresses, which percolate the foam and thus are mainly responsible for the load transmission through the foam.

A number of assumptions has been applied to the random model, namely:

- all solid material is distributed in struts and not in vertices;
- all struts are of the same and constant cross-section (leads to a stiffening of the model);
- the solid material in all struts has constant properties;
- the strut cross-section is simplified by a circle instead of the Plateau-Gibbs border (introduces a decrease of the struts bending stiffness).

Moreover, the struts positioned at the boundaries of the random model cause an additional stiffness of the model. Nevertheless, the random model showed a good agreement with the regular cubic model of Gibson and Ashby, which, as opposed to the random model, presents fitting of the experimental data and, therefore, is not useful for studying the effect of parameters like anisotropy and degree of randomness.

Investigating the dependence of Young's modulus on the foam density, indications are found that the normal deformation is of increasing importance relative to bending deformations for higher densities. The overall Young's modulus of random foams has been found to obey the Gibson and Ashby (1988) estimate to a very good accuracy for foam densities ρ_f/ρ_s smaller than 0.03.

When the foam relative density ρ_f/ρ_s exceeds $(0.3\ldots0.5)$, the random model described above becomes invalid. This is explained by the fact that, within the range of the model's validity, open-cell foam contains slender struts that are consequently implemented in the FE program as beam elements. Outside of this range, concentrations of the solid material in vertices (see Fig. 2.44) cannot be neglected anymore and the assumption of slender struts that have a constant cross-sectional area becomes invalid.

The random model has been extended to perform nonlinear analyses. The foams are subjected to uniaxial stress, either tensile or compressive, and the nonlinear analyses are accomplished by modelling the struts as beams and using standard FE techniques. The nonlinear elastic analyses are applied to random and regular microstructures, where the Voronoi tessellation is based on randomly distributed nuclei and nuclei stacked according to the bcc and fcc distributions, respectively.

The stiffness of the regular foams is virtually constant when the strains remain sufficiently small. In this region, the struts deform primarily by bending. With increasing strain, the region is entered where the stiffness increases linearly. The stiffness of the foams is determined here by the continuously changing combination of bending and axial deformation of struts. It is illustrated that the reason for this lies in the gradual re-orientation of the struts in the global stress direction. The influence of the axial strut deformation increases with increasing strain, and at a certain strain level, the global stiffness becomes constant. In this region, the majority of struts is aligned in the global stress direction and they deform axially only.

The axial deformations of struts in the random foam model are important even at very small strains. This is explained by the existence of chains of struts that are percolating the unit cell and which are loaded axially already in the initial deformation stage. At large tensile strains, the limiting stiffness is approached, which is found to be lower than that of the

regular models. The effective unit cell cross-section A_{eff} is an important factor for the foam stiffness under large tensile strains. The model with the highest minimum A_{eff}, or with the strongest "weak" place, will possess the highest stiffness in the large global deformations region. In this way, it can be understood why the regular rhombic dodecahedron model having a constant A_{eff} is the stiffest at large strains. The same high A_{eff} cannot be reached by a random foam model with the same foam density.

The above results are obtained for a linear elastic response of the struts. In the case of a nonlinear material behaviour, the deformation of the struts will remain roughly the same, so that the ultimate axial stiffness of struts determines the final foam stiffness.

During the compressive deformation of foam, the elastic collapse stress of the random foam model is found to obey the estimate Eq. (2.7) of Gibson and Ashby (1988) which was based on experimental observations. The accuracy of the model can be improved by incorporating the nonlinear material behaviour in compressed struts instead of the more simple linear elastic material used here. The importance of this effect grows with an increasing relative foam density.

Application of a simple bilinear constitutive model for the solid material in struts gives a more realistic elastomeric foam behaviour than linear elastic. This increases the accuracy and applicability of the model.

Due to the Voronoi technique, a new kind of geometrical anisotropy—primary anisotropy of the nucleation points—is described. This allows for variation of the regular cell shape without changing the average cell dimensions. The primary geometrical anisotropy is related to the anisotropic distribution of the nuclei before their growth and the nucleation process during the growth. The secondary geometrical anisotropy is associated with the extension of the foam structure due to the effects of extrusion and growth. The combination of the primary and secondary anisotropy factors makes it possible to choose the cell in such a way that the geometrical and mechanical anisotropy factors of cells of the model have a direct correspondence with that of a real foam macrostructure. The degree of initial anisotropy, n, is implemented to evaluate the ratio between the primary and the secondary geometrical anisotropy factors.

A series of regular bcc-based models with constant geometrical anisotropy ratios and various n is created. To determine a regular model that correlates best with the measured values, seven anisotropic open-cell foam types with various anisotropy ratios A_{ij} are tested and their mechanical anisotropy ratios E_{ij} are compared with those of the regular models. The value of n is chosen to be 0.15. The relative error comprises 23% at most in comparison with the measured values. This shows a good agreement of the model with the

experimental results.

A similar method is applied to the random foam model to introduce anisotropy effects. It was found that the initial anisotropy degree n influences the strut orientations distribution in the model. To choose the adequate model, the strut angles distributions in the open-cell S08 foam have been measured and the model with the corresponding strut angles distributions has been found. The respective n was equal to 0.38. The results of the modelling of the measured foam are satisfactorily good. They predict the mechanical anisotropy of the real foam structure better than the cubic model of Huber and Gibson and better than the anisotropic tetrakaidecahedron model.

The assumption has been made that the value of n is approximately the same for the whole set of the available foam structures. Based on this assumption, the same value of the initial anisotropy degree has been applied to the models of the other six foam structures and mechanical anisotropy has been determined. The obtained values of E_{ij} were in almost all cases the same as or better than the ones predicted by the cubic model of Gibson and Ashby.

To evaluate the anisotropic linear elastic open-cell foam model, an aluminium foam has been measured and tested. The mechanical properties of the solid aluminium in the foam were known and, for this reason, the aluminium foam was ideal for the verification of the adequacy of the model geometry. The estimation has been made that the initial anisotropy degree n was equal to 0.38, as measured for the PUR foam. The struts were modelled by the circular beams in the FE model. The density of the model was corrected by taking into account the concentrations of the solid material in the vertices. The resulting Young's moduli of the model occurred to be somewhat lower than the measured values. After application of the struts having the Plateau-Gibbs cross-section, the Young's moduli of the foam were predicted very accurately.

The further development of the random anisotropic model may be conducted by:

- Measuring the strut angles orientations in 3D instead of 2D strut projections.
- Measuring a greater number of struts, instead of approximately 2000 per direction as done here.

However, these improvements would be extremely elaborate, offering only limited additional accuracy and limited additional insight into the mechanical behaviour of foam.

3. Closed-cell foams

3.1 Introduction

Closed-cell foams as opposed to the open-cell foams contain cells with membranes. Due to this difference, closed-cell foams possess quite different properties and, therefore, find different applications. For example, closed cells contain gas which increases the thermal isolation properties of foam. As a result, closed-cell foams found numerous applications as an isolation material. Moreover, the presence of the cell membranes increases the mechanical properties of foam considerably and this leads to the use of such foams as a structural material, e.g., as a core in sandwich panels. For instance, the side walls of trucks for transportation of frozen food are sandwich structures.

As it has been shown in Chapter 2, there are only two features that determine the mechanical properties of the open-cell foams—the properties of the solid material in struts and geometry. As far as closed-cell foams contain gas inside the cells, the gas also might affect the mechanical properties of closed-cell foam. Figure 1.1 demonstrates the main influencing factors comprising the mechanical properties of this class of foams.

Typical examples of closed-cell foams are shown in Fig. 3.1. All three components from Fig. 1.1 are different for these two foams, which will be discussed first. The solid material is polymethacrylimide (PMI) in Fig. 3.1a and extruded polystyrene (XPS) in Fig. 3.1b. The difference in the mechanical properties of these two solids also affects the difference in the mechanical properties of corresponding foams. The other aspect—cell geometry—has also decisive influence onto the foam properties. A number of geometrical features of foams and their effects have already been mentioned in Chapter 1. Geometrical anisotropy of cells clearly seen in Fig. 3.1b is one of them. Irregularity of the structure is

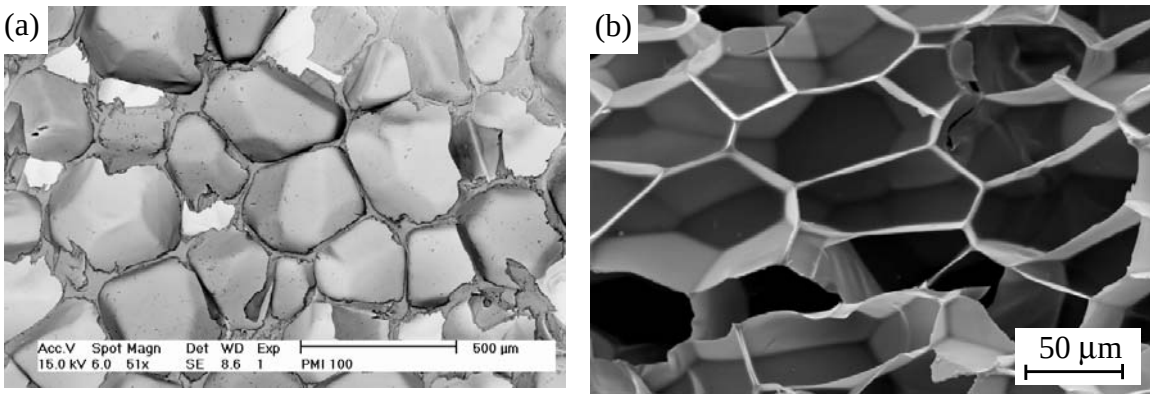

Fig. 3.1. Views of (a) PMI and (b) XPS foams.

also visible. Geometrically, the foam structure may be described as a cell network consisting of the cell faces, edges and vertices. For the low-density foams, faces and edges may be simplified by walls of a constant thickness and struts of a constant cross-sectional area. In addition, vertices are assumed to be knots, not containing any material concentrations and negligibly small.

To make an adequate model of the closed-cell foam, all these components should be accounted for.

3.2 Survey of the existing models

To predict mechanical properties of foams, several types of models have been used. In general, the situation with the closed-cell foams modelling is much less satisfactory than with the open-cell foams. The most well-known models may be subdivided in two groups:

- models based on space symmetrical packing (rectangular prisms, rhombic dodecahedra, tetrakaidecahedra)
- an aggregate model that uses the averaging of a small structural volume element over all possible orientations in 3D.

Cubic model

An isotropic closed-cell foam is modelled by Ashby and Gibson (1988) who give an approximate foam Young's modulus related to the solid Young's modulus as a function of the fraction of the solid material in struts ϕ by

$$\frac{E_f}{E_s} \approx C_1 \phi^2 \left(\frac{\rho_f}{\rho_s} \right)^2 + C_1'(1-\phi)\frac{\rho_f}{\rho_s} + \frac{p_0(1-2\nu_f)}{E_s(1-\rho_f/\rho_s)}, \tag{3.1}$$

where p_0 is the gas pressure inside cells, C_1 and C_1' are constants of proportionality, given as $C_1 \approx C_1' \approx 1$. The three terms here correspond to the bending of the solid material in struts, axial deformation of the solid material in walls and the gas pressure inside cells. In many cases of the synthetic foams, the gas pressure inside cells is very close to the atmospheric pressure $p_{at} = 0.1$ MPa and the last term in Eq. (3.1) can be neglected.

Plastic collapse stress Σ_{pl} of foam under compression related to the yielding stress $\sigma_{y,s}$ of the solid material is obtained by

$$\frac{\Sigma_{pl}}{\sigma_{y,s}} = C_2 \left(\phi \frac{\rho_f}{\rho_s} \right)^{3/2} + C_2'(1-\phi)\frac{\rho_f}{\rho_s} + \frac{p_0 - p_{at}}{\sigma_{y,s}}, \tag{3.2}$$

where C_2 and C_2' are constants, determined by fitting of the experimental data and correspondingly equal to 0.3 and 1.

In tension, the cell walls are assumed to become aligned when the global tensile strain ε_f exceeds $1/3$ and to deform consequently axially. Therefore, the collapse stress of foam Σ_{el} in tension is defined as

$$\frac{\Sigma_{el}}{\sigma_{y,s}} \approx \frac{\rho_f}{\rho_s}. \tag{3.3}$$

Tetrakaidecahedron

Another group of models is related to the space-filling polyhedra shown in Figs. 2.2b-d. The most popular of them is the tetrakaidecahedron from Fig. 3.2a, for which the mechanical properties have been studied with the help of FEM by, e.g., Renz and Ehrenstein (1982). This regular cell is the closest from the space-filling regular cells to real foam cells, as has been shown in Table 2.1. Figure 3.2b demonstrates a $1/8$ part of the tetrakaidecahedron used in the analysis. As a result, initial Young's moduli of low-density PVC and PUR foams have been computed. The cell walls thickness δ and strut length l have been measured from the real foams. Various material distributions between cell walls and struts have been used for these two foam models. The deviation between computed and measured Young's moduli comprised 50% at most for PVC foam where only walls are assumed, i.e., the fraction of the solid material in struts $\phi = 0$. In the case of PUR foam, ϕ in the model varied between 1 and 0.8. The measured fraction of solid in struts ϕ was between 0.95 and 0.9. Measured Young's modulus of PUR foam occurred to

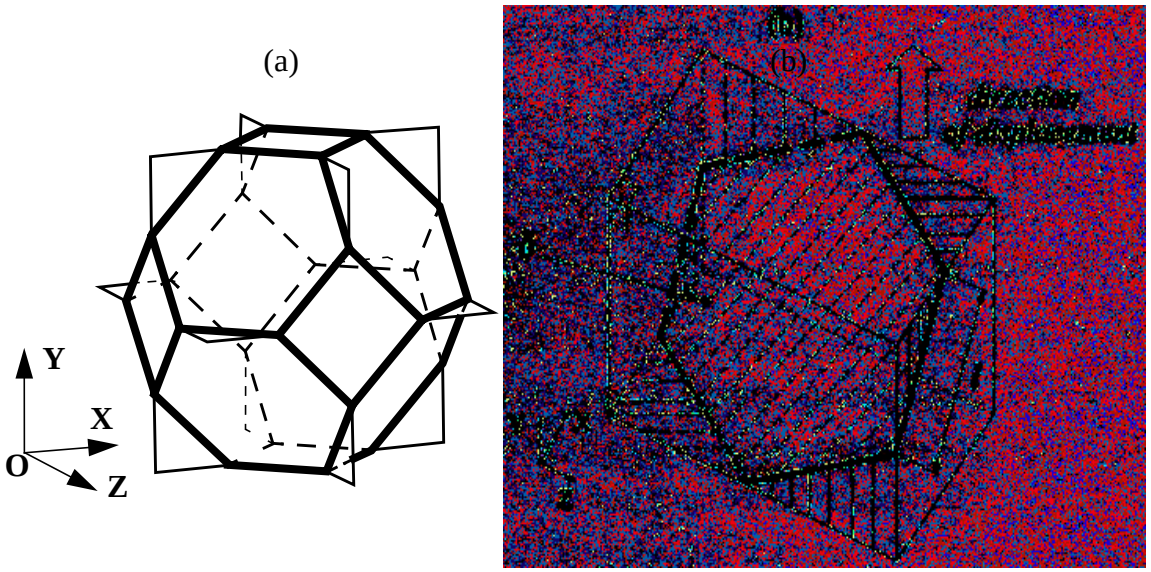

Fig. 3.2. (a) A tetrakaidecahedron and (b) its $1/8$ part.

coincide with the model containing a fraction 0.8 of the material in struts. The corresponding deviation between the measured modulus of the low-density PUR and the model was found to be nearly 100%. This result was called a “good agreement” [Renz and Ehrenstein (1982)].

The situation with the anisotropic closed-cell foam modelling is even less satisfactory than with the anisotropic open-cell foams, described in Section 2.2.1. An anisotropic tetrakaidecahedron with $A_2 = A_3$ has been used by Van Vuure (1997) to predict the Young’s moduli of the anisotropic foams. The resulted Young’s moduli in the rise and the third directions yielded

$$\frac{E_1}{E_s} = \gamma A_{13}\left(\frac{A_{13}}{A_{13}+2}\right)^2\phi^2\left(\frac{\rho_f}{\rho_s}\right)^2 + \beta\left(\frac{A_{13}}{2A_{13}+1}\right)\left(\frac{2}{3}A_{13}^2+\frac{1}{3}A_{13}\right)(1-\phi)\frac{\rho_f}{\rho_s} \qquad (3.4)$$

and

$$\frac{E_3}{E_s} = \frac{\gamma}{2}\left(\frac{A_{13}}{A_{13}+2}\right)^2\left(\frac{1}{A_{13}}+\frac{1}{A_{13}^4}\right)\phi^2\left(\frac{\rho_f}{\rho_s}\right)^2 + \frac{\beta}{3}\left(\frac{A_{13}}{2A_{13}+1}\right)\left(\frac{1}{A_{13}^2}+\frac{1}{A_{13}}+1\right)(1-\phi)\frac{\rho_f}{\rho_s}, \qquad (3.5)$$

where coefficients γ and β are taken to be 9 and 3 correspondingly.

3.3 Regular closed-cell foam modelling

Further development of the regular isotropic closed-cell tetrakaidecahedron has been performed. The low-density closed-cell XPS foam with density $\rho_f = 31\ kg/m^3$ depicted in Fig. 3.1b is a subject of study and experiments. First, a number of experiments and measurements are performed to determine the geometrical features of the foam and the mechanical properties of the foam.

3.3.1 Experiments

Compression test

The compression tests for anisotropic XPS foam, illustrated in Fig. 3.3a, are done with a specimen geometry and dimensions according to the ASTM D1621 testing procedure for rigid foams. The cross-section has a square shape with an area of 1600 mm^2. The height is 40 *mm*. The specimens are stored more then 40 hours before the test in a standard atmosphere of $23°C \pm 1°C$ and a relative humidity of $50\% \pm 2\,\%$.

Because the foam is anisotropic and has three main directions, the experiments are

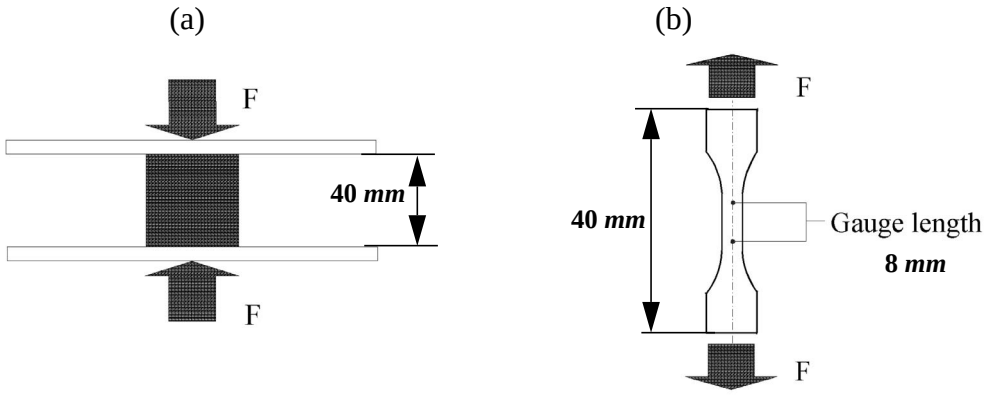

Fig. 3.3. (a) Compression and (b) tensile tests of the XPS foam.

performed in all three directions. 5 samples are tested in each direction and the specimens are deformed to 90% of their original size. The chosen deformation ratio is 0.25 min^{-1}. The results of the experiments are presented in Fig. 3.4 in the form of the mean values without standard deviation which was negligibly small.

Tension test

The tension tests for XPS foam are done with so-called dogbone-shaped specimens. The dimensions are smaller than the normalised specimens because of the limited dimen-

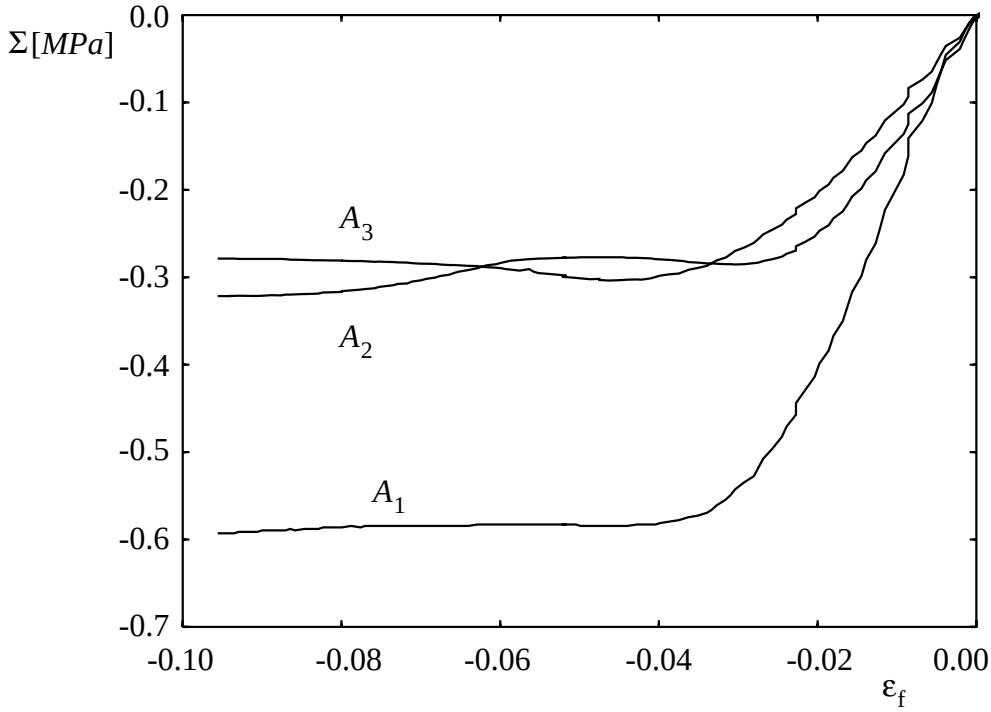

Fig. 3.4. Results of the compression experiments (averaged over 5 samples) on XPS foam in three directions.

sion of the available foam in rise direction (40 *mm*). The tested cross-section area (6 mm^2) however consists of more than 2000 cells (cell diameter $D = 60\ \mu m$), consequently continuum behaviour is approximated. Because the influence of the boundaries is relatively high, in total 16 samples are tested. The specimen shape is displayed in Fig. 3.3b. The specimens are stored more then 40 hours in standard atmosphere in which testing takes place before the actual test. The specimens are prepared by using an aluminium form with dogbone shape and cut with a 0.1 *mm* thick hot wire.

To prevent breaking of the specimen at the clamping edges, the clamping force is regulated in such a way that breaking at the clamps and slipping of the specimen in the clamp is prevented. Sandpaper between the clamps and the specimen was used additionally in order to enhance friction. The results of the tensile experiments in three directions with confidence interval are shown in Fig. 3.5.

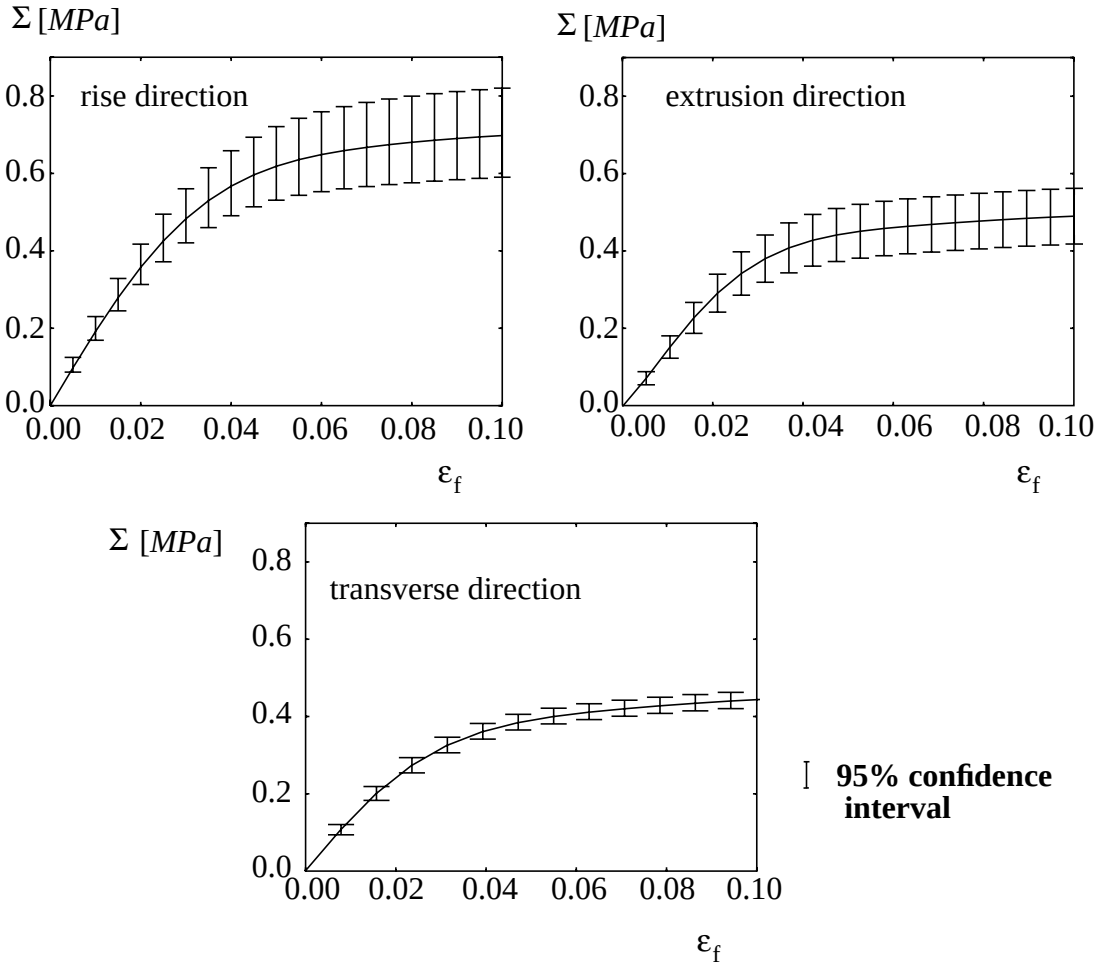

Fig. 3.5. Results of the tension experiments (average over 5 samples with confidence interval) on XPS foam in three orthogonal directions.

3.3.2 Model

Geometry and density of foam

For the regular tetrakaidecahedron structure the density of foam can be determined as a function of the geometry and density of the basic material, ρ_s.

A tetrakaidecahedron in Fig. 3.2b contains 36 struts of the length l and cross-section a. The volume of the $1/8$ part of the tetrakaidecahedron is

$$V = 2\sqrt{2}l^3. \tag{3.6}$$

If the weight of the cell is concentrated in struts and walls (the mass of the gas inside of the cell is neglected), and taking into account that walls and struts at the border of the unit cell are shared by two neighbouring elements, the mass of one element is

$$M = \left[3al + \frac{3+6\sqrt{3}}{4}\delta l^2\right]\rho_s. \tag{3.7}$$

The density of foam is

$$\rho_f = \frac{M}{V} \text{ or } \rho_f = \frac{1}{2\sqrt{2}l^2}\left[3a + \frac{3+6\sqrt{3}}{4}\delta l\right]\rho_s. \tag{3.8}$$

a and l are measured from the SEM micrographs taken at 9 different places of a foam plate with the dimensions $250 \times 60 \times 4\ cm^3$.

The surface of the microscopic slide is observed in order to find intersected struts. Once an intersection is found, the slide is turned in such a way that the strut length is in the plane of the picture. Now the strut length can be measured from the picture or the screen, taking into account the realised magnification. This procedure is repeated 2 times for each of the 9 mentioned parts of the plate.

The detection of the cross-sectional area a of a strut is analogous to the above mentioned procedure.

Tension-compression deformation

A one-eighth part of the tetrakaidecahedron is a representative part of the structure due to the geometrical and load symmetry. A constraint is implemented in the model that allows the opposite pairs of surfaces to remain parallel during the deformation. The distance between opposite surfaces is allowed to change from one increment to another.

Walls are assumed to have constant thickness δ. Struts of the foamlike structures are known to have a shape of Plateau-Gibbs borders as in Fig. 2.11a. For the simplification of the model, struts are assumed to be straight and to have a constant circular cross-section a.

Using data for the density of the solid XPS given by Van Krevelen (1976), ρ_s, and Eq. (3.8), the wall thickness δ has been determined. It is given in Table 3.1. Mechanical properties of polymers are time dependent. However, published data are in general obtained with deformation rates similar to those chosen here (0.25 min^{-1}). Consequently, the time scales and mechanical properties are similar and specific attention to time dependent polymer behaviour is not necessary.

Preliminary FEM analyses indicated that strut local strains, associated with the struts bending, are relatively small as compared to wall strains, related to the walls stretching. Consequently, a simplification can be made for the later computations: the basic polymer in struts is assumed to deform elastically. At the same time, the material in walls is considered to have a yielding point at the yielding stress, σ_y, and the corresponding elastic collapse strain, ε_e, and after that it has a constant positive work hardening slope until the point of the ultimate stress, σ_u, and the plastic strain, ε_p, is reached [data from Van Krevelen (1976) is given in Table 3.1]. After that, the material has perfectly plastic behaviour. Von Mises yield condition has been adopted, i.e., the yielding occurred, when the equivalent stress was equal to the yield stress σ_y from the uniaxial test. The equivalent stress is calculated by

$$\sigma_{eq} = \sqrt{\frac{(\sigma_1 - \sigma_2)^2 + (\sigma_2 - \sigma_3)^2 + (\sigma_3 - \sigma_1)^2}{2}}, \tag{3.9}$$

where σ_i ($i = 1,2,3$) are the principal stresses.

Polymers are known to be pressure dependent. The compression yield stress is higher than the tensile yield stress. So far this effect is also neglected.

Table 3.1. Properties of solid polymer and geometrical features of the XPS foam

Plastic	ρ_s [kg/m^3]	ρ_f [kg/m^3]	σ_y [MPa]	ε_e [%]	σ_u [MPa]	ε_p [%]	E_s [GPa]	a [μm^2]	l [μm]	δ [μm]	A_{13} [-]	A_{23} [-]
XPS	1050	31	30	0.9	50	1.6	3.4	2.1	35	0.82	1.68	1.27

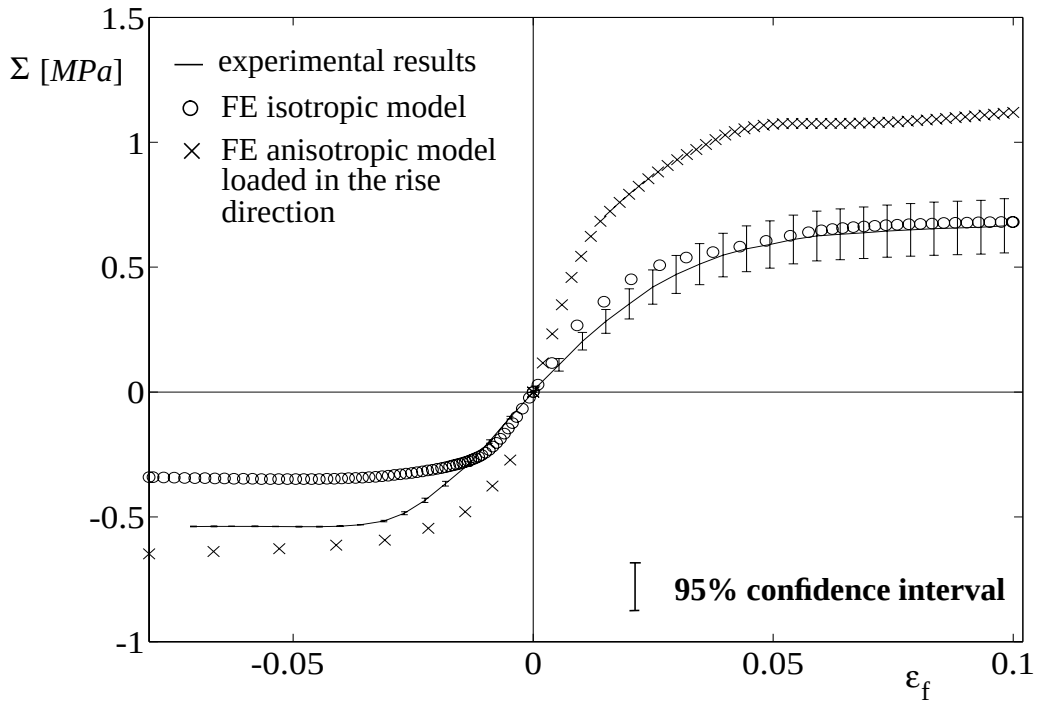

Fig. 3.6. Stress-strain curves for tension-compression of XPS foam and the model in the rise direction.

The finite element computations have been done by the standard MARC FEM program. In the first case, the model is assumed to be isotropic, i.e., the dimensions of a cell in Fig. 3.2b, will stay the same in the 3 main directions. In the other case, the anisotropic effects of the real cell shape is taken into account and 1/8 part of the tetrakaidecahedron is extended in the rise direction with the anisotropy factor A_{13} and in the extrusion direction with the factor A_{23}. This way of the anisotropy introduction corresponds only to the secondary anisotropy ratio described in Section 2.3.4. Both A_{ij} values are estimated from SEM micrographs and are given in Table 3.1.

Subsequently, the FEM simulation of the uniaxial compression and tension tests of foam in the rise direction is performed. The updated Lagrangian method has been used, i.e., the geometry is updated after every load increment. This increases the accuracy in the large displacement analysis. The results of the computations and experiments in the form of a stress–strain diagram for the XPS foam, that contained $\phi = 0.0615$ of the polymer in struts, are represented in Fig. 3.6. The Young's modulus of the isotropic model, $E_{\mathrm{f}}^{\mathrm{iso}} \approx 29.5$ *MPa*, occurred to be approximately equal to that, obtained from the experiments for the rise direction, $E_{\mathrm{f,\,1}}^{\mathrm{test}} \approx (23.5 \pm 4.5)$ *MPa*. The results obtained from the anisotropic foam model occurred to overestimate the stiffness and strength of the foam considerably. The explanation of this can be found in the wrong way of the introduction of anisotropy (secondary anisotropy only). This problem is similar to that discussed in Sec-

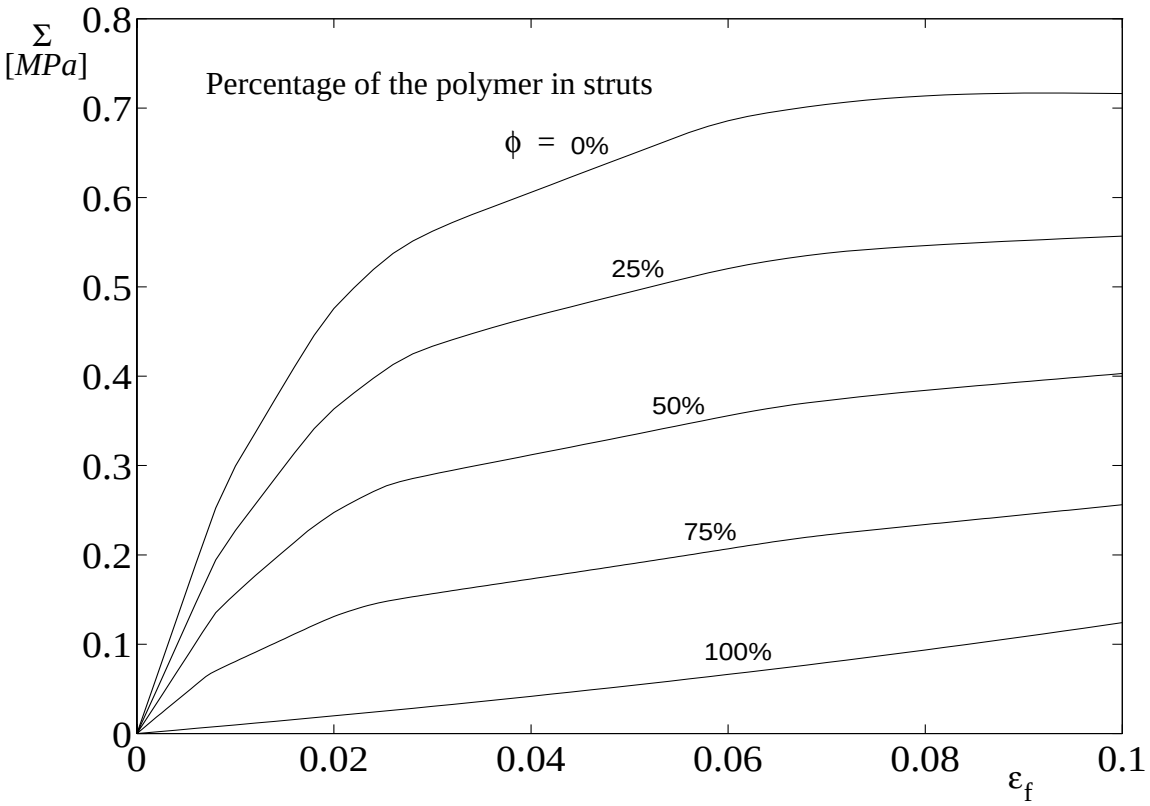

Fig. 3.7. Dependence between distribution of the material between walls and struts and mechanical properties of the XPS foam with constant density.

tion 2.3.4.

However, the model is very much consistent with the experiment in the yielding plateau in tension. But the isotropic model was too weak in comparison with the real foam regarding plastic yielding plateau in compression. The difference might be explained by the use of the isotropic foam model for the prediction of the behaviour of the anisotropic real foam.

Influence of the material distribution between walls and struts on the mechanical properties of the foam

The model is also applied to evaluate the influence of the distribution of the material between walls and struts, ϕ, on the mechanical properties. The density of the foam ρ_f is kept constant while the thickness of the walls δ and the cross sectional area of the struts a are changed accordingly. In this way the relative quantity of material in struts in comparison with that in walls varied from 0% to 100%. The results for the tensile behaviour of the XPS foam model in Fig. 3.7 show an almost linear dependence between the thickness of walls (as a linear function of the percentage of the polymer in walls) and the stress (at the same strain).

3.4 Random unit cell

3.4.1 Linear elastic behaviour

All regular foam models mentioned above are simple and easy to handle. But in comparison with the real irregular foam, their geometry is too regular. The effect of the irregularity has already been demonstrated for the open-cell foam models in Section 2.3.2 and has been observed to be considerable. This effect has not been investigated yet for the closed-cell foams. This phenomenon will be an issue of the interest here.

As it has been shown in Chapter 2 for the open-cell foams, the Voronoi tessellation can successfully be used to simulate the foam growing process. In this technique, the final geometry of the model is completely determined by the nuclei set. The same method is used here to model the closed-cell foam. The modelling is started from the regular nuclei sets based on the body-centred cubic (bcc) and face-centred cubic (fcc) packings illustrated in Figs. 2.6a and b. Resulting structures form rhombic dodecahedra and tetrakaidecahedra foam models correspondingly, which have cubic symmetry as well as fcc and bcc nuclei sets. Due to this symmetry, these regular structures may directly be used to fill a cubic unit cell. An attempt to randomize the foam model geometry raises immediately the question concerning the symmetry conditions to be kept at the boundaries of the cubic unit cell. In the open-cell foam modelling, struts crossing the boundary surfaces have been rotated to become perpendicular to these surfaces. This technique is schematically shown in Fig. 2.10. This method cannot be used for the closed-cell modelling, because then Plateau's laws are violated at the unit cell boundaries, where the originally planar cell walls would become distorted.

To avoid this, another approach is applied to arrange symmetrical boundaries of the unit cell. Symmetry conditions are being provided at the stage of the nuclei positioning by placing the nuclei lattice, represented in Fig. 3.8a as points, at the boundaries of the unit cell with edges of the length L_{uc} in the bcc- or fcc- order at the depth d. At the same time, the core of the unit cell may be any, as it is shown in Fig. 3.8a, where the model has bcc-based boundaries and a random core. The random core is obtained by a random placing of nuclei in space.

This technique has an important advantage which supplies the cubic unit cell with symmetrical boundaries. On the other hand, regular boundaries will affect the properties of the whole unit cell to some extent. To evaluate the influence of the regular boundaries on the mechanical properties of the foam model, the relative volume of the random core will be increased by increasing the cubic unit cell edge length L_{uc}. Because the regular

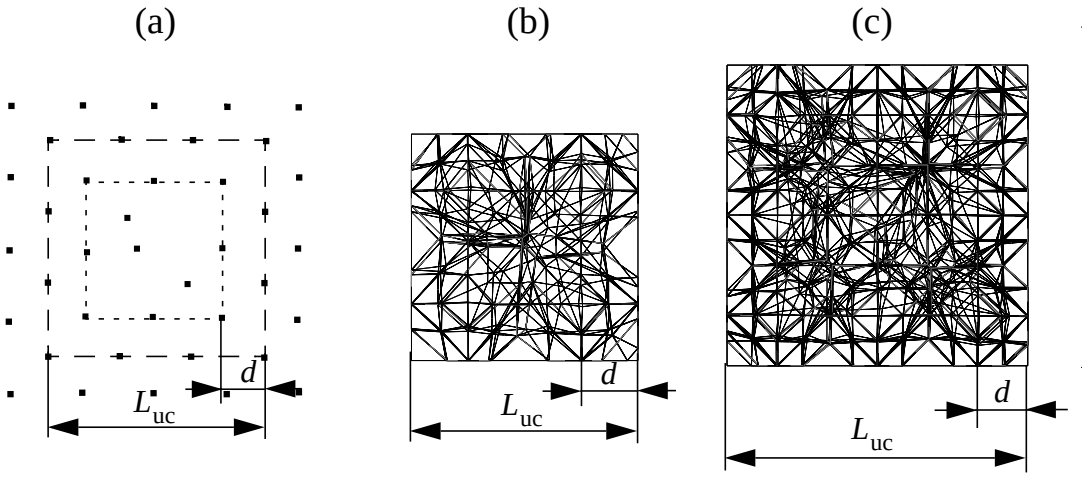

Fig. 3.8. Unit cell construction. (a) Providing unit cell symmetry conditions by placing a bcc-based lattice at the boundaries. (b) 2D projection of the foam structure with bcc-based boundaries resulting from the Voronoi tessellation with $(1-2d/L_{uc})^3$=0.125 and (c) 0.296.

layer stays constant with the depth equal to d, the relative volume of the random part, or relative random volume, $(1-2d/L_{uc})^3$ increases. It will be adopted as the relative random volume of the model unit cell. The maximum value of the relative random volume is limited by the computer capacities. Note that large unit cells contain more than 17400 beam and shell elements. Figures 3.8b-c demonstrate two examples of the models with a different $(1-2d/L_{uc})^3$.

The foam model geometrical parameters, e.g., a wall thickness, δ, and the area of the strut cross-section, a, are obtained from the measurements of the real closed-cell foam. The volumetric fraction of the solid in the struts, ϕ, yields directly from these geometrical parameters. ϕ was shown (Section 3.3.2) to be an important parameter that influences the choice of the kind of unit cell.

Simulations with Systematic Geometry Variations

Two kinds of the boundaries, fcc- and bcc-based, are chosen for the closed-cell foam model. The core stays always random. The relative random volume varies from 0%, or regular model, to 57.87% for both models and a linear elastic analysis is performed in the standard FE program MARC. A relative volume larger than 58% would result in excessive computation time. Two kinds of elements are used. The first one is the straight two-nodes elastic beam element, also used in the open-cell foam modelling in Chapter 2. Each foam strut is represented with one finite beam element. The second kind of elements used is a

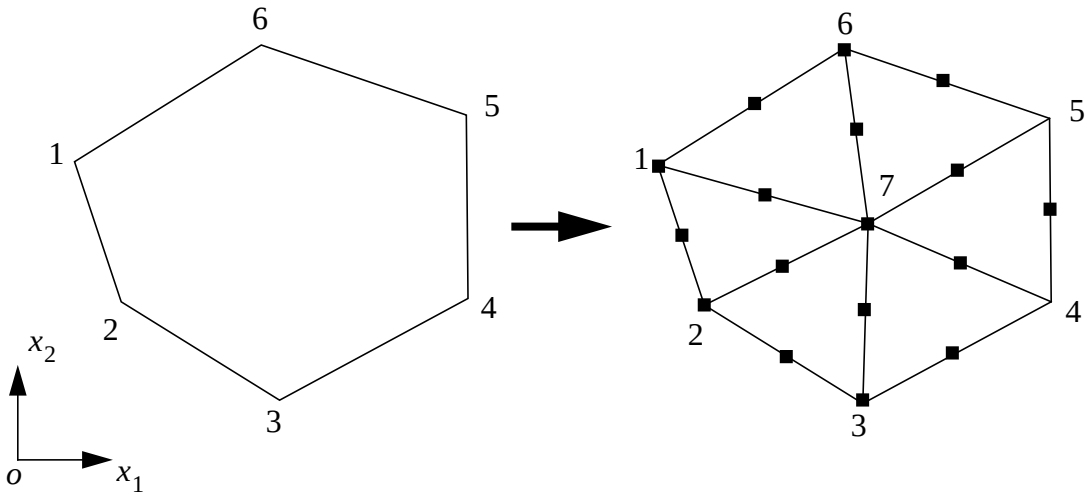

Fig. 3.9. Meshing of the cell walls.

six-nodes triangular thin shell element. Each cell wall is meshed in the way demonstrated in Fig. 3.9. A node is added at geometric centre of a cell wall.As a result, each cell wall is meshed with a number of triangular elements corresponding to the number of wall sides.

The shown element meshing is rather coarse and might give inaccurate solutions. To investigate the influence of the meshing on the results of the FE computations, the regular model in Fig. 3.2b has been simulated twice with two meshings. First, 1/8 tetrakaidecahedron is modelled by 24 triangular elements, as shown in Fig. 3.10a. The same FE model is simulated with a fine mesh using 563 quadrilateral thin shell elements. Figure 3.10b demonstrates this model. Both these models are loaded in tension in OY direction and the linear elastic analysis is performed. The resulting stress distributions can be seen in Fig. 3.10. The Young's modulus of the coarsely meshed model is approximately 8% higher than that of the finely meshed. The kind of mesh used in the FE analysis will influence the computation time considerably. As far as quite large structures with many elements are expected to be modelled, the coarse meshing is to be used here. The gain in the computation time then is reached at the sacrifice of about 8% of the model accuracy. However, it must be noticed that the accuracy of the nonlinear analysis may decrease significantly, because the buckling effects of the cell walls, also shown in the view of the closed-cell PUR foam in Fig. 3.11, cannot be modelled with such a coarse meshing.

Another parameter that varies in the unit cell is the distribution of the solid material between walls and struts. To study this parameter, all unit cells are modelled with the volumetric fraction of the material in struts ϕ equal to 1 (open-cell foam), 0.9, 0.5, 0.1 and 0 (all material is concentrated in walls).

(a)

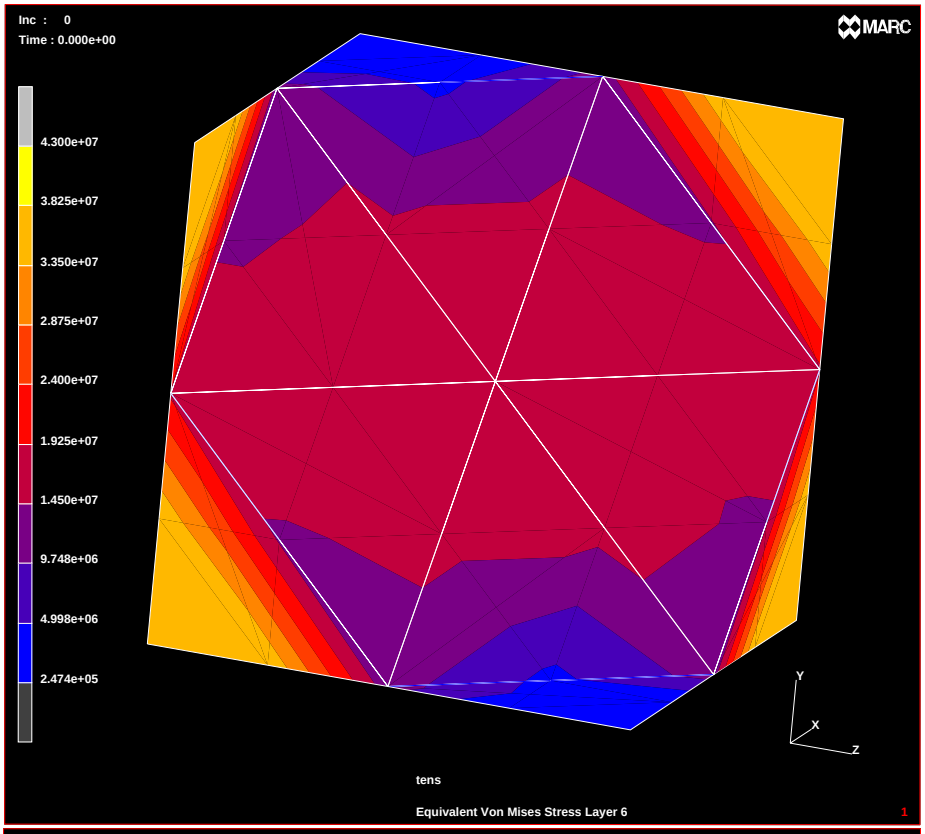

(b)

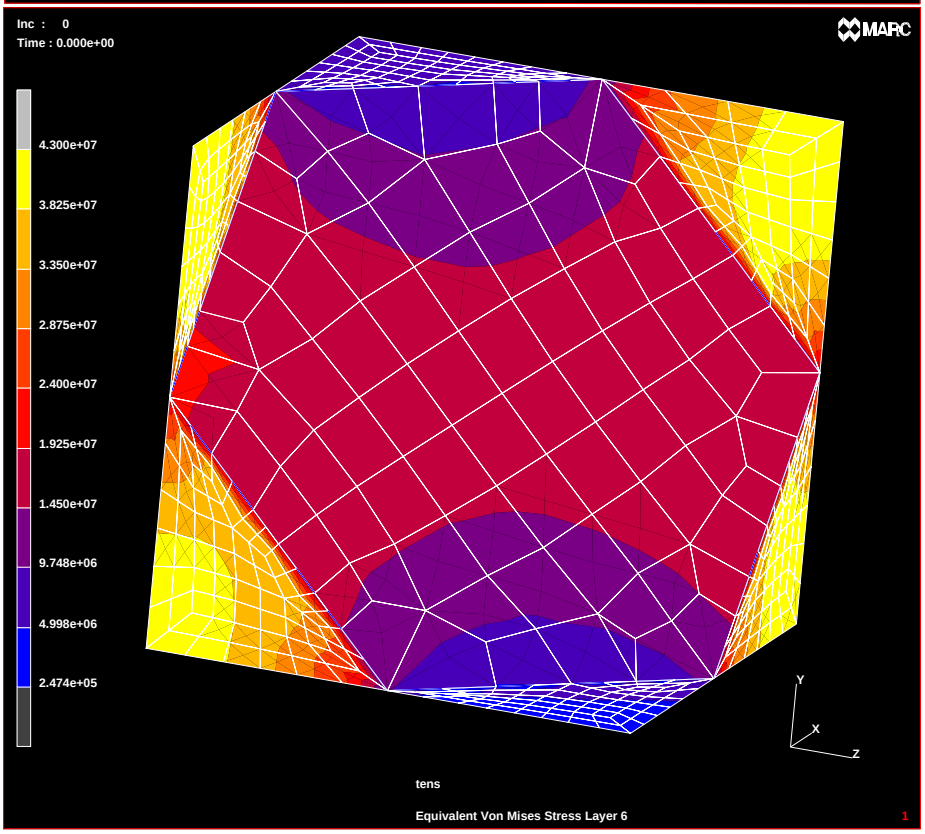

Fig. 3.10. (a) Coarse and (b) fine mesh of 1/8 part of the tetrakaidecahedron. Both models are loaded in tension and Von Mises stresses distribution is shown.

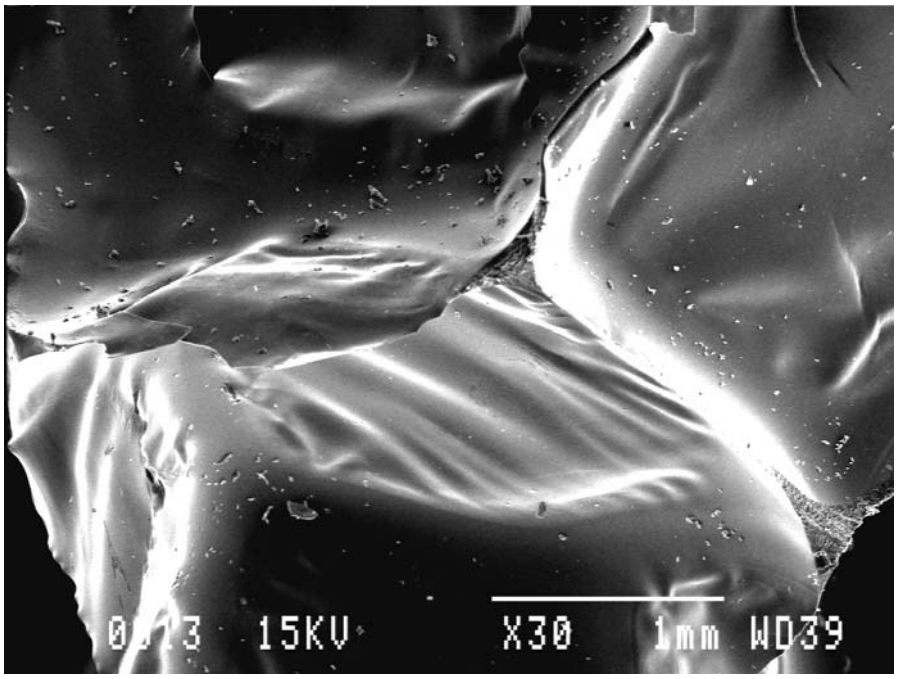

Fig. 3.11. View of the closed-cell PUR foam of Recticel N.V. showing buckling.

Each unit cell type with its distinct set of $(1-2d/L_{uc})^3$ and ϕ is created in the FEM program based on three various nuclei distributions and each unit cell is uniaxially loaded in three orthogonal directions. As a result, nine values of the foam Young's modulus yield an averaged value for the bcc- and fcc-based structures for each situation. The resulting map shown in Fig. 3.12a illustrates the dependence of the initial Young's modulus of models with the fcc- and bcc-based boundaries and having the relative foam density $\rho_f/\rho_s = 0.025$, on the material distribution and on the relative random volume. The relative Young's modulus E_i/E_{100} in Fig. 3.12b represents the ratio between Young's modulus of a regular model and that of the completely randomized model, which is extrapolated from the available data, as indicated in Fig. 3.12b.

The closed-cell foam models with material completely concentrated in cell walls ($\phi = 0$) converge quite quickly to the Young's modulus of the model with 100% random volume. Moreover, the effect of the random foam geometry is small. A random foam shows about 10% lower stiffness as compared to a regular fcc-based model. Already at a randomization degree $(1-2d/L_{uc})^3$ equal to 0.422, the fcc- and bcc-based models give accurate predictions of the extrapolated Young's modulus of the random model. An increase of material content ϕ in struts leads to a decreasing convergence of the bcc-based model to the random model. The same effect occurs in the fcc-based model if ϕ becomes higher than 0.5. For the open-cell foam models ($\phi = 1$) the convergence is poor and the

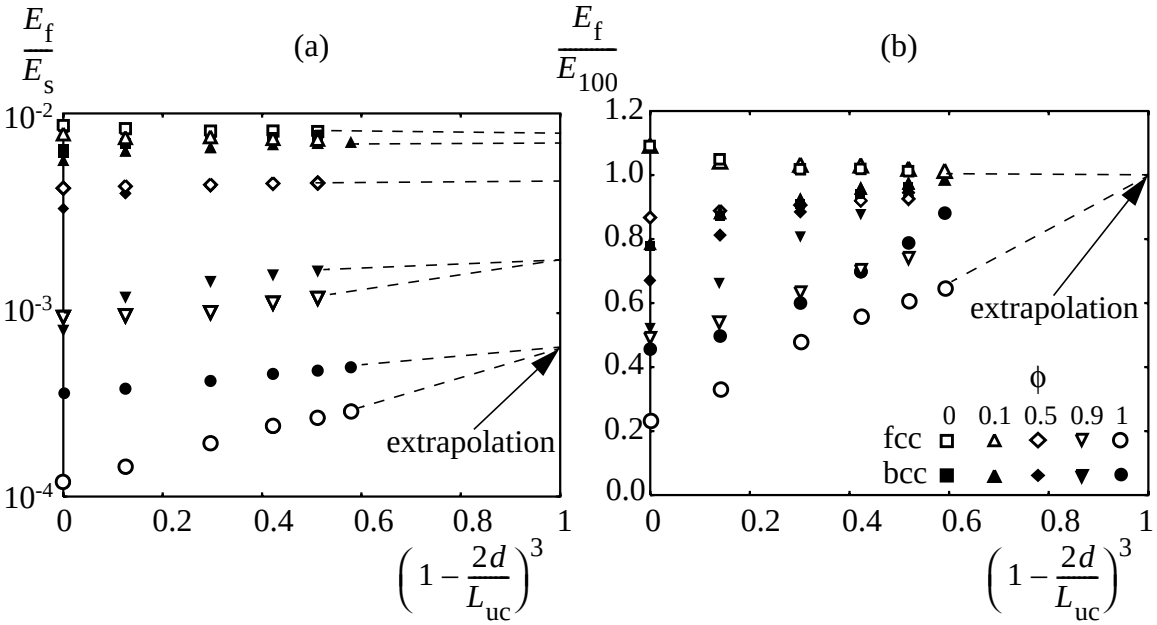

Fig. 3.12. Young's modulus of the foam models as a function of the unit cell type.

use of the regular boundaries arrangement is not recommended. In this case the method should be used as described in Section 2.3.1. However, the extrapolated value for the Young's modulus of the open-cell foam in Fig. 3.12 agrees with that determined in Section 2.3.2.

Foam models with high values of ϕ have a low stiffness, but they appear to become stiffer if randomized. As mentioned before, the opposite applies to a fcc model with $\phi = 0$; however, to a small extent only. Models with intermediate ϕ values appear to provide intermediate behaviour.

Simulation of Glass Foam

To verify the model, a glass foam (Pittsburgh Corning Nederland b. v.) has been modelled. The important difference with the plastic foams modelled above is that the properties of the solid material (glass) inside the walls and struts of the glass foam are known. Views in Fig. 3.13 highlight some important specifications of this foam. One of them is the presence of the gaseous phase inside the struts and walls. Glass is foamed at two levels: mesolevel shown in Fig. 3.13a and microlevel, or the level of walls and struts, shown in Figs. 3.13b-d. This effect has been observed also with other materials, for instance, in starch foam by Warburton *et al.* (1990). The measured density of the material in walls occurred then to be lower than of the original unfoamed solid because of the foaming effect in the walls. It is clearly seen from the views in Figs. 3.13c-d that both the walls and the struts in the foam are considerably foamed too. This effect should be taken into

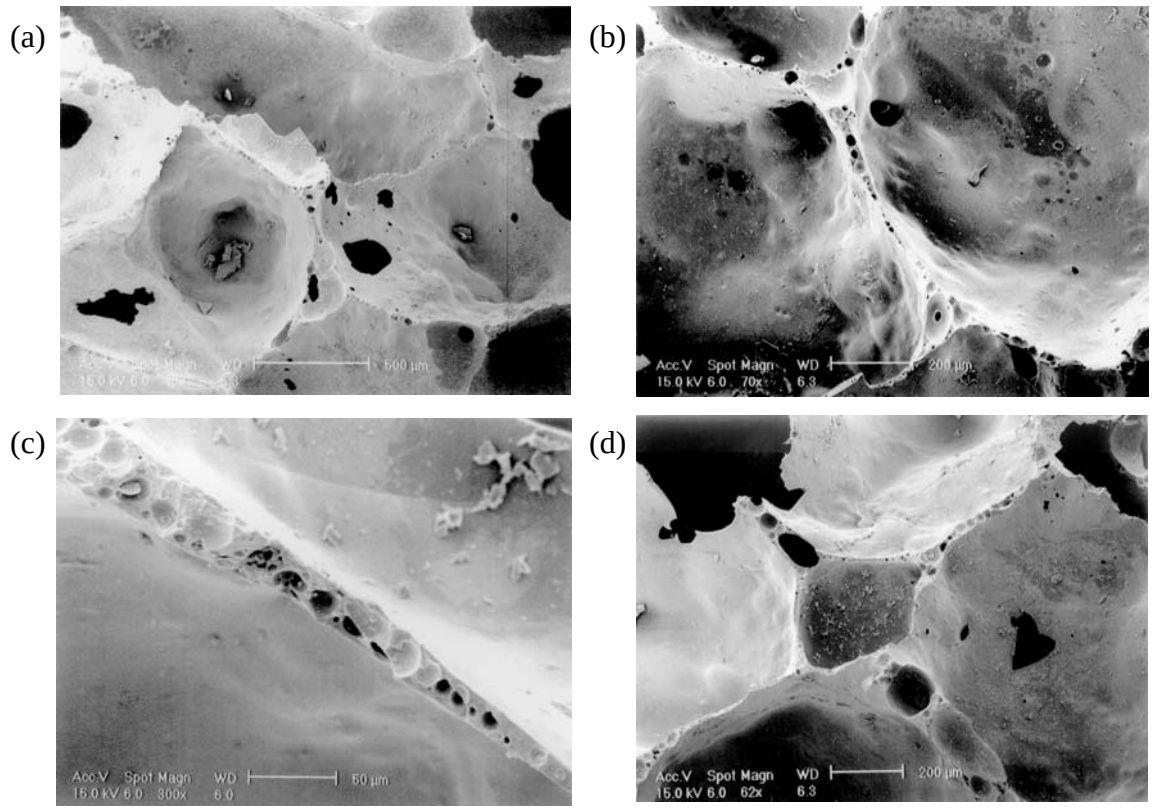

Fig. 3.13. Scanning electron micrographs of closed-cell glass foam: (a) overview; (b) a wall between two cells; (c) a foamed wall section; (d) foamed strut sections.

account during the modelling.

First, the views of the glass foam have been studied with the image processing technique to determine the geometrical features of the foam. The cell walls thickness δ and the struts cross-section a have been measured by SEM and are presented in Table 3.2. The foam structures have been studied with the image processing technique, as described by Waterman and Phillips (1974), to determine the average cell diameter D. By measuring the average diameter of cells in the real foam D and the cell diameter in the model D', the scale factor $M = D'/D$ has been determined. Further, the model wall thickness and the struts cross-section are determined as $\delta' = M\delta$ and $a' = M^2 a$. Knowing the total walls area $\sum S_{\text{walls}}$ and the total struts length $\sum l_{\text{struts}}$ in the unit cell, the model density ρ_f' may be obtained from

$$\rho_f' V_{uc} = \rho_s (\delta' \sum S_{\text{walls}} + a' \sum l_{\text{struts}}) \ , \tag{3.10}$$

where V_{uc} is a volume of the unit cell. The model density ρ_f' is approximately a factor three different from the measured foam density ρ_f. This points to the fact that the density

Table 3.2. Glass foam characteristics

Foam characteristic	Value
Solid density, ρ_s [kg/m^3]	2400
Measured foam density, ρ_f [kg/m^3]	111
Mean measured membranes thickness, δ [μm]	26 ± 6
Mean measured struts cross-section, a [μm^2]	3200 ± 900
Fraction of the material in struts, ϕ	28.5
Cell diameter, D [mm]	0.72 ± 0.12
Model cell diameter, D' [m]	0.15
Magnification (scaling) factor, $M = D/D'$	209
Total walls surface in the model, $\sum S_{walls}$ [m^2]	4.08
Total struts length in the model, $\sum l_{struts}$ [m]	62.97
Struts cross-section in the model, a' [m^2]	0.000140
Walls thickness in the model, δ' [m]	0.005434
Computed foam density, ρ'_f [kg/m^3]	344
Computed struts cross-section in the model with the simplification from Fig. 3.14a, a' [m^2]	0.000045
Computed walls thickness in the model with the simplification from Fig. 3.14a, δ' [m]	0.00175
Solid Young's modulus, E_s [MPa]	70000

of the walls and struts is three times lower than it would be in the foam with unfoamed walls and struts. In other words, two various foam densities can be introduced for this foam. First, conventional relative foam density ρ_f/ρ_s and the relative density (or porosity) of the material in struts and walls.

There are two possibilities to model the glass foam from Fig. 3.13. The first one is schematically depicted in Fig. 3.14a and assumes the structural elements of the foam to be unfoamed and to have, therefore, three times lower sections. This simplification will lead

to a drop in the bending stiffness of the struts and walls, while axial stiffness will remain the same. To keep both, axial and bending stiffness of the structural elements of the model adequate, the cell walls and struts thickness can be kept as measured and the Young's modulus of the material can be reduced proportionally to the porosity of the material in struts and walls. This can be motivated by the fact that the struts and walls are high-density foams for which the properties are about proportional to the relative foam density [see Meinecke and Clark (1973)]. The corresponding modelling is shown in Fig. 3.14b.

Both model simplifications are used in the FEM modelling to predict the Young's modulus of the glass foam. The model has been generated 4 times and the Young's modulus in three orthogonal directions is determined. The results are presented in Table 3.3. The small difference in the initial Young's moduli of the models arranged in two different ways (as shown in Figs. 3.14a and b correspondingly) demonstrates that the axial (in-plane) deformations in the closed-cell foam are dominant. Both models agree very good with the experimental data. The cubic model of Gibson and Ashby (1988) is also used to predict the Young's modulus of the closed-cell glass foam. The cubic models based on the simplifications from Figs. 3.14a and b [see Eq. (3.1)] overestimate the measured Young's modulus considerably.

The presented modelling demonstrates a very good agreement between the Young's modulus predicted by the random model and the measured Young's modulus of the closed-cell foam. The random model provides much better results than the widely-used cubic model. This occurs due to the geometry of the closed-cell random model which approaches the geometry of the real foam much closer than the regular foam models.

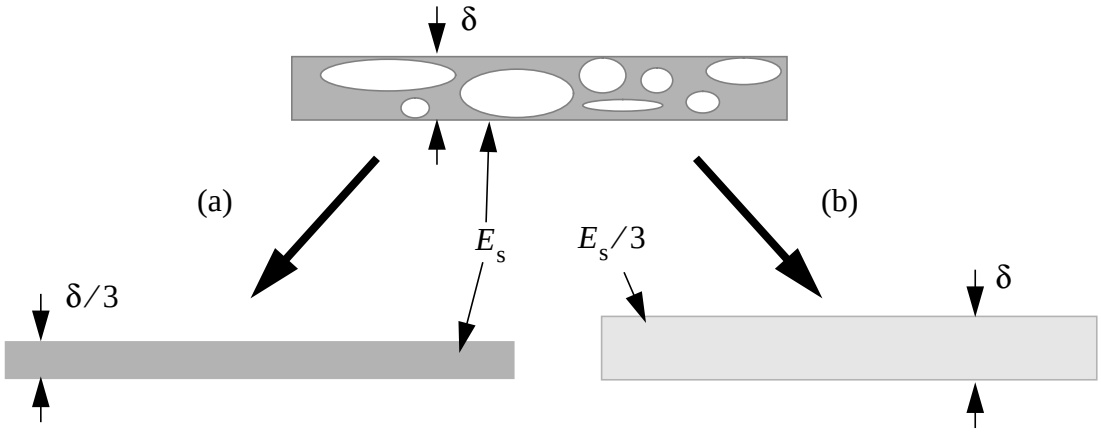

Fig. 3.14. Modelling of the cell walls by (a) decreasing the cell walls thickness and (b) by decreasing the cell walls stiffness.

Table 3.3. Analysis of the random isotropic model and measurements of the closed-cell glass foam in compression

Model	**Young's moduli of foams E_f with thin walls (Fig. 3.14a) and $\frac{\rho_f}{\rho_s} = 0.046$ [*MPa*]**	**Young's moduli of foams E_f with low E_s (Fig. 3.14b) and with $\frac{\rho_f}{\rho_s} = 0.14$ [*MPa*]**
1	833; 881; 846	841; 888; 853
2	892; 857; 859	908; 874; 872
3	789; 844; 909	801; 852; 919
4	862; 871; 891	873; 882; 902
Average	**861 ± 32**	**872 ± 32**
Measured	**800**	**800**
Gibson and Ashby cubic model	**2327**	**2373**

Simulation of PMI Foam

The same approach is used to simulate the linear elastic properties of polymer foam. For the computations concerning the Young's modulus of a closed-cell foam, the bcc-based foam model with a randomization degree $(1 - 2d/L_{uc})^3 = 0.512$ is applied. To verify the random foam model, two closed-cell foams, PMI-30 and PMI-110 of RÖHM, are studied. Scanning electron micrographs of both foams are presented in Fig. 3.15. PMI-30 from Fig. 3.15a has relatively thin walls and struts and somewhat larger cells dimensions in comparison with PMI-110 from Fig. 3.15b, having a higher density. The geometry of the foams, like the struts cross-section a, cell diameter D and the cell walls thickness δ (see Figs. 3.15c and d), is measured by SEM as it has also been done for the glass foam. The results are given in Table 3.4 together with the calculation results. The foam model density is determined by Eq. (3.10). The deviations of the model densities ρ_f' from the measured foam densities ρ_f are small, indicating that the model resembles the real foam. It is remarkable that the estimated density of PMI-30 is much closer to reality, than that of PMI-110. As it has been shown in Section 1, the geometry of foam can be subdivided into walls, struts and vertices. As far as low-density foams are considered here, the material in vertices is ignored. With the increasing foam density, the relative part of the material in vertices increases too. In both PMI foams models, the material in vertices is not taken into account and, therefore, a minor error is produced which is lower for the lower-density foams. Mechanically, the material in vertices is hardly loaded and may be neglected.

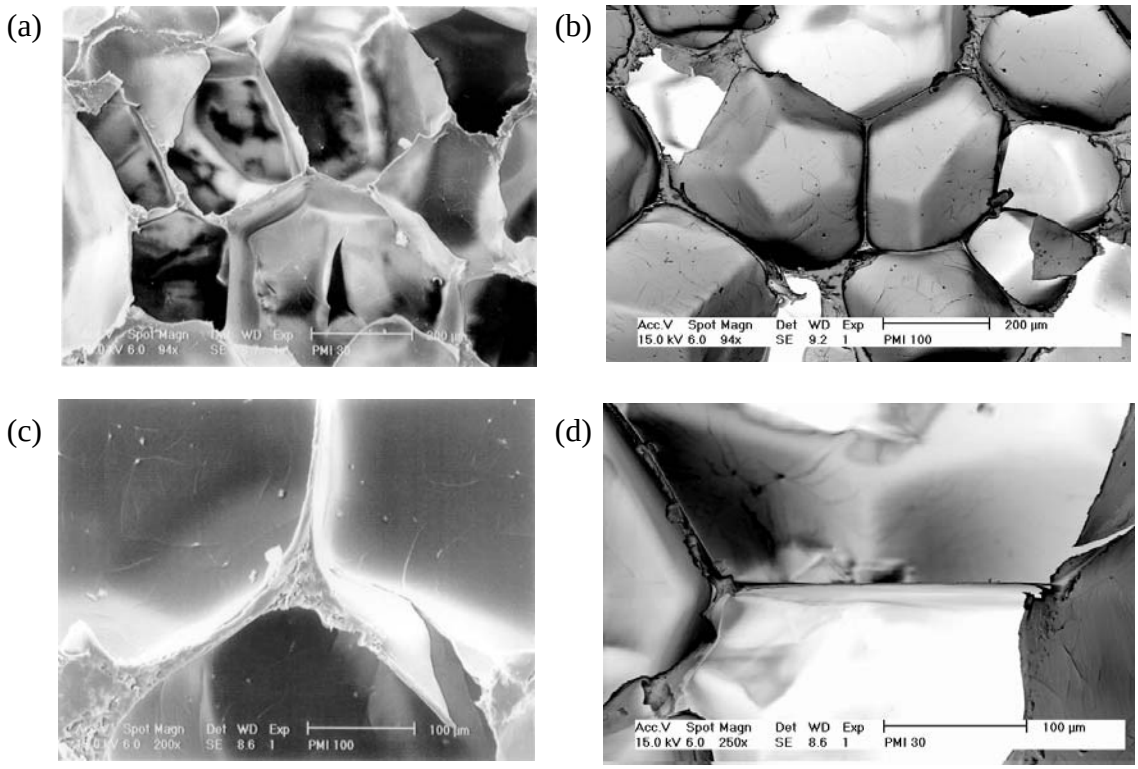

Fig. 3.15. Closed-cell PMI foams. Overview SEM images of (a) PMI-30 and (b) PMI-110. (c) A strut cross-section and (d) a wall between two cells in PMI-30.

Blocks of solid PMI were provided by RÖHM. As far as PMI is a thermoplastic and the foaming process is only a physical one, its mechanical properties are assumed not to change significantly during the foaming processes. The modulus of elasticity of the solid material, E_s, is measured in uniaxial tension and compression experiments. For this purpose, two kinds of samples are cut from the blocks of solid PMI. Compression tests of 4 samples as shown in Fig. 3.16a are performed according to ASTM D695 at a deformation rate of 0.044 min^{-1}. The resulting Young's modulus comprises $E_s = 7060 \pm 200\ MPa$. Tension experiments are performed on 7 solid PMI "dogbone"–samples illustrated in Fig. 3.16b according to ASTM D638 at the same deformation rate between the clamps. The corresponding Young's modulus of the solid PMI in tension has a value of $E_s = (6490 \pm 450)\ MPa$. The difference between the determined Young's moduli in tension and compression points to an asymmetric behaviour of the polymer. The averaged value of 6780 *MPa* is used in the model.

The FE model computations give results (see Table 3.4) which are closer to the real foam than the values predicted by Eq. (3.1) of Gibson and Ashby (1988). However, the Young's moduli predicted by the random model of both PMI foams overestimate the measured values. A possible reason for this may be the idealization of the model by

Table 3.4. Geometrical features and Young's moduli of the PMI foams

Foam feature	PMI-30	PMI-110
Measured solid density, ρ_s [kg/m^3]	1192±2	
Measured foam density, ρ_f [kg/m^3]	37.7±0.4	116.0±2.0
Measured walls thickness, δ [μm]	1.9±0.2	3.6±0.4
Measured struts cross-section, a [μm^2]	183± 40	470± 20
Measured average cell diameter, D [μm]	~425	~370
Model average cell diameter, D' [m]	0.2	
Scale factor, $M = D/D'$	470	540
Model cell walls thickness, δ' [m]	0.00089	0.00194
Model cell struts cross-section, a' [m^2]	41×10^{-6}	137×10^{-6}
Content of the solid material in struts, ϕ	0.41	0.51
Calculated model foam density, ρ_f' [kg/m^3]	36.3	96.3
Measured average solid Young's modulus, E_s [MPa]	6780	
Measured foam Young's modulus, E_f [MPa] (from the compression experiment, deformation rate 0.027 min^{-1})	20.1	83.2
Gibson–Ashby model Young's modulus, E_f' [MPa]	130	360
Computed foam Young's modulus, E_f' [MPa]	43.3	100.5
Computed foam Young's modulus with $\vartheta = 0.3$, [MPa]	22.5	75.7

assuming the walls to have a constant thickness which is also the same for all cells. Also the coarse modelling (about 8% stiffer behaviour) contributes to the difference. Moreover, the model contains only unruptured cell walls, while real closed-cell foams contain also some open cells.

Berlin and Shutov (1980), who studied closed-cell PUR foams, suggest that the fraction of open cells, ϑ, is a function of the foam relative density. In the region of the low-density foams the factor ϑ is approximately equal to 0.3 for foams in their study. They explain this effect by the fact, that in low-density foams the membranes become very thin

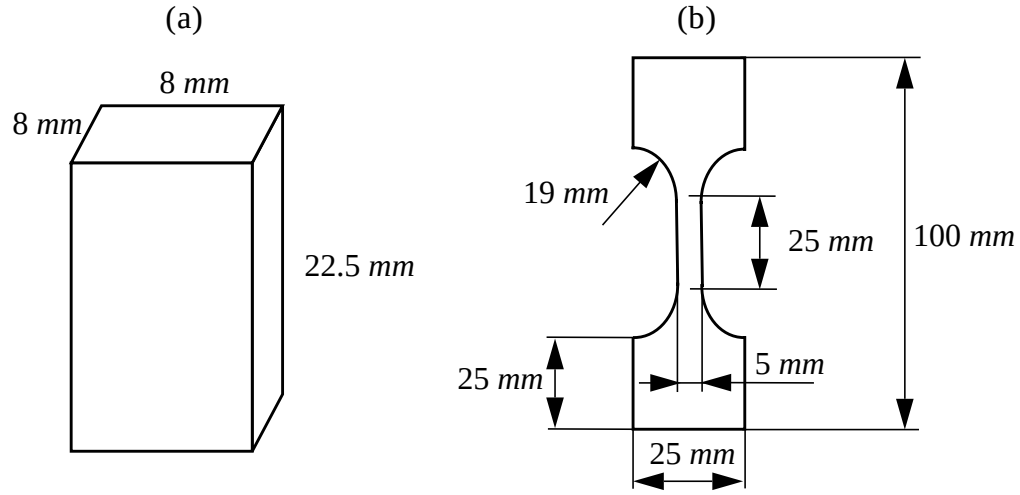

Fig. 3.16. Specimens of PMI solid for (a) compression and (b) tension tests.

and can easily rupture during or after the processing.

In order to study the effect of the presence of open cells, a bcc-based model with the randomization parameter $(1-2d/L_{uc})^3 = 0.512$ has been created where 30% of all walls were removed. The Young's modulus of this model, given in Table 3.4, predicts the real PMI-30 foam modulus much better. The Young's modulus of PMI-110 is now underestimated. Considering the mentioned effect of density on the open cell fraction, this is understood. The open cell fraction ϑ in PMI-110 will be less than of PMI-30 and less than 0.3.

To create a model of a real foam, the geometry of the foam should be known, including the fraction of open cells ϑ in the closed-cell foam. An air flow method has been described by Yasunaga *et al.* (1996) where air is blown through a closed-cell foam and the drop in air pressure has been measured. A correlation between air flow and fraction of

Table 3.5. Percolation thresholds for various 3D packings [from Stauffer (1985)]

Type of packing	Bond
Diamond	0.3880
Simple cubic	0.2492
BCC (tetrakaidecahedron)	0.1785
FCC (rhombic dodecahedron)	0.1190

open cells ϑ has been found. Moreover, a typical value of ϑ is obtained, a so-called "threshold", under which no air flow has been measured through the foam. It occurred to be equal to approximately $\vartheta = 10\,\%$. It is known from the percolation theory [see, for example, Stauffer (1985)], that there is always a threshold value of open bonds between cells in 3D, above which continuous channels of open bonds can be found in the structure from one side to the opposite one. This value of open bonds is dependent on the type of structure. Table 3.5 demonstrates percolation thresholds of some of them.

The same method is used to measure the fraction of open cells in the two available PMI foams. In both cases, no air flow occurred through the samples. As far as a real cell shape corresponds to that of tetrakaidecahedron (as shown in Table 2.1), a foam with nearly 18% of ruptured walls will have no air flow through it. This means that at most about 18% of the walls in the PMI-30 and PMI-110 foams can be ruptured. This is less than the 30% applied in the calculations. Obviously, the overestimation of the stiffness of PMI-30 calculated without ruptured cell walls cannot be explained entirely by the presence of open cells.

Another very important effect that can affect the mechanical properties of foams is the effect of the blowing agent on the mechanical properties of the solid material in struts and walls. During the production, blowing agent always influences the properties of solid, making it weaker. Some blowing agents might remain in the solid. This might also explain the discrepancy in the measured and computed Young's modulus of foam.

3.4.2 Alternative nonlinear modelling of the anisotropic closed-cell foam

Complete random "model"

Further development of the model concerns complete randomization of the model. It means that no regular boundaries are present. This can be achieved at the sacrifice of the "unit cell" concept. In both previous cases of the unit cell construction, the open-cell unit cell in Section 2.3.1 and the closed-cell unit cell in the last Section, boundaries have been arranged in such a way, that the created structure could be repeated in space by mirrorizing the original unit cell. The behaviour of the whole structure could be represented by the behaviour of a unit cell, by prescribing the corresponding boundary conditions.

All related complications vanish if boundaries have no symmetry conditions. The characteristic dimension of such a model should be sufficiently large to allow the assumption that this model is a representation of a real foam. The resulting structure should contain at least several tens of cells. The non-symmetrical boundaries are arranged then in the following way. First, randomly distributed nuclei are placed in a box with the minimum

distance d between them. Consequently, Voronoi tessellation is applied and the structure containing cells with walls and struts arises. To obtain the model cell, a box with smaller dimensions L is introduced inside the already existing box, as it has been done in the open-cell foam modelling described in Section 2.3.1 and shown in Fig. 2.10b. As opposed to the open-cell foam modelling, the border of the closed-cell random model is arranged in another way. All walls passing the model border are "cut" with that border and only an inner part of the wall is included in the "model". The representation of this arrangement is given in Fig. 3.17. All points at a boundary are connected with each other in a way to keep boundaries shear stress-free and flat during the deformation. The prescribed flatness is chosen in order to simulate the effect of adjacent foam material to some extent. The resulting model is a direct analogue of the cubic sample cut out of the real foam. In comparison with the closed-cell foam model presented in Section 3.4.1, where the boundaries were regular and the core remained random, the present model does not contain any regular part at all and, therefore, has no influence of any regular structure. Moreover, the model may stay smaller than that with the regular boundaries. This technique leads to vanishing of the conventional micromechanical concept of "unit cell". Its application is motivated by the relatively large dimensions of the model in comparison with the regular models used earlier.

Dimensions analysis

The value of L/d can be a good measure of the model dimensions similar to the modelling with the regular boundaries in Section 3.4.1. The dimensions parameter L/d was chosen here to be 1, 2, 3, 4 and 5. For each value of the dimensions parameter, three isotropic model cells are created with the relative foam density $\rho_f/\rho_s = 0.025$ and with the equally distributed solid material between the cell walls and struts, i.e., $\phi = 0.5$. Each model cell is uniaxially loaded subsequently in the three directions (see Fig. 2.5) in the standard FE program. Consequently, nine results are obtained for each condition. Aver-

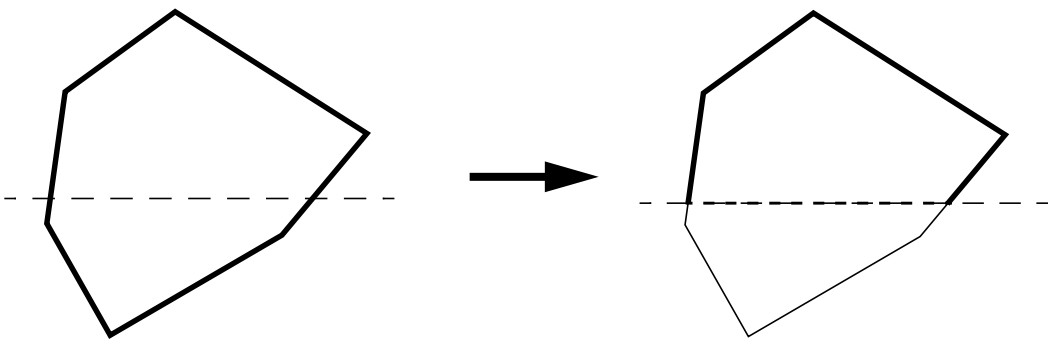

Fig. 3.17. Arrangement of the border of the closed-cell random model.

aged values of the Young's modulus are plotted against the model cell dimensions in Fig. 3.18. The models with $L/d = 3$, 4 and 5 have the same value of the Young's modulus as the extrapolated value in Fig. 3.12. The random model with the dimensions $L/d = 3$ is accepted as the smallest model that is sufficiently accurate and it will be used in all further computations.

Modelling of the XPS foam

This model is used here to estimate the nonlinear mechanical properties of the anisotropic closed-cell XPS foam shown in Fig. 3.1b and modelled in Section 3.3. Geometrical features of the XPS foam are measured in the way similar to the PMI and glass foams and are presented in Table 3.1. In contrast to the closed-cell foams discussed above, XPS foam is anisotropic. To simulate the mechanical behaviour of this foam, the same principles of the anisotropy introduction in the foam model as for the open-cell foam model in Section 2.3.5 are to be used here. Similarly, the same initial anisotropy ratio n equal to 0.38 will be applied to the model. This approach is based on the assumption that both open- and closed-cell foams are produced in a similar way. The only difference is that in the case of open-cell foams, walls are being removed from the structure by physical or chemical treatments without any impact on the geometry of the foam structure.

All geometrical features of the XPS foam are taken from the measurements used in the regular modelling in Section 3.3 and given in Table 3.1. The random model is generated based on the randomly distributed nuclei with the primary anisotropy ratio

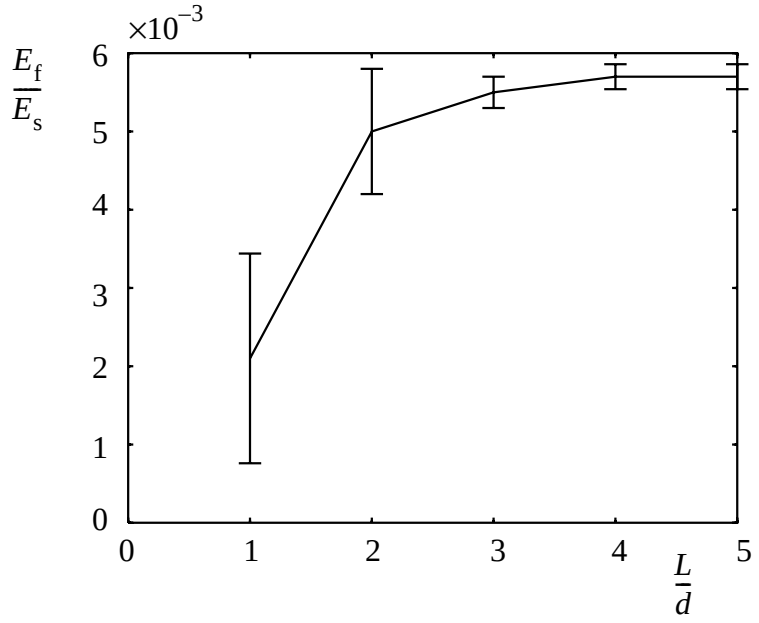

Fig. 3.18. Young's modulus with the standard deviation as a function of the foam model dimensions.

$A'_{ij} = A_{ij}^{0.38}$, as it has been demonstrated in Fig. 2.39. After the 3D Voronoi tessellation is completed, the boundaries of the model are arranged as shown in Fig. 3.17. Next, the model is geometrically extended in the directions of the anisotropy with the secondary anisotropy ratio $A''_{ij} = A_{ij}^{0.62}$. Finally, global compression and tension loads are applied to the model boundaries and large displacements analysis can be completed. The solid material in struts and walls is assumed to have nonlinear behaviour according to the data for XPS obtained from Van Krevelen (1976) [see Table 3.1].

The random XPS foam model has been generated five times based on five various nuclei distributions and each model has been loaded in tension and compression in FEM. Because the solid content in struts is very small ($\phi = 0.0615$), struts are eliminated from the model. This leads to a considerable saving of computation time without losing accuracy. Table 3.6 summarizes the results of the five random XPS foam simulations and the measurements and predictions of the foams Young's moduli by the regular anisotropic tetrakaidecahedron with the initial anisotropy degree $n = 0$. The random model predicts the ratio of the Young's moduli better than the regular tetrakaidecahedron, because the random structure with the chosen value of initial anisotropy degree n is geometrically much closer to the real foam. Unfortunately, no other model is available to predict properties of an anisotropic closed-cell foam. However, verification can take place by comparison to experimental results.

It is clearly seen from Table 3.6 that the tensile strength and compression collapse stress are predicted very good by the model in all three directions. Moreover, the stiffness ratios of the XPS foam are also predicted very accurately. However, the Young's moduli in three directions are overestimated by the random model. Remarkable is that the difference in the Young's moduli of the model and of the real foam are always nearly a factor two. This points out that the geometry of the random foam model corresponds to that of the XPS foam. The most reasonable explanation of the observed discrepancy is an incorrect Young's modulus of the solid XPS, E_s, used in the modelling. This discrepancy may arise from a possible difference in the mechanical properties of the solid XPS taken from the tables [for instance, from Van Krevelen (1976)] and actual mechanical properties of the foamed material inside the struts and walls. In the above case, the basic material in the XPS foam might be expected to have a two times lower Young's modulus E_s in comparison with the solid Young's modulus given in Table 3.1. In fact, this discrepancy is similar to the result with the other polymer (PMI) in the previous section. The discussion on the observed discrepancy for PMI will also apply to the present XPS case.

Table 3.6. Computations of the random anisotropic model (XPS) and measurements

Model	Relative Young's moduli			Moduli anisotropy	
	E_1/E_s	E_2/E_s	E_3/E_s	E_{13}	E_{23}
1	0.0126	0.0083	0.0058	2.17	1.43
2	0.0131	0.0098	0.0072	1.82	1.36
3	0.0130	0.0090	0.0069	1.88	1.30
4	0.0133	0.0087	0.0063	2.11	1.38
5	0.0130	0.0091	0.0063	2.06	1.44
Average	**0.0130**	**0.0090**	**0.0065**	**2.00**	**1.38**
Measured	0.0068	0.0042	0.0032	2.12	1.31
Tetrakaidecahedron with $n = 0$	0.0159	0.0087	0.0044	3.61	1.98

Model	Tensile strength [*MPa*]			Compression collapse stress [*MPa*]		
	$\Sigma_{pl,1}$	$\Sigma_{pl,2}$	$\Sigma_{pl,3}$	$\Sigma_{c,1}$	$\Sigma_{c,2}$	$\Sigma_{c,3}$
1	0.76	0.53	0.40	0.43	0.31	0.20
2	0.75	0.57	0.51	0.48	0.36	0.30
3	0.75	0.59	0.47	0.45	0.30	0.27
4	0.73	0.54	0.46	0.47	0.29	0.26
5	0.73	0.58	0.42	0.51	0.26	0.28
Average	**0.74**	**0.56**	**0.46**	**0.47**	**0.30**	**0.26**
Measured	0.76	0.55	0.54	0.60	0.33	0.28

3.5 Discussion and Conclusions

A regular tetrakaidecahedron model was used to predict the behaviour of the anisotropic closed-cell foam. The FEM computations were based on the properties of monolitic polymer and on the geometrical features of the adopted foam structure as a tetrakaidecahedron regular cell structure. The simplicity of the geometry is one of the most attractive features of this model. However, compared to the geometry of the real foam, the tetrakaidecahedron is too regular to describe the real foam behaviour. The FEM simulations with the isotropic regular model showed a reasonable agreement with the experiment. Although, the accuracy in the compression region was limited. The reasons of that lay, probably, in the wrong introduction of the anisotropy and in the ignoring of the asymmetric behaviour typical for polymers. Moreover, some buckling effects in the membranes could not be reproduced because of the coarse meshing in the FE analysis.

Low-density isotropic closed-cell foam was consequently modelled using 3D Voronoi tessellation of space. Unit cells containing various numbers of foam cells were composed to be applied in the linear elastic FE computations. Boundaries of a unit cell were kept regular by placing the nucleation points in a fcc- or bcc-pattern at the border of the unit cell. Special attention was paid to the distribution of the material between struts and walls of cells.

Analyses for unit cells of various dimensions and material distributions showed that for a model without struts (all material in walls) even a small unit cell (several foam cells) with a low random volume percentage was quite representative for the elastic behaviour of closed-cell foam and the effect of randomness was small. In the case of a model without walls (open-cell foam), the effect of randomness was large, but the applied method of the boundaries arrangement was found to be inefficient. The method of the unit cell boundaries arrangement used in Section 2.3.1 would be more efficient and is recommended for the open-cell foam random modelling.

For the foams with solid material distributed between walls and struts, the unit cell with bcc-boundaries containing a relative random volume of 0.512 and about 200 foam cells exhibited a behaviour similar to that of the unit cell that would be completely random. This unit cell has been used in the computations to predict the linear elastic properties of the closed-cell PMI foam. The geometrical features of foam and solid material properties have been obtained from measurements of the real foam. Computed values of the Young's moduli of foams overestimated that of the real foam. To approach the real closed-cell foam structure which always contains open cells, 30% of the cell walls has been removed from the model. The obtained elastic moduli predicted the measured values

much better. However, the percentage of the open cells has been estimated from the literature data on a different foam and, therefore, may not be reliable. Moreover, the air flow measurements indicated that probably less than 30% of the cell walls were ruptured in the closed-cell PMI foam. The adopted percentage of open cells is probably overestimated. Measurement of the fraction of open cells in the closed-cell foam is difficult.

The randomized model has been used to simulate isotropic glass foam. Glass foam was found to be foamed at two levels, i.e., the struts and the walls of the foam were also foamed. For this reason, the randomized model has been adopted in two various ways. First, all structural elements of the foam were scaled by a factor, corresponding to the relative density of the foamed struts and walls. Second, the thickness of the walls and the struts was kept as measured and the stiffness of the solid material (the Young's modulus of glass) was reduced respectively. Both models gave a foam Young's modulus very similar to the measured value. The following two main inferences can be drawn from this:
1. **The dominant deformation mechanism in the closed-cell glass foam is in-plane deformation in the foam cell walls.** This conclusion is based on the fact, that the main difference in the two above described approaches (reduction of the walls and struts thicknesses or reduction of the stiffness) is the changing of the bending stiffness of the walls and struts. In the second modelling, the bending stiffness of the struts and walls increased significantly in comparison with the first modelling, while the axial stiffness remained the same. The stiffness of the two models occurred to differ by about 1% only.
2. **The randomized closed-cell foam model predicts the stiffness of the isotropic closed-cell foams correctly**, if two conditions are met: a) the constitutive behaviour of the solid material in struts and walls is determined correctly and b) all geometrical features of the closed-cell foam, like the struts and the walls thickness, are taken into account.

A complete random model has been created by the introduction of a cube filled by foam cells and by arranging boundaries without geometrical symmetry, but with flat and shear stress free boundaries. This model does not include a regular part and, therefore, it shows a better converge to the correct result then the model with the regular part. This allows the use of a smaller model, because the geometry is very close to that of the real closed-cell foam structure.

The complete anisotropic closed-cell foam model including large deformation analysis with nonlinear solid material behaviour was successfully used to simulate the anisotropic XPS foam. Anisotropy has been introduced in a way similar to that used in the open-cell foam modelling. The Young's moduli ratios, global compressive collapse stress and tensile stress are predicted very accurately in all three directions. However, the absolute values of the Young's moduli were overestimated in all three directions with the same

factor. This fact might be explained by the use of the Young's modulus of the solid PS before the foaming and without taking into account changes in the properties of the solid because of the foaming. This overestimation also occurred in PMI foam, and might be typical for foams made of polymers.

As a result of the modelling, it was found that:

- The topological model based on the geometry of the tetrakaidecahedron is a good approximation of the Young's modulus of the real foam structure with considerable content of the solid material in walls.
- Anisotropy effects enhance the mechanical properties of the foam in the rise direction.
- The mass distribution of polymer over struts and walls has a considerable impact on the mechanical properties of the foam. The stiffness and yield stress of the foam increase with an increasing portion of polymer in walls; 100% material in walls appears to be optimal. Apparently, the cell walls are dominant structural elements in closed-cell foams.
- Walls experience higher stresses and strains than struts.
- The fraction of open cells in a closed-cell foam impacts the properties of the foam. Measurements are recommended for the future investigations.
- Special attention should be paid to the mechanical properties of the solid material in the foamed structure. This may differ strongly from the original properties of the solid before the foaming processes.
- The anisotropic random model with the initial anisotropy degree $n = 0.38$ gives adequate results for the Young's moduli anisotropy of a real foam. This indicates that the described geometry in the model is correct.

4. Discussion and Conclusions

A comprehensive low-density foam model is created and described in Chapters 2 and 3. Due to the application of the geometrical features of real foam, the mechanical properties of foams can be modelled. The geometry of the real foam is emulated by the application of the 3D Voronoi tessellation which closely resembles the growing of bubbles during the foaming processes. The subsequent implementation of the geometry in the FE analysis and the application of the correct mechanical properties of the solid material logically leads to a model that is able to emulate the behaviour of foams.

The main deformation mechanisms in foams could be analysed and the effect of various topological features of the foam morphology could be investigated in detail using the geometry which is close to the geometry of the real foam. First of all, the main deformation mechanism in the open-cell foam is strut bending, while the axial deformation of struts was also found to play a certain role in the stiffness of foams even in the initial state, especially for foams with a random morphology. On the other hand, in-plane stiffness of cell walls influences the Young's modulus of the closed-cell foam. In general, the open-cell foam can be defined as the closed-cell one with cell walls having zero thickness. From this point of view, an important conclusion can be made about the linear elastic deformation of foams: the Young's modulus of foam is governed by the in-plane deformation of cell walls and bending of struts; the amount of the solid material in walls determines the stiffness of a foam to a very large extent. Bending struts represent flexible (micro-)structural elements, whereas walls experience predominantly in-plane stresses and, therefore, they represent stiff (micro-)structural elements.

In comparison with regular foam models, the presented random model includes irregularities of the geometry typical for the real foams. This fact allows to analyse the influence of the structural irregularities on the mechanical properties of foams. It was found, that the Young's modulus of foam is dependent on the degree of the foam irregularity. Moreover, the open-cell foam model was very sensitive to the irregularities, while the randomness had a small impact on the Young's modulus of the closed-cell foam without struts (cell walls only). However, the randomization degree of the foam structure is still important for the large deformation of foams.

The other advantage gained from the Voronoi approach is the possibility of the introduction of a new kind of the geometrical anisotropy in the foam structure. As opposed to the previous anisotropic foam models, the link can be made between the structure of the foam model and the production process of the observed foam. This leads to a more correct

modelling of the geometry of the anisotropic foam and to a more accurate prediction of the real foam behaviour.

One more advantage of the presented model as compared with the foregoing models is the possibility to vary the geometrical features within the model. For instance, the struts cross-sectional area and the walls thickness may be variable. Moreover, the usage of a considerable number of foam cells in the model allows to remove a number of cell walls and study the effects on foam properties. This modelling corresponds to the real closed-cell foam structure, where some cell walls are ruptured during or after the foaming process.

To keep the model practical, a number of ***simplifications*** has been accepted. First of all, gas pressure inside cells in closed-cell foams has not been taken into account. As mentioned above, the mechanical properties of foam depend, besides the gas pressure, on the foam geometry and solid material in the geometrical elements of foams. Consequently, two main groups of simplifications are distinguished — the foam *geometry* and the *solid material* simplifications. The additional group results from the *limitations of the computer capacities*.

The first group includes simplifications concerning struts and walls **geometry**. First, struts cross-section and wall thickness are assumed to be constant within each strut and wall. Moreover, this thickness is kept constant for all struts and walls (except Section 2.3.2, where struts have various cross-sections). These assumptions are shown to be acceptable, because only low-density foams are modelled. Struts are modelled by a circular cross-section instead of the much more complicated Plateau-Gibbs border. This simplification decreases the bending stiffness of struts. Nevertheless, all effects in foam, like occurrence of the percolating chains of axially loaded struts, remain unchanged. The following assumption used in the presented modelling is related to the walls in the random model. They are flat in the undeformed state due to the 3D Voronoi tessellation based on the nuclei that grow with the same rate. This can be violated in real foams where the curved walls are sometimes observed. Consequently, mechanical properties of the foam would change. However, presence of the gas inside the cells of real foams has stabilizing effect for the walls and curved walls are not expected to considerably change the properties of foams. Moreover, the dominant deformation mechanism found in closed-cell foams is the in-plane deformation of cell walls.

In **the second group** of simplifications of the model, the behaviour of the **solid material** in struts and walls is simplified. First of all, the mechanical properties of the solid material in foam should be determined carefully. The properties of the base material

before foaming are very often very different from those inside the walls and struts. Moreover, mechanical properties of the material in walls can differ from those in struts, because of the different way of the material orientation in struts and walls. This is especially appropriate for the polymeric foams, where macromolecules of the solid polymer may get unidirectional orientation inside struts and two dimensional alignment inside walls. The resulting material might posses higher stiffness than the original unfoamed bulk polymer. This phenomenon requires determination of the properties of the material inside the struts and walls by, for example, direct experiments on walls and struts. Unfortunately, this is often impossible because of the needed small scale of the testing equipment. Moreover, the solid material behaviour in the linear elastic analyses is assumed to be linear and time-independent, while structural elements of foam will have various strain rates. Consequently, material in struts and walls of foam made of polymers will respond diversely and this can influence the global behaviour of foam. Further, solid polymers may behave asymmetrically in compression and tension and this effect should be taken into account. Moreover, no failure criteria are applied to the solid material inside struts and walls. As a result, the foam model presented cannot predict failure of foam.

The other important group of the simplifications pertains to the restrictions of the **computer capabilities**. First, the use of a rather rough meshing in the closed-cell foam modelling introduces a certain error in the modelling. This error, still small in the linear analysis of closed-cell foams due to absence of walls buckling, becomes larger when non-linear analysis is applied. Secondly, the possible contact between walls and struts during the foam deformation was not incorporated. This simplification leads to the impossibility of the modelling of the densification effect in the compression region of foams. In addition, the unit cell dimensions are still limited due to the number of elements that could be used in the FE computations.

A worthwhile future development of the model is seen in the elimination of the main simplifications of the random model, namely, by:

- more accurate determination of the mechanical properties of the solid material inside walls and struts;
- introduction of failure criteria of the solid material in the FE model;
- application of a variable wall thickness within walls in foam cells in such a way, that walls become thinner in the middle, and not all walls have equal thickness;
- substitution of the simplified circular cross-section of struts by a more complicated one having a Plateau-Gibbs border shape;
- exact determination of the fraction of open cells (or ruptured walls) in the closed-cell foam and application of that open cells fraction in the model;

- taking into account gas pressure inside the cells in closed-cell foams, which is especially important in the large deformation analysis;
- the use of the larger computer capacities which would allow finer FE meshing and larger unit cell dimensions;
- adoption of a “unit element” concept with a considerable amount of random foam cells, but without symmetric boundaries, instead of the more conventional in view of the prescribed symmetry conditions “unit cell” concept which needs a regular boundary layer.

APPENDIX

This Appendix discusses the procedure adopted to carry out the FE analyses using the nonlinear material behaviour of the struts (B or C in Fig. 2.23 in the main text). An incremental, Updated Lagrange approach is used in which the incremental (or tangent) stiffness against tension and bending are determined from the integrated deformation history of the cross-section. This integration is carried out numerically by subdividing the cross-section into N_r by N_t segments as shown in Fig. A1. The axial strain $\varepsilon^{(ij)}$ at segment (i,j), with coordinates $\left(x^{(ij)}, y^{(ij)}\right)$, follows from standard kinematics as

$$\varepsilon^{(ij)} = \varepsilon_a + \kappa_x y^{(ij)} + \kappa_y x^{(ij)}, \tag{A1}$$

where ε_a is the average axial strain of the strut, κ_x and κ_y are curvatures about corresponding local x- and y-axis. For the nonlinear constitutive relations in Fig. 2.23, the local tangent $D^{(ij)}$ at this segment is a function of the local strain $\varepsilon^{(ij)}$. The local incremental response $\Delta\sigma^{(ij)} = D^{(ij)}\left(\varepsilon^{(ij)}\right)\Delta\varepsilon^{(ij)}$ at all segments is then used together with the incremental form of Eq. (A1) to determine the global incremental relations for normal force F and bending moments M_x, M_y in terms of the global incremental deformations $\Delta\varepsilon_a$, $\Delta\kappa_x$ and $\Delta\kappa_y$ through

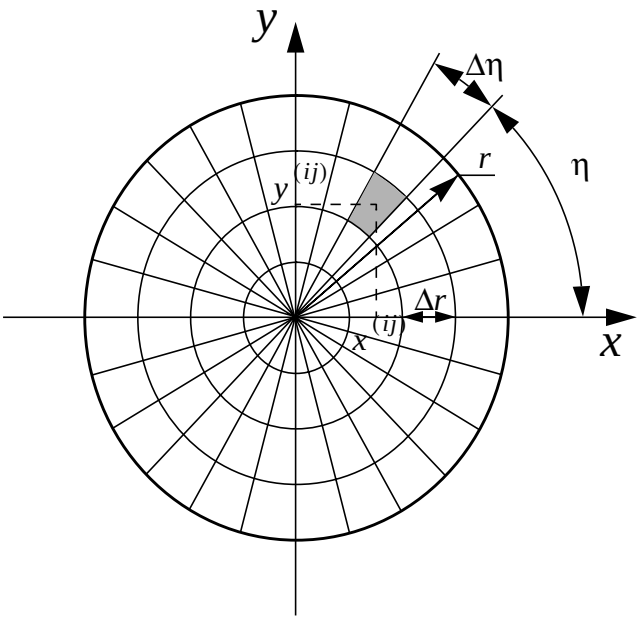

Fig. A1. Strut cross-section discretisation, where the area is divided in radial and circumferential directions. The middle of segment (i,j) (shaded gray) has coordinates $x^{(ij)}$, $y^{(ij)}$, where $0 < i \le N_r = r/\Delta r$ and $0 < j \le N_t = 2\pi/\Delta\eta$.

$$\Delta F = \sum_{i=1}^{N_r} \sum_{j=1}^{N_t} \Delta\sigma^{(ij)} a^{(ij)} \ , \ \Delta M_x = \sum_{i=1}^{N_r} \sum_{j=1}^{N_t} \Delta\sigma^{(ij)} a^{(ij)} y^{(ij)} \quad \text{and}$$

$$\Delta M_y = \sum_{i=1}^{N_r} \sum_{j=1}^{N_t} \Delta\sigma^{(ij)} a^{(ij)} x^{(ij)} \ . \qquad \text{(A2)}$$

Here, $a^{(ij)}$ is the area of segment (i, j) in the undeformed configuration (geometric non-linearity associated with contraction of the cross-section is neglected throughout).

Because of the relatively small torsional strains found in the foam (see Section 2.3.2), material nonlinearity is neglected in the torsional resistance. Thus, the torsional stiffness is taken to be determined by the initial shear modulus $E_s / 2\,(1 + \nu_s)$ of the solid material.

Bibliography

Berlin, A.A., and F.A. Shutov (1980). *Chemistry and Processing of Foamed Polymers* (in Russian). Moscow, Nauka .

Beukers, A., S. de Winter and W.D. Brouwer (1997). *Self-Supporting Refrigerated Truck.* European Patent Nº 97200124.2-2306.

Boetes, R. (1986). *Heat Transfer Reduction in Closed Cell Polyurethane Foams.* Ph.D.-thesis, Delft.

Boots, B.N. (1982). *The Arrangement of Cells in "Random" Networks*. Metallography, 15, 53-62.

Brezny, R., and D.J. Green (1990). *The Effect of Cell Size on the Mechanical Behaviour of Cellular Materials.* Acta metall. mater., 38, 2517-2526.

Brodt, K. (1995). *Thermal Insulations: CFC-Alternatives and Vacuum Insulation.* Ph.D.-thesis, Delft.

Chan, R., and M. Nakamura (1969). *Mechanical Properties of Plastic Foams.* J. of Cellular Plastics, 5, 112-118.

Cunningham, A. (1981). *Modulus Anisotropy of Low-density Cellular Plastics: Aggregate model.* Polymer, 22, 882-885.

Cunningham, A. (1984). *The Mechanical Anisotropy of Low-density Cellular Plastics.* Cellular Polymers, 3, 133-143.

Cunningham, A., and N.C. Hilyard (1994). *Low Density Cellular Plastics* (eds. N.C. Hilyard and A. Cunningham). London, UK: Chapman & Hall.

Dementjev, A.G., and O.G.Tarakanov (1970a). *Influence of the Cellular Structure of Foams on their Mechanical Properties* (in Russian). Mechanics of Polymers, 4, 594-602.

Dementjev, A.G., and O.G.Tarakanov (1970b). *Modelling and Design of the Cellular Foam Structure of a PUR Type* (in Russian). Mechanics of Polymers, 5, 859-865.

du Cauze de Nazelle, G.M.R. (1995). *Thermal Conductivity Ageing of Rigid Closed Cell Polyurethane Foams.* Ph.D.-thesis, Delft.

Euler, L. (1746). *Thoughts on the elements of bodies*. Memoirs of the Prussian Academy of Sciences, Berlin.

Fedorov, E.S. (1971). *Symmetry of Crystals.* American Crystallographic Association, Pittsburgh.

Gent, A.N., and A.G.Thomas (1959). *Failure of Foamed Elastic Materials.* J. of Appl. Polym. Sci., 2, 354-357.

Gent, A.N., and A.G.Thomas (1963). *Mechanics of Foamed Elastic Materials.* Rubber Chem.Technol., 36, 597.

Gibson, L.J., and M.F. Ashby (1988). *Cellular Solids: Structure and Properties.* Oxford, UK: Pergamon Press.

Gibson, L.J., and M.F. Ashby (1982). *The Mechanics of Three-Dimensional Cellular Materials.* Proc. Roy. Soc., A382, 43-59.

Gioumousis, G. (1963). *Shapes of Cells in Polymer Foams.* J. of Appl. Polym. Sci., 7, 947-957.

Hagiwara, H., and D.J. Green (1987). *Elastic Behavior of Open-Cell Alumina.* J. Am. Ceram. Soc., 70, 811-815.

Hall, R. (1993). *Effective Moduli of Cellular Materials.* J. of Reinforced Plastics and Composites, 12, 186-197.

Huber, A.T., and L.J. Gibson (1988). *Anisotropy of Foams.* J. of Mater. Sci., 23, 3031-3040.

Ko, W.L. (19 65). *Deformations of Foamed Elastomers.* J. of Cellular Plastics., 1, 45-50.

Kann, K.B. (1989). *Capillary hydrodynamics of foams* (in Russian). Nauka, Novosibirsk.

Kumar, S., and S.K. Kurtz (1994). *Simulation of Material Microstructure Using a 3D Voronoi Tessellation: Calculation of Effective Thermal Expansion Coefficient of Polycrystalline Materials.* Acta metall. mater., 42, 3917-3927.

Lakes, R., P.Rosakis and A.Ruina (1993). *Microbuckling instability in elastomeric cellular solids.* J. of Materials Sci., 28, 4667-4672.

Lederman, J.M. (1971). *The prediction of the Tensile Properties of Flexible Foams.* J. Appl. Polym. Sci., 15, 693-703.

Meinecke, E.A., and R.C. Clark (1973). *Mechanical Properties of Polymeric Foams.* Technomic Publishing Co., Westport (USA).

Morgan, J.S., J.L. Wood and R.C. Bradt (1981). *Cell Size Effects on the Strength of Foamed Glass.* Mater. Sci. Engng 47, 37-42.

Ogibalov, P.M., V.A. Lomakin and B.P. Kishkin (1975). *Mechanics of Polymers* (in Russian). Moscow University Publishing, Moscow.

Papka, S.D., and S. Kyriakides (1994). *In-plane Compressive Response and Crushing of Honeycomb.* J. Mech. Phys. Solids, 42, 1499-1532.

Pertsov, A.V., A.E. Simonov and E.V. Porodenko (1992). *Plateau-Gibbs Borders: Calculation of Shape and Volume.* Mendeleev Commun., 114-115.

Plateau, J. (1873). *Statique Experimentale et Theorique des Liquides Soumis aux Seules Forces Moleculaires.* Gauthier-Villars, Paris.

Renz, R., and G.W. Ehrenstein (1982). *Calculation of Deformation of Cellular Plastics by Applying the Finite Element Method.* Cellular Polymers, 1, 5-13.

Rusch, K.C. (1969). *Load-compression behaviour of flexible foams.* J. Appl. Polym. Sci., 13, 2297-2311.

Stauffer, D. (1985). *Introduction to Percolation Theory.* Taylor & Francis, London.

Vainshtein, B.K., V.M. Fridkin and V.L. Indenbom (1995). *Structure of Crystals.* FRG: Springer–Verlag, Berlin.

Valuyskikh, V. (1990). *Study of Elastic Foamed Plastics*. Cellular Polymers, 9, 12-24.

Van de Weygaert, R. (1991). *Voids and the Geometry of Large Scale Structures.* Ph.D.–thesis, Leiden.

Van Krevelen, D.W. (1976). *Properties of Polymers: Their estimation and correlation with chemical structure.* Elsevier Scientific Publishing Co, Amsterdam.

Van Vuure, A.W. (1997). *Composite Panels Based on Woven Sandwich-Fabric Preforms.* Ph.D.–thesis, Leuven (Belgium).

Voronoi, G. (1908). *Nouvelle Applications des Paramètres Continus à la Théorie des Formes Quadratiques.* J. Reine und Angew. Math., 134, 97.

Vos, R. de, D. Rosbotham and J. Deschaght (1994). *Open-Celled Polyurethane Foam Based Vacuum Panel Technology: a Fully Polyurethane-Based Composite Technology for Vacuum Insulated Appliances.* Proc. ICI Polyur. SPI Confer., Boston (USA).

Warburton, S.C., A.M. Donald and A.C. Smith (1990). *The Deformation of Brittle Starch Foams.* J. of Mater. Sci., 25, 4001-4007.

Warren, W.E., and A.M. Kraynik (1987). *Foam Mechanics: the Linear Elastic Response of Two-Dimensional Spatially Periodic Cellular Materials.* Mechanics of Materials, 6, 27-37.

Warren, W.E., and A.M. Kraynik (1988). *The Linear Elastic Properties of Open-Cell Foams.* ASME Journal of Applied Mechanics, 55, 341-347.

Warren, W.E., and A.M. Kraynik (1994). *Low Density Cellular Plastics* (eds. N.C. Hilyard and A. Cunningham). London, UK: Chapman & Hall.

Warren, W.E., and A.M. Kraynik (1997). *Linear Elastic Behavoir of a Low-Density Kelvin Foam with Open Cells.* To be published in the ASME J. of Appl. Mech.

Waterman, N.R., and P.J. Phillips (1974). *The mechanical Properties of High-Density Rigid Polyurethane Foams in Compression: Yield Behaviour.* Polymer Engin. and Sci., 14, 72-75.

Weaire, D., and M.A. Fortes (1994). *Stress and Strain in Liquid and Solid Foams.* Advances in Physics, 43, 685-738.

Yasunaga, K., R.A. Neff, X.D. Zhang and C.W. Macosko (1996). *Study of Cell Opening in Flexible Polyurethane Foam*. J. of Cellular Plastics, 32, p.427-448.

Zhu, H.X., J.F. Knott and N.J. Mills (1997). *Analysis of the Elastic Properties of Open-Cell Foams with Tetrakaidecahedral Cells.* J. Mech. Phys. Solids, 45, p.319-343.

SUMMARY

Foamed materials are applied in many products, because of the special combination of mechanical properties and low density. The mechanical properties of foams are determined by the properties of the solid material inside the foam and the topology of the foam structure. This makes it possible to model the mechanical behaviour of foams with the help of a Finite Element Method. In this thesis, FE analyses are performed on various types of foams and the effects of various geometrical features of the foam geometry are studied.

The majority of the existing models is based on regular structures consisting of struts and walls associated with the structural elements in foams. The main advantage of the presented random model in comparison with already existed ones is the use of a geometry very close to the real foam geometry. This allows to understand the dominant deformation mechanisms in foams and, therefore, to predict the behaviour of foams. The FE analysis results were compared to the results of experiments from which the mechanical properties were obtained. The experimental investigations of foams also comprised a microscopic analysis of the geometrical features of the foam. Various types of foams were studied in this way: polyurethane, polystyrene, polymethacrylimide, glass and aluminium foams.

First, an open-cell random foam model has been created with the help of the 3D Voronoi technique. The deformation behaviour of regular foams is dominated by bending of struts. This has already been recognized by several other scientists. However, it has been shown in this thesis that the behaviour of random foams is different. Axial deformations in random foams play an important role even in the initial stage of the deformations. This is opposed to the regular models often used in practice. The FE analyses showed that the stiffness of a random foam model is higher than that of corresponding regular models due to the “coincidental” percolations of chains of randomly oriented struts. These chains bear a significant axial load. The random open-cell model showed that axial deformation becomes dominant in all foams under large tensile strains.

Geometrical anisotropy of open-cell foam is also modelled. It is described by the introduction of two kinds of anisotropy. This technique allows to reach a close correspondence between the geometrical features of real foams and those of the model. Consequently, the behaviour of foam can be modelled and predicted.

Similar to the open-cell foams, also a closed-cell random foam model is created. It has been shown that the geometry of a model is important for the prediction of the mechanical properties of foams. The distribution of the solid material between struts and walls in

foam is very important, and foams with all material inside the walls (struts are not pronounced) exhibit the highest mechanical properties. Moreover, not all walls are closed in closed-cell foams. Some of them are ruptured during or after processing. This is also one of the geometrical features which influence the foam behaviour considerably. Comparison of regular and random foam models showed that simple fcc- and bcc-based foam models can be used to predict the Young's modulus of isotropic foam, if the main part of the material in the modelled foam is concentrated in walls. Otherwise, if the fraction of solid in struts is considerable, regular models give inaccurate results and the use of the random model is advisable.

Furthermore, the anisotropy in closed-cell foam is described analogous to that in the open-cell foam model. The predicted Young's modulus in real foam is much more accurate than previously described (literature) models. Finally, a complete random anisotropic closed-cell foam model is created and successfully used to predict both linear and nonlinear mechanical behaviour of a real anisotropic closed-cell foam.

Vladimir Shulmeister

SAMENVATTING

Geschuimde materialen worden in veel produkten toegepast wegens hun bijzondere combinatie van lage dichtheid met goede mechanische eigenschappen. De mechanische eigenschappen van geschuimde materialen worden bepaald door de eigenschappen van het materiaal waar het schuim van gemaakt is en door de topologie van de schuim structuur. Dit maakt het mogelijk de mechanische eigenschappen van een schuim te modelleren met behulp van de Eindige Elementen Methode (EEM). In dit proefschrift wordt een EEM analyse gepresenteerd van de invloed van diverse geometrische factoren op de mechanische eigenschappen van verschillende schuimsoorten.

De meerderheid van de bestaande modellen zijn gebaseerd op regelmatige structuren, bestaande uit kleine staven “struts” en celwanden “walls” als elementaire constructieve elementen waaruit het schuim is opgebouwd. In dit proefschrift zijn ook meer onregelmatige, z.g. gerandomiseerde structuren onderzocht. Het voordeel t.o.v. de eerder beschreven regelmatige structuren is dat de onregelmatige structuren veel beter overeen komen met de waargenomen werkelijke structuur van schuimen. Zo is het nu mogelijk de dominante vervormingsmechanismes in geschuimde materialen beter te begrijpen en het gedrag beter te voorspellen. De resultaten van de EEM modeleringen zijn vergeleken met experimenteel bepaalde schuim-eigenschappen. Verder zijn er diverse microscopische analyses uitgevoerd om de topologische karakteristieken van de schuimgeometrie te bepalen. De experimenten zijn uitgevoerd voor diverse materialen: polyurethaan, polystyreen, polymethacrylimide, glas en aluminium schuimen.

Opencellige schuimen worden het eerst gemodelleerd. Een topologisch schuimmodel is gemaakt met behulp van een drie-dimensionale Voronoi methode. Het vervormingsgedrag van regelmatige schuimen blijkt gedomineerd te worden door buiging van de “struts”. Dit is al eerder herkend door verschillende andere onderzoekers. Uit het onderzoek in dit proefschrift blijkt echter dat axiale vervormingen belangrijk worden wanneer de schuimstructuur gerandomiseerd wordt. De stijfheid van een “volledig gerandomiseerd” onregelmatig schuim is een factor twee tot vier hoger dan van een regelmatig schuim, afhankelijk van het type model voor het regelmatige schuim waarmee wordt vergeleken. De EEM analyse toonde dat de stijfheidstoename ontstaat door het “toevallig” optreden van ketens van “struts” die in de belastingsrichting georiënteerd zijn. Deze ketens dragen een relatief grote axiale belasting. Dit effect wordt in geen van de eerder gepubliceerde modellen beschreven.

Het effect van geometrische anisotropie van opencellige schuimen op de mechanische eigenschappen is ook gemodelleerd. Er is een nieuwe manier gevonden om geometrische

anisotropie te modelleren. Daarbij worden twee verschillende soorten anisotropie onderscheiden. Op deze manier blijkt het mogelijk de werkelijke topologie van anisotrope schuimen zeer goed te benaderen en het gedrag realistisch te modelleren. De mechanische eigenschappen van opencellige anisotrope schuimen konden op deze manier goed voorspeld worden.

Op een analoge manier zijn ook geslotencellige schuimen gemodelleerd. Ook hier blijkt de topologie van het gemodelleerde schuim belangrijk te zijn. De verdeling van het materiaal over “struts” en “walls” heeft grote invloed op de stijfheid van het schuim. Schuimen met veel materiaal in de celwanden (“walls”) blijken relatief stijf te zijn. Het blijkt dat niet alle celwanden in geslotencellig schuim ook werkelijk gesloten zijn. Sommige celwanden zijn beschadigd tijdens of na de produktie van het schuim. Hoe meer celwanden open zijn, hoe lager de stijfheid van het schuim is.

Een vergelijking van regelmatige en onregelmatige structuren blijkt voor geslotencellige schuimen een veel kleiner verschil op te leveren dan voor de eerder genoemde opencellige schuimen. Simpele fcc en bcc modellen voldoen hier, zolang het grootste deel van het materiaal aanwezig is in de celwanden.

Het effect van geometrische anisotropie in geslotencellige schuimen is gemodelleerd op een analoge manier als voor opencellige schuimen. De resulterende stijfheden komen veel beter overeen met de gemeten stijfheid van echte schuimen dan de stijfheden volgens eerder gepubliceerde modellen uit de literatuur. Tenslotte is een onregelmatig anisotroop model geconstrueerd voor geslotencellig schuim. Hiermee kon het mechanisch gedrag in het lineaire en het niet lineaire gebied van een echt schuim goed beschreven worden.

Vladimir Shulmeister

Acknowledgements

First of all I would like to thank prof. G.P. Nerubenko (in spite of some unfortunate "nonlinearities" in my relation with him based on a difference of opinion on some non-scientific subjects) and prof. P. Meijers for the initiation of my connections with Delft University of Technology in 1991.

My unconditional deep gratitude also goes to my promotor prof. Roel Marissen for his daring act of taking a yet unknown young Ukrainian man as his first (!) PhD student and for his encouraging help.

Throughout these four years I had a lot of fun in my work thanks to my colleague and friend Nico Lousberg whose south-Limburg temperament was quite similar to the south-Ukrainian one of mine. Moreover, we even found some time to complete useful experiments used in the thesis.

This most considerable part of work in my life up to now would surely not be possible without the friendly help of Leonid Timochouk (formerly PhD student at the Mathematics department at TUDelft) who introduced me to the world of Unix! My friendship with PhD students from the Technical Mechanics department of the TUDelft Geert Stam, Sander Steenbrink and Marc van der Burg led to wonderful moments during my life in Delft and, consequently, very fruitful cooperation regarding modelling of foams with Marc and his supervisor prof. Erik van der Giessen. I've learned a lot from them both scientifically and in general.

In times of difficulty my colleagues at Fibre Reinforced Plastics group — Leo, Jan, Lydia, Wim, Huib, René and Bertus Nijhof — were always nearby and ready to help. Thanks!

My special gratitude to our system manager Jan Booij whose excellent work is difficult to evaluate by words.

At the final stage of the work on the thesis I received a number of useful advises about the use of the English language (articles are useless!) from my schoolmates Greg Krasnov and Artjem Nagorny.

Propositions

accompanying thesis
"Modelling of Mechanical Properties of Low-Density Foams"

Vladimir Shulmeister
January, 1998

1. The main drawback of the regular foam models is not their inability to predict the behaviour of foamed materials. To make it work, some adaptive coefficients may be used (and are used!). The main problem is the inability of the regular models to demonstrate "why" it is so.
2. Chaos is difficult to predict. From this point of view, the mechanical properties of polymer foams are very difficult to model not only because of their irregular (chaotic) geometry, but also due to the chaotic structure of the solid polymer itself on the macromolecular level within the structural elements of the foam.
3. Nature is at least three-dimensional.
4. From the geometrical point of view, the cover of this thesis is very close to the evolution process.
5. One of the problems of models that use the fitting of the experimental data is that they plot different materials with very different parameters on one graph and then try to fit this data for one of the parameters without taking the others into account. This drawback is much easier to overcome in the sort of modelling presented in the thesis, where one may change only one parameter and be sure about the purity of the comparison among several models.
6. Everything can be explained! And even in several ways!
7. An important thing in the life of a person is his communication with the world around, or with other people. His situation may be modelled by a hammock. When some of the connections break (ropes rupture), the load is redistributed among the other ropes. At a certain point the load may exceed the limit and, if no new connections are made, a crisis ensues.
8. Everything starts from nothing. And it ends there too...
9. Every PhD student has a right to write a dissertation and everybody else has a right not to read it.
10. One of the formulations of the meaning of life is to be happy. Everybody just fills this meaning with his own understanding of happiness.
11. A human being is originally lazy. From this point of view, "success" may be defined as "overcome laziness multiplied by a fortune factor".
12. An understanding of the purpose of life is to leave some remembrance after. It can be realized through "children" and through "work". Many people choose only the first realization (often due to their "original laziness", see the foregoing proposition) without being conscious that "the main work" comes after the children are made.
13. Number 13 may be a lucky number. Just believe in it!

Stellingen

behorende bij het proefschrift

"Modelling of the Mechanical Properties of Low-Density Foams"

Vladimir Shulmeister
January, 1998

1. Het belangrijkste nadeel van de huidige schuimmodellen is niet het feit dat men er het gedrag van geschuimde materialen niet mee kan voorspellen. Om ze te laten werken, kunnen immers enige variabele coëfficiënten worden gebruikt (en dat wordt ook gedaan!). Het grootste probleem is het feit dat de huidige modellen niet kunnen verklaren waarom dingen zijn zoals ze zijn.
2. Chaos is moeilijk te voorspellen. Hieruit volgt dat de mechanische eigenschappen van polymeerschuimen zeer moeilijk te modelleren zijn, niet alleen vanwege hun onregelmatige (chaotische) geometrie maar ook vanwege de chaotische structuur van de vaste polymeren zelf op het macromoleculaire niveau binnen de structurele elementen van het schuim.
3. De natuur is tenminste drie-dimensionaal.
4. Vanuit een geometrisch gezichtspunt komt de omslagillustratie van dit proefschrift sterk in de buurt van het evolutieproces.
5. Eén van de problemen met modellen waarin experimentele resultaten worden verdisconteerd is het feit dat diverse materialen met zeer diverse parameters in één grafiek worden samengebracht en dat men daarna probeert deze gegevens te laten kloppen voor één parameter zonder de andere in acht te nemen. Aan dit nadeel is veel eenvoudiger te ontkomen bij het type modellering dat in dit proefschrift wordt gepresenteerd; hierin mag men maar één parameter veranderen en kan men zeker zijn van de zuiverheid bij een vergelijking van de diverse modellen.
6. Alles kan worden uitgelegd! En zelfs op verschillende manieren!
7. Een belangrijk aspect in het leven van een mens is zijn communicatie met de wereld om hem heen of met andere mensen. Zijn situatie kan vergeleken worden met een hangmat. Als enkele verbindingen verbroken worden, dan wordt de belasting herverdeeld over de andere verbindingen. Op een zeker punt kan de belasting een grens overschrijden en zal, indien geen nieuwe verbindingen worden gemaakt, een crisis intreden.
8. Alles begint vanuit niets. En daar eindigt het ook...
9. Elke promovendus heeft het recht een proefschrift te schrijven en ieder ander heeft het recht dit niet te lezen.
10. Eén van de formuleringen voor 'de zin van het leven' is: gelukkig zijn. Iedereen vult dit in aan de hand van zijn eigen opvatting van geluk.
11. Een mens is van origine lui. Vanuit dit gezichtspunt kan "succes" gedefinieerd worden als "overwonnen luiheid, vermenigvuldigd met een geluksfactor".
12. Eén van de opvattingen over het doel van het leven is: het achterlaten van een herinnering. Dit kan worden gerealiseerd middels "kinderen" en middels "werk". Veel mensen kiezen alleen voor de eerste optie (vaak vanwege hun "oorspronkelijke luiheid", zie de voorgaande stelling) zonder dat zij zich ervan bewust zijn dat "het echte werk" begint nadat de kinderen zijn gemaakt.
13. Het getal 13 kan een geluksgetal zijn. Je moet er gewoon in geloven!